

Electronic Thesis and Dissertation Repository

---

9-11-2018 2:00 PM

## Matrix-Assisted Laser Desorption/Ionization Mass Spectrometry Imaging of ZP1609 and Amyloid Beta

Jasmine S. H. Wang, *The University of Western Ontario*

Supervisor: Yeung, Ken K.-C., *The University of Western Ontario*

Co-Supervisor: Whitehead, Shawn N., *The University of Western Ontario*

A thesis submitted in partial fulfillment of the requirements for the Doctor of Philosophy degree in Chemistry

© Jasmine S. H. Wang 2018

Follow this and additional works at: <https://ir.lib.uwo.ca/etd>

 Part of the [Analytical Chemistry Commons](#)

---

### Recommended Citation

Wang, Jasmine S. H., "Matrix-Assisted Laser Desorption/Ionization Mass Spectrometry Imaging of ZP1609 and Amyloid Beta" (2018). *Electronic Thesis and Dissertation Repository*. 5744.  
<https://ir.lib.uwo.ca/etd/5744>

This Dissertation/Thesis is brought to you for free and open access by Scholarship@Western. It has been accepted for inclusion in Electronic Thesis and Dissertation Repository by an authorized administrator of Scholarship@Western. For more information, please contact [wlsadmin@uwo.ca](mailto:wlsadmin@uwo.ca).

## Abstract

The revolutionary development of soft ionization techniques like matrix-assisted laser desorption/ionization (MALDI) has opened up the possibilities for mass spectrometry (MS) in protein detection, identification, and sequencing. The ability of MALDI MS to acquire images of intact tissue sections offer an additional dimension of analysis where location information can be attained. Visualization of biological systems help to unravel the complexities of cells, drug pathways, and disease pathology. However, the capabilities of MALDI MS imaging are often being questioned, as signals are typically biased towards the most abundant component within a complex sample. Within biological tissue samples, the most abundant components are salts and lipids making it difficult for compounds such as proteins and peptides to ionize and be detected.

In this thesis, sample preparation techniques are investigated to help improve the detection sensitivity of MALDI MSI for proteins and peptides through investigation of ZP1609 and the amyloid  $\beta$  (A $\beta$ ) protein. ZP1609 is an antiarrhythmic drug designed to protect against cardiac ischemia-reperfusion injury, and A $\beta$  oligomers are strongly correlated with Alzheimer's disease (AD) pathology. Both of which are considered lower abundance compounds within samples analyzed, and therefore ideal candidates for the work described herein. This thesis presents MALDI MS capabilities in the detection of noncovalent complexes by distinguishing variations in *in vitro* A $\beta$  composition for different sample preparatory procedures. Furthermore, a reduction in ion suppression effects by salts and lipids was demonstrated with increased MALDI MSI detection sensitivity for the target peptide. Most noticeably, an

additional acidification protocol generated images of greater detection sensitivity, and spatial resolution. Introduction of solid-phase extraction (SPE) by means of magnetic bead application was designed to improve the extraction of proteins from tissue sections. The C18 functionalized magnetic beads provided signal enhancement capabilities for varying concentrations of A $\beta$ <sub>1-42</sub> samples, however difficulties were encountered when applied for MALDI MSI analysis. Nonetheless, the application of SPE for targeted analyte extraction prior to MALDI MS analysis was beneficial in improving detection sensitivity of A $\beta$  proteins with and without the presence of contaminants from tissue sections.

## **Keywords**

MALDI TOF MS, MALDI MSI, Alzheimer's disease, amyloid beta oligomers, matrix application, detection sensitivity, protein imaging, peptide imaging, solid-phase extraction, magnetic beads.

## Co-Authorship Statement

Chapters 3 and 4 contain published materials in the following journals:

1. Jasmine S.H. Wang, Shawn N. Whitehead, and Ken K.-C. Yeung. Detection of Amyloid Beta (A $\beta$ ) Oligomeric Composition Using Matrix-Assisted Laser Desorption Ionization Mass Spectrometry (MALDI MS), *J. Am. Soc. Mass Spectrom.*, **2018**, 29(4), 786-795.
2. Jasmine S. H. Wang, Moises Freitas-Andrade, John F. Bechberger, Chris C. Naus, Ken K.-C. Yeung, Shawn N. Whitehead. Matrix-Assisted Laser Desorption/Ionization Imaging Mass Spectrometry of Intraperitoneally Injected Danegaptide (ZP1609) for Treatment of Stroke-Reperfusion Injury in Mice. *Rapid Commun Mass Spectrom.*, **2018**, 32(12), 951-958.

All the data presented in each article was collected by the author. The author also prepared the first draft of the manuscripts. Article 1 was edited by Drs. Shawn Whitehead and Ken Yeung.

Article two was edited by Drs. Chris Naus, Ken Yeung, and Shawn Whitehead. The mice brain retrieval and treatment protocols were provided and performed by Moises Freitas-Andrade and John F. Bechberger.

## **Acknowledgments**

I would like to express my sincere gratitude for my supervisors Dr. Ken Yeung, and Dr. Shawn Whitehead for their continuous support, patience, and guidance throughout my graduate studies. I would like to thank Dr. Yeung for his attention to detail and thoughtful advice over the years. His encouragement, wisdom, and careful considerations have been instrumental in the completion of my thesis. I would like to thank Dr. Whitehead for his endless motivation, enthusiasm, and encouragement for out-of-the-box thinking. His valuable insight, dedication and passion for research has been incredibly inspirational. I am extremely grateful to have two supervisors who were always available for questions, discussions, and to provide feedback on my written work. I would not have been able to complete my studies without their support and expertise.

I would like to thank Western University for the financial support and facilities needed to carry out my work. Thank you to my committee members, Dr. Lars Konermann, Dr. Len Luyt, and Dr. Brian Pagenkopf for your guidance and interest in my research progress. My appreciation is also extended to my examiners, Dr. Lars Konermann, Dr. Len Luyt, Dr. Gilles Lajoie and Dr. Derek Wilson.

During my studies, I have had the pleasure of working alongside and learning from Kristina Jurcic, who has been incredibly supportive. Her knowledge and advice has been immensely helpful throughout this journey. I would also like to thank Sarah Caughlin for her support and understanding as we both worked towards completing our degrees, Lynn Wang for her advice and helpfulness, and the Vulnerable Brain team. A special thank you to the past and present

members of the Yeung lab: Shirley Fan, Hanadi Ibrahim, and Chao Chao Chen. It has been extremely encouraging working with such a supportive, helpful, and caring group of people.

Finally, I would like to express a heartfelt thank you to my husband Nicholas Yu, my parents Connie Hsiao and Steven Wang, and my brother and sister-in-law Eric and Stacey Wang. I cannot thank them enough for their unconditional love, encouragement, prayer and patience throughout this whole process.

# Dedication

To God, my husband, and my parents.

# Table of Contents

Abstract.....	i
Co-Authorship Statement.....	iii
Acknowledgments.....	iv
Dedication.....	vi
Table of Contents.....	vii
List of Tables.....	xiii
List of Figures.....	xiv
List of Equations.....	xvi
List of Symbols and Abbreviations.....	xvii

## **Chapter 1: Introduction of Mass Spectrometry in Protein and Peptide Analysis.....22**

1.1 Overview of Protein Analysis.....	23
1.1.1 Amino Acid Building Blocks.....	23
1.1.2 Protein Structure.....	26
1.1.3 Biological Functions & Interactions of Proteins.....	27
1.2 Protein Analysis.....	28
1.3 Theory and Instrumentation for Mass Spectrometry.....	31
1.3.1 Instrumentation for Mass Spectrometry.....	31
1.3.1.1 Principles of Time-Of-Flight Mass Analyzers.....	34
1.3.1.2 Applications of TOF Analyzer.....	38
1.3.1.3 Detectors.....	39



1.3.2 Soft Ionization Methods.....	40
1.3.2.1 Electrospray Ionization (ESI) .....	40
1.3.2.2 Matrix-Assisted Laser Desorption/Ionization (MALDI).....	43
1.4 Application of MALDI Mass Spectrometry .....	45
1.4.1 Role of MALDI Matrices.....	45
1.4.2 MALDI Matrices and Deposition Methods .....	46
1.5 Introduction of MALDI Mass Spectrometry Imaging (MALDI MSI) .....	50
1.5.1 Theory of MALDI MSI .....	50
1.5.1.1 Ionization of Analytes from Intact Tissue Sections.....	50
1.5.1.2 Signal Detection Sensitivity versus Image Spatial Resolution ..	54
1.5.2 Applications of MALDI MSI.....	55
1.5.2.1 Tissue Collection and Storage .....	55
1.5.2.2 Tissue Sectioning and Mounting .....	57
1.5.2.3 Matrix Application Methodology .....	58
1.5.2.4 Sample Rehydration Methodology .....	63
1.6 References .....	64

## **Chapter 2: Alzheimer’s Disease and the Amyloid Cascade Hypothesis 70**

2.1 Introduction to Alzheimer’s Disease.....	71
2.1.1 Alzheimer’s Disease Pathology .....	72
2.1.2 Amyloid Cascade Hypothesis (ACH).....	75
2.2 Amyloid Beta .....	76
2.2.1 Physical Properties.....	76

2.2.2 A $\beta$ Assemblies .....	77
2.2.3 Biological Functions & Neurotoxicity of Amyloid Beta.....	80
2.3 Amyloid Beta Imaging.....	83
2.4 Overview of Thesis .....	84
2.5 References .....	86

**Chapter 3: Matrix-Assisted Laser Desorption/Ionization Mass Spectrometry Imaging of Intraperitoneally Injected Danegaptide (ZP1609) for Treatment of Stroke-Reperfusion Injury in Mice .....91**

3.1 Introduction .....	92
3.1.1 MALDI MSI Analysis of Small Peptides .....	92
3.1.2 Biological Significance of Danegaptide (ZP1609) .....	93
3.2 Experimental .....	96
3.2.1 Apparatus .....	96
3.2.2 Samples and Reagents.....	97
3.2.3 Treatment Conditions for Tissue Samples .....	97
3.2.4 Tissue Preparation for MALDI MSI Analysis.....	98
3.2.5 MALDI MSI Analysis .....	99
3.3 Results and Discussion.....	100
3.3.1 Identification of Danegaptide Peaks .....	100
3.3.2 Effects of Variation in Matrix Selection.....	102
3.3.3 Effects of Tissue Washing in Signal Detection .....	104

3.3.4 Effects of Variation in Methods of Matrix Application.....	105
3.3.5 Acidification Effects on Signal Detection Sensitivity .....	108
3.3.6 MALDI MSI Analysis of Intraperitoneally Injected ZP1609.....	110
3.4 Conclusion .....	114
3.5 References .....	115

**Chapter 4: Detection of Amyloid Beta Oligomeric Composition Using Matrix-Assisted Laser Desorption/Ionization Mass Spectrometry (MALDI MS).....118**

4.1 Introduction .....	119
4.2 Experimental .....	123
4.2.1 Apparatus .....	123
4.2.2 Samples and Reagents.....	123
4.2.3 Amyloid Beta Sample Preparation.....	124
4.2.4 Molecular Weight Cut-Off Filtration.....	125
4.2.5 Amyloid Beta Toxicity for Embryonic Rat Cortical Neuron Cultures .....	125
4.2.6 MALDI MS Analysis.....	126
4.3 Results and Discussion.....	126
4.3.1 MALDI MS Detection of A $\beta$ <sub>1-42</sub> and A $\beta$ <sub>1-40</sub> Oligomer Composition.....	126
4.3.2 Validation of MALDI MS Detection Capabilities.....	128
4.3.2.1 Analysis of A $\beta$ Fragments with Various Propensities for Oligomerization .....	130
4.3.2.2 Molecular Weight Cut-Off Filtration Analysis.....	131

4.3.3 Effects of Variations Among Amyloid Beta Preparatory Protocols .....	136
4.3.3.1 Monomerization Solvents .....	136
4.3.3.2 Oligomerization Solvents.....	139
4.3.4 In Vitro Amyloid Beta Toxicity Assessment.....	141
4.4 Conclusion .....	144
4.5 References .....	145

**Chapter 5: Enhancements in Detection Sensitivity for the Amyloid Beta Protein with Matrix-Assisted Laser Desorption/Ionization Mass Spectrometry Imaging (MALDI MSI).....149**

5.1 Introduction .....	150
5.1.1 MALDI MSI of Proteins in Intact Tissue Sections.....	150
5.1.2 Magnetic Bead Solid - Phase Extraction .....	151
5.2 Experimental .....	153
5.2.1 Apparatus .....	153
5.2.2 Samples and Reagents.....	154
5.2.3 Amyloid Beta Sample Preparation.....	155
5.2.4 Variations in Magnetic Bead Extraction Efficiency .....	155
5.2.5 Magnetic C18 Dynabeads on Plate Extraction Efficiency.....	158
5.2.6 Sample Preparation for MALDI MSI Analysis .....	158
5.2.6.1 Tissue Extraction and Postmortem Amyloid Beta Injections ..	158
5.2.6.2 Tissue Mounting and Preparation .....	159
5.2.6.3 On Tissue Magnetic Bead Extraction .....	159

5.2.6.4 Matrix Deposition & Tissue Rehydration.....	160
5.2.7 MALDI MSI Parameters.....	161
5.3 Results and Discussion.....	161
5.3.1 Enhancement of Detection Sensitivity Facilitated by C18 Magnetic Bead Extraction.....	161
5.3.1.1 Magnetic Bead Selection .....	161
5.3.1.2 A $\beta$ Signal Enhancement Effects using C18 Magnetic Beads ..	165
5.3.2 Signal Enhancement Effects of Magnetic Beads for Amyloid Beta Using MALDI MSI .....	170
5.4 Conclusion .....	174
5.5 References .....	175
<b>Chapter 6: Conclusions &amp; Future Work.....</b>	<b>178</b>
6.1 Conclusions and Future Work.....	179
6.2 References .....	183
<b>Appendix 1 – Copyright Permission .....</b>	<b>184</b>
<b>Curriculum Vitae.....</b>	<b>189</b>

## List of Tables

<b>Table</b>	<b>Description</b>	<b>Page</b>
<b>1.1</b>	Amino acid residues are listed with both the 3- and 1- letter symbols associated with each. The polarity of each amino acid has been provided.	25
<b>1.2</b>	Alternative matrices developed for MALDI MS analysis, and the target analyte of interest each matrix is most successfully used for have been listed. Unfortunately, as a result of the uncertainties with the ionization mechanism, these are all simply guidelines when choosing a matrices for experiments. The guidelines help to narrow down the selection, however trial-and-error is required to determine the optimal selection for the target analyte.	49
<b>3.1</b>	Peaks identified through MALDI MS analysis of standard ZP1609 samples were recorded. These peaks include dipeptide fragmentation as well as any salt ions, and adducts formations detected within the $m/z$ range of 100 – 550.	101

## List of Figures

<b>Figures</b>	<b>Descriptions</b>	<b>Page</b>
1.1	Schematics for both linear (A) and reflectron (B) modes of MALDI TOF mass analyzers.	37
1.2	Illustration of an ESI ion source in positive mode.	42
1.3	The structure of three commonly used matrices in MALDI MS.	47
1.4	A schematic of the MALDI MSI workflow.	53
1.5	Sublimation apparatus.	62
2.1	A simplified schematic demonstrating factors that influence AD development and progression modified from Anand et al. [1].	74
2.2	Amino acid sequence of pathogenic amyloid beta peptides 1-40 and 1-42.	76
2.3	Different stages of the A $\beta$ aggregation pathway.	79
3.1	ZP1609 dipeptide structure.	95
3.2	ZP1609 signal detection capabilities of SA (A), and DHB (B).	103
3.3	Effects of tissue washing protocols on resulting images acquired.	106
3.4	Extraction efficiency of ZP1609 using wet versus dry matrix application methods.	107
3.5	Extended tissue acidification.	109
3.6	Detection of IP injected ZP109.	111
3.7	MALDI MSI detection of ZP1609 in samples treated with preclinical trial conditions.	113
4.1	Mass spectra of oligomers prepared from A $\beta$ <sub>1-42</sub> (A-B) and A $\beta$ <sub>1-40</sub> (C-D).	129

<b>4.2</b>	Oligomerization of wild-type A $\beta$ <sub>1-40</sub> (A) was compared to scrambled A $\beta$ <sub>1-40</sub> (B), and mutations (Gln <sup>22</sup> ) A $\beta$ <sub>1-40</sub> (C).	132
<b>4.3</b>	Mass spectra of oligomerized A $\beta$ <sub>1-40</sub> after passing through 10 kDa (A) and 30 kDa (B) filters.	133
<b>4.4</b>	Oligomerized sample of A $\beta$ <sub>1-40</sub> diluted to 50 $\mu$ M.	135
<b>4.5</b>	Mass spectra of A $\beta$ <sub>1-40</sub> after treatment with four monomerization solutions: HFIP (A), HCO <sub>2</sub> H (B), TFA (C) and NH <sub>4</sub> OH (D).	138
<b>4.6</b>	Mass spectra of oligomerized A $\beta$ <sub>1-40</sub> prepared in two oligomerization solutions, PBS (blue) and F12 (green), and in water (red).	140
<b>4.7</b>	Rat cortical neuron cell death determined under the treatment of A $\beta$ monomers and oligomers.	143
<b>5.1</b>	In-vial binding efficiency of BcMag and Dynabead magnetic beads.	157
<b>5.2</b>	Effects of varying Dynabead concentrations applied per sample spot.	163
<b>5.3</b>	Evaluation of the optimal C18 Dynabeads concentration.	164
<b>5.4</b>	Assesment of Dynabead extraction capabilities with different concentrations of A $\beta$ <sub>1-42</sub> .	166
<b>5.5</b>	On Tissue Dynabead extraction capabilities for A $\beta$ <sub>1-42</sub> .	169
<b>5.6</b>	MALDI MSI of wildtype and transgenic rat brains injected with A $\beta$ <sub>1-40</sub> and A $\beta$ <sub>1-42</sub> .	173



## List of Equations

		<b>Page</b>
1.1	$R = \frac{M}{\Delta M}$	32
Eq. 1.2	$zeV = \frac{1}{2}mv^2$	35
Eq. 1.3	$v = \sqrt{\frac{2zeV}{m}}$	35
Eq. 1.4	$\frac{m}{z} = t^2 \left( \frac{2ev}{L^2} \right)$	35

## List of Symbols and Abbreviations

3D	Three-dimensional
$\alpha$	Alpha
$\beta$	Beta
$\Gamma$	gamma
$\lambda$	Wavelength
$\Delta M$	Peak width at 50% peak height
$\mu\text{g}$	Microgram ( $1 \mu\text{g} = 10^{-6} \text{g}$ )
$\mu\text{L}$	Microliter ( $1 \mu\text{L} = 10^{-6} \text{L}$ )
$\mu\text{m}$	Micrometer ( $1 \mu\text{m} = 10^{-6} \text{m}$ )
$\mu\text{M}$	Micromolar ( $1 \mu\text{M} = 10^{-6} \text{M}$ )
A	Alanine
AAP	Anti-arrhythmic peptide
A $\beta$	Amyloid beta
ACH	Amyloid cascade hypothesis
ACN	Acetonitrile
AD	Alzheimer's disease
AFM	Atomic force microscopy
Ala	Alanine
ANOVA	Analysis of variance
APOE	ApolipoproteinE
AP	Ammonium hydrogen phosphate
APP	Amyloid precursor protein
Arg	Arginine
Asn	Asparagine
Asp	Aspartic Acid
BBB	Blood brain barrier
C	Cysteine
CD	Circular dichroism
CHCA	$\alpha$ -cyano-4-hydroxycinnamic acid

CI	Chemical ionization
Cys	Cysteine
D	Aspartic Acid
Da	Dalton, 1 Da = 1 u (atomic mass standard)
DAN	1, 5 - diaminonaphthalene
DAPI	4'-6-diamidino-2-phenylindole
DC	Direct current
DE	Delayed extraction
DHAP	Dihydroxyacetone phosphate
DHB	2,5 dihydroxybenzoic acid
DMSO	Dimethyl sulfoxide
e	Electron volt, 1 e = 1.6 x 10 <sup>-19</sup> Joule
E	Glutamic Acid
E22Q	Modified version of Aβ <sub>1-40</sub> with the 22 <sup>nd</sup> residue replaced by Gln
EI	Electron ionization
EM	Electron multiplier
e/m	Charge-to-mass
ESI	Electrospray ionization
F	Phenylalanine
F12	Ham's F-12 nutrients mixture
FAB	Fast atom bombardment
FFPE	Formalin-fixed paraffin embedded
FRET	Fluorescence resonance energy transfer
FT-ICR	Fourier transform ion cyclotron resonance
g	grams
G	Glycine
Gln	Glutamine
Glu	Glutamic Acid
Gly	Glycine
H	Histidine
HABA	2 - (4 - hydroxyphenylazo)benzoic acid

HBSS	Hank's balanced salt solution
HDX	Hydrogen/deuterium exchange
HFIP	Hexafluoroisopropanol
His	Histidine
HPLC	High-performance liquid chromatography
HSD	Honest significant difference
I	Isoleucine
Ile	Isoleucine
IMS	Ion mobility spectrometry
IP	Intraperitoneally
ITO	Indium tin oxide
IV	Intravenously
K	Lysine
kDa	KiloDalton (1 kDa = $10^3$ Da)
kg	Kilogram (1 kg = $10^3$ g)
kHz	Kilohertz (1 kHz = $10^3$ Hz)
L	Leucine
LC	Liquid chromatography
Leu	Leucine
Lys	Lysine
M	Methionine
M <sup>+</sup>	Molecular ion
MALDI	Matrix assisted laser desorption ionization
MB	Magnetic bead
Met	Methionine
mg	Milligram (1 mg = $10^{-3}$ g)
min	Minute
mm	Millimeter (1 mm = $10^{-3}$ m)
mM	Millimolar (1 mM = $10^{-3}$ M)
MRI	Magnetic resonance imaging
MS	Mass spectrometry

MS/MS	Tandem mass spectrometry
MSI	Mass spectrometry imaging
MW	Molecular weight
MWCO	Molecular weight cut-off
m/z	Mass-to-charge ratio
n	Sample size
N	Asparagine;
Nd:YAG	Neodymium-doped yttrium aluminum garnet
NFTs	Neurofibrillary tangles
NGF	Nerve growth factor
nL	Nanoliter (1 nL = 10 <sup>-9</sup> L)
nm	Nanometer (1 nm = 10 <sup>-9</sup> m)
NMR	Nuclear magnetic resonance
NP	Normal phase
P	Proline
PBS	Phosphate buffered saline
PET	Positron emission tomography
Phe	Phenylalanine
pH	Potential of hydrogen
PI	Propidium iodide
PPI	Protein-protein interactions
ppm	Parts per million
Pro	Proline
PTMs	Post translational modifications
q	Net charge of an ion
Q	Glutamine; or Quadrupole
QIT	Quadrupole Ion Trap
R	Arginine; or Resolution
RF	Radio frequency
ROI	Region of interest
RP	Reverse phase

RPC	Reverse phase chromatography
rpm	Revolutions per minute
S	Serine
SA	Sinapinic acid
sAPP $\alpha$	Soluble amyloid precursor protein alpha
SDS	Sodium dodecyl sulfate
SDS-PAGE	Sodium dodecyl sulfate polyacrylamide gel electrophoresis
SEM	Standard error of the mean
Ser	Serine
S/N	Signal-to-noise ratio
SPE	Solid-phase extraction
SPR	Surface plasmon resonance
t	time
T	Threonine
TFA	Trifluoroacetic acid
THAP	2, 4, 6 - trihydroxyacetophenone
Thr	Threonine
tMCAO	Transient middle cerebral artery occlusion
TOF	Time-of-flight
TOF/TOF	Tandem time-of-flight
Trp	Tryptophan
Tyr	Tyrosine
UV	Ultraviolet
v	Velocity
V	Valine
Val	Valine
W	Tryptophan
Y	Tyrosine
z	Net charge of the ions
ZP123	Rotigaptide drug
ZP1609	Danegaptide drug

# **Chapter 1: Introduction of Mass Spectrometry in Protein and Peptide Analysis**

## 1.1 Overview of Protein Analysis

### *1.1.1 Amino Acid Building Blocks*

As building blocks of cellular systems, proteins play a critical role in the structure, function, and regulation of biological systems. They are comprised of 20 naturally occurring amino acid residues with molecular weights ranging from 57 – 186 Da. These residues group together to form polypeptide chains predetermined by the genetic code. As indicated in Table 1.1, amino acids can be classified as either polar, or nonpolar based on the side chain composition [1-3]. Having awareness of the polarity of each residue helps to understand the hydrophobicity of amino acids, and in turn, predict the resulting protein structure. However, there is controversy surrounding the level of hydrophobic properties each residue possesses. Variations exist because of the difference in methods used to assess the relative hydrophobicity of each amino acid residue [4-7]. The measure of hydrophobicity is often achieved through either examination of the 3D protein structure, or by looking at the physical properties of the sidechains and observing how the amino acid partitions in water versus nonpolar solvent environments. Differences in the results obtained occurs when two different methods are used. Since the former evaluates the amino acid as part of a polypeptide chain, while the latter looks at the free amino acid residues, the two methods yield different results for residues that possess levels of opposing properties. In addition to the differences in evaluation, hydrophobic properties of the 20 amino acid residues is a relative unit of measure. Alternative factors such as the surrounding environment also play a role in the hydrophobicity of the amino acid. The polarity and hydrophobic properties of



cysteine and tyrosine at times are a topic of controversy. Cysteine possesses an –SH group which makes it a polar amino acid residue, but when investigating the 3D structure of proteins, cysteine is often found embedded within the core of the protein leading to misinterpretation that it is hydrophobic. However, this behaviour can be a result of the residue's affinity to form disulfide bonds found in the core of the protein. Alternatively, tyrosine is an aromatic amino acid, and therefore should be considered nonpolar [2, 8]. Despite the aromatic ring, tyrosine also possesses an- OH group, and its contributions towards hydrogen bonding causes conflicting results when the level of hydrophobicity is assessed in different environments. For the purposes of the work described here, both cysteine and tyrosine will be regarded as a polar amino acid residues.

**Table 1.1** Amino acid residues are listed with both the 3- and 1- letter symbols associated with each. The polarity of each amino acid has been provided.

<b>Amino Acid</b>	<b>3-Letter Symbol</b>	<b>1-Letter Symbol</b>	<b>Polarity</b>
Alanine	Ala	A	Nonpolar
Arginine	Arg	R	Polar
Asparagine	Asn	N	Polar
Aspartic Acid	Asp	D	Polar
Cysteine	Cys	C	Polar
Glutamic Acid	Glu	E	Polar
Glutamine	Gln	Q	Polar
Glycine	Gly	G	Nonpolar
Histidine	His	H	Polar
Isoleucine	Ile	I	Nonpolar
Leucine	Leu	L	Nonpolar
Lysine	Lys	K	Polar
Methionine	Met	M	Nonpolar
Phenylalanine	Phe	F	Nonpolar
Proline	Pro	P	Nonpolar
Serine	Ser	S	Polar
Threonine	Thr	T	Polar
Tryptophan	Trp	W	Nonpolar
Tyrosine	Tyr	Y	Polar
Valine	Val	V	Nonpolar

### *1.1.2 Protein Structure*

Amino acids join together through a condensation reaction with the amino group of one amino acid, and the carboxyl group of the other. This reaction releases water, forming the backbone of polypeptide chains. This unique backbone has minimal intrinsic mobility due to the partial double bond characteristics it possesses [2, 9]. The  $\alpha$ -helical or  $\beta$  sheet secondary structure of a polypeptide chain is generated through intra- and inter-strand hydrogen bonding respectively. The  $\alpha$  helix conformation is developed when hydrogen bonding occurs between the carbonyl and the amino group of an amino acid four residues away in the polypeptide sequence [10]. The  $\beta$  sheet structure is generated when hydrogen bonding occurs between the NH and CO groups of amino acids in different polypeptide chains. The formation of  $\beta$  sheets can be in both anti-parallel or parallel orientations.

After formation of the secondary structure, these proteins then fold and bend to form the three dimensional tertiary structure. At this stage, structural formation is determined primarily from the amino acid sequence. However, the protein's environmental surroundings also play a key role in structural formation. Proteins will acquire the tertiary structure which provides the greatest stability, and in turn, the lowest energy state. In general, amino acids with hydrophobic side-chains will be buried within the protein structure, while the polar amino acids reside on the surface. In comparison to the secondary form, the tertiary structure of proteins appear to be irregular and unstructured. However, these three dimensional formations are developed and stabilized by the interactions between amino acid side-chains, and the hydrophobic backbone [11-12]. These interactions

include, hydrogen bonding, and the formation of salt or disulfide bridges. Protein quaternary structures then reflect the interaction between globular protein subunits which aggregate and develop into larger protein complexes.

### *1.1.3 Biological Functions & Interactions of Proteins*

Based on just 20 different amino acid building blocks, countless proteins that serve key roles in structure, function and transport for all biological systems are generated. They can be categorized as antibodies, assembly proteins, blood proteins, enzymes, hormones, membrane proteins, or nucleoproteins. In attempts to understand biological systems, a growing list of protein interactions continue to be uncovered year after year. The majority of protein interactions are identified as protein-protein interactions (PPI), but interactions also exist between protein-lipids (often involving membrane proteins), and proteins with carbohydrates.

Studying PPI can help researchers in furthering the understanding of protein function. The nature of the interaction differs depending on the protein affinity, composition, as well as whether the interaction is permanent or transient [13]. The key driving force in these interactions involve the protein concentration within a system, and the free energy of the complex in comparison to the energy of the protein in alternative states. PPI can be distinguished based on the structural and functional groups of the proteins involved, and the physical characteristics of the interaction. Complexes are considered either obligate, or non-obligate [13-14]. Where the former does not exist *in vivo* as stable structures, and the

latter can be found *in vivo* as stable, independent complexes. Alternatively, protein interactions are also classified as transient or permanent based on the lifetime of the resulting complex. Aside from PPI, lipid-protein interactions encompass another division that is integral in the functionality of biological systems as a whole. Lipids play a key role in the unique functionality, and physical properties of cellular membranes [15-17]. This type of interaction can be characterized as integral membrane proteins, peripheral membrane proteins, and soluble protein interactions [18-21].

## 1.2 Protein Analysis

Understanding the physical and chemical properties of proteins helps to elucidate biological systems and processes. This investigation involves identifying the molecular weight of proteins, studying the amino acid sequence, analyzing the 3D structure, understanding protein interactions, and to obtain location information for the presence of proteins within a biological tissue sample. Since protein functions are highly dependent on their structure, the study of intact proteins has become a primary target for many researchers [22-24]. With advancements in analytical techniques, researchers are now able to study intact protein structures, expression, and interactions. This information can aid the understanding of disease pathology to facilitate the development of therapeutics, detection of disease development, and possible preventative measures.

Continuous development in analytical techniques provided additional platforms for the investigation of protein characteristics. X-ray crystallography, nuclear magnetic resonance (NMR), and electron microscopy are popular methods for the analysis of the 3D structure

of proteins. Alternatively, chemical crosslinking, fluorescence resonance energy transfer (FRET), and protein arrays are often used for studying protein interactions [25-31]. Proteomic research is an exponentially growing field of study, continuously expanding based on the development of available techniques. A large area of interest resides in protein identification within biological systems through the separation and detection of proteins based on molecular weight and sequencing. Sodium dodecyl sulfate polyacrylamide gel electrophoresis (SDS-PAGE) and mass spectrometry are commonly used techniques in the separation and identification of proteins. SDS-PAGE is capable of isolating target proteins or peptides using electrophoresis. Application of SDS denatures the protein sample while providing an environment with a negative net charge. The proteins within the mixture then separate as they travel towards the anode. The negative environment disrupts the complex structures of proteins so the rate at which proteins travel is predominantly based on the molecular mass of the polypeptide.

SDS-PAGE is an effective technique in identifying proteins for targeted approaches, however mass spectrometry (MS) provides a method to perform targeted and untargeted analysis of a wide range of molecules. This technique only requires microliter amounts of sample for analysis, and does not need the addition of dyes or antibodies for detection. Conventional ionization techniques, chemical ionization (CI), electron ionization (EI), and fast atom bombardment (FAB) limited MS to small, thermostable compounds. These ionization techniques resulted in severe fragmentation of relatively larger molecules which generated complex spectra that is difficult to interpret. In the late 1980s, development of two ionization techniques, electrospray ionization (ESI) and matrix-assisted laser desorption/ionization (MALDI) made MS available for analysis of larger molecules such

as proteins [22]. These two ionization techniques reduces the fragmentation of larger molecules, and therefore retains the original, intact molecule during the ionization process making it possible to directly study larger peptides and even intact proteins.

The development of imaging techniques provided a methodology to obtain location information for target proteins. Traditionally, staining and labelling techniques such as, immunohistochemistry (IHC), magnetic resonance imaging (MRI), fluorescence microscopy, and positron emission tomography (PET) were used for targeted identification of proteins within biological systems. Although effective, these techniques are dependent on the successful staining or labelling of target molecules, and therefore successful localization of these proteins are directly affected by the specificity of the stains and labels used.

Introduction of matrix-assisted laser desorption/ionization mass spectrometry imaging (MALDI MSI) presented a powerful technique which provides two dimensional information regarding target samples. This platform is not only capable of the characterization and identification of proteins and complex molecules, but it also possesses the ability to map out protein expression within intact tissue sections. Similar to standard MALDI MS analysis, information is extracted as the laser hits the matrix coated sample. As the laser moves along the tissue section, each ablation spot allows for information to be extracted and acts as “pixels” for the image generated. This method of analysis provides information regarding protein expression within a biological sample, which would typically be lost in standard protein extraction, purification or separation protocols.

## 1.3 Theory and Instrumentation for Mass Spectrometry

### *1.3.1 Instrumentation for Mass Spectrometry*

Mass spectrometry has come a long way since the development of the first instrument by Sir J. J. Thomson [32-33]. As the instrument matured, its capabilities continues to expand beyond a tool for physicists. From initially detecting the charge-to-mass ( $e/m$ ) for particles such as electrons, to the ongoing expansion of applications in all fields of science. Overall, three processes occur in mass spectrometers, ion generation, separation, and detection. These three processes are achieved using an ion source, mass analyzer, and the ion detector respectively.

The ion source is where sample ions are generated. A variety of ionization sources are available, with the most prominent ones in proteomic research being electrospray ionization (ESI), and matrix-assisted laser desorption/ionization (MALDI). These “soft” ionization systems produce ions with minimal fragmentation, therefore providing intact gaseous sample ions for analysis of larger biomolecules. The ions generated are then transferred to the mass analyzer, where they are separated based on their mass-to-charge ratios ( $m/z$ ). The five most commonly use mass analyzers are, time-of-flight (TOF), quadrupole (Q), quadrupole ion trap (QIT), orbitraps, and fourier-transform ion cyclotron resonance (FT-ICR) [34]. Analyzer selection is decided by the necessary sensitivity, resolution, mass accuracy, and mass range to encompass specifications required for the target analysis.



In mass spectrometry, sensitivity refers to the ratio of the maximum number of ions recorded at a given  $m/z$  (of  $M$ ) to the signal of the background at an adjacent  $m/z$  (of  $M + 1$ ) [35]. It takes into account the relationship between maximum useable signals acquired, versus the minimum useable signal (detection limit). Although detection sensitivity of the mass analyzer can provide a relative indicator of the maximum discernable concentrations of analyte within a sample, detection of low abundance components within a sample is also dependent on other factors such as the instrument's resolving power. A mass spectrometer's resolving power is the ability of the mass analyzer to effectively separate, define, and generate two distinct signals from components within a mixture with minor differences in  $m/z$ . Simply put, the narrower the peak, the higher the resolution. The resolution ( $R$ ) for a single peak can be measured with,

$$R = \frac{M}{\Delta M} \quad (\text{Eq. 1.1})$$

Where  $M$  is the peak position ( $m/z$ ), and  $\Delta M$  is the width of the peak at the position of 50% peak height [36]. Resolving power becomes increasingly important when performing untargeted analysis, and when characterizing molecules with near identical masses. Mass accuracy in MS refers to the error in mass measurement. It evaluates the difference between measured, and actual  $m/z$  values of the target analyte. This measurement is usually provided in parts per million (ppm), and is calculated by dividing the difference of observed and true  $m/z$  values, by the true  $m/z$  of the analyte. The mass accuracy of an analyzer is directly correlated with its resolving power. Therefore, the higher the mass resolution, the greater

the mass accuracy. The mass range refers to the range of  $m/z$  for which the analyzer can detect ions with sufficient resolution to differentiate between adjacent peaks. For many analyzers, increasing the mass range results in compromise with the signal detection of lower  $m/z$  ions, therefore the upper limit is a relative maximum, at which point the instrument performance becomes severely compromised.

Different analyzers possess different mass range capabilities, and this is often the limiting factor when deciding upon a suitable instrument for analysis. For quadrupole mass analyzers,  $m/z$  selection is achieved through variations in the magnitude of radio frequency (RF), and the direct current (DC) applied to the four electrode rods [37-38]. The application of RF and DC determines the trajectory of the ions passing through, allowing for ion mass selection or identification. Ions with unstable trajectories are eventually neutralized through collision with the quadrupole electrode rods. These analyzers provide good reproducibility, but is limited with the resolution obtained. In conjunction with an ion trap, QIT mass analyzers possess a similar mechanism for  $m/z$  selection, however instead of the stable ion being selected, mass selection for QIT is achieved through ion instability [35, 39]. In QIT mass analyzers, a three dimensional electric field is applied, which effectively traps the ions. As the RF increases, ions with higher  $m/z$  are ejected. The manipulation of DC and RF voltages allow for extensive MS/MS analysis of high resolution and sensitivity. Orbitraps contains a spindle-like inner electrode and a barrel-like outer electrode. As the voltage applied increases, ions are introduced into the trap. The ions oscillate along the horizontal axis of the inner electrode and  $m/z$  selection is achieved as ions of differing  $m/z$  reach the desired orbit within the trap. FT-ICR analyzers operate based on the same mechanism as QIT by storing ions and selecting  $m/z$  through manipulation of voltages

applied [39]. However, the ions travel in a circular path within a magnetic field. The ion mass can then be determined by detection of the cyclotron frequency for the ion's circular motion. Among the available mass analyzers, FT-ICR provides the highest level of mass resolution, but possesses a limited mass range. For TOF mass analyzers, the ion mass is determined by measuring the amount of time it takes to travel through a flight tube. TOF mass analyzers are extremely fast, and provide a high mass range. Therefore, TOF mass analyzers are very desirable for targeted and untargeted protein analysis.

#### *1.3.1.1 Principles of Time-Of-Flight Mass Analyzers*

Decades after J. J. Thomson constructed the first spectrometer, time-of-flight (TOF) mass analyzers were introduced [33, 40]. TOF mass analyzers were conceptualized in 1946, however the first commercial TOF analyzer was not introduced until the 1950s. The mass analyzer promoted was based on designs by William Wiley, and I. H. McLaren. At this time, the attainable resolution was so poor that the technique was not viable for MS applications. Improvements in the resolution of TOF analyzers wasn't possible until the development of reflectron by Boris Mamyrin. From then on, TOF analyzers continued to improve in resolution, and developed into an indispensable tool for mass spectrometry.

TOF analyzers separate ions based on their mass, and measures the mass-dependent time required for the ions to travel through the drift tube to the detector. To start, ions generated in the "plume" are released from the source in sets, these ions with mass,  $m$ , and a charge of  $q = ze$ , are collected in an acceleration region until max capacity is reached [34, 41].

Once full, a difference of potential applied between the sample plate and an extraction grid accelerates the ions towards the drift tube. Since the kinetic energy acquired by each ion is equal, separation of the ions result solely from the ion mass. High mass ions will possess a lower velocity in comparison to smaller mass ions. The ion velocity is then recorded based on the amount of time it takes for the ions to reach the detector. With the known length of the flight tube, and the measured ion velocity, mass-to-charge can then be calculated with the equation,

$$zeV = \frac{1}{2}mv^2 \quad (\text{Eq. 1.2})$$

$$v = \sqrt{\frac{2zeV}{m}} \quad (\text{Eq. 1.3})$$

$$\frac{m}{z} = t^2 \left( \frac{2ev}{L^2} \right) \quad (\text{Eq. 1.4})$$

Here,  $m/z$  represents the mass-to-charge ratio of ions,  $t$  and  $v$  represent the time required for ions to reach the detector, and the velocity of the ions respectively [34]. Lastly,  $L$  is the length of the flight tube in which the ions travel through. From the equations above, ions with different  $m/z$  values will travel at different velocities, and therefore reach the detector at different times (Eq. 1.4). With velocity in consideration, the ions can either be positively, or negatively charged depending on the voltage polarity used.

The mode of analysis outlined above directly measures the amount of time required for ions to travel through the flight tube and reach the detector. With TOF mass analyzers, this mode is categorized as the linear mode of analysis. However, when ions are formed in the desorption plume, differences in initial kinetic energies exist. These differences result in a corresponding shift of arrival times at the detector for ions of the same mass which contributes to a decrease in mass resolution. In order to compensate for these shifts, a delayed extraction (DE) technique can be applied [42]. This delay permits the ions generated within the plume to expand into a field-free region in the source. The electric field applied remains consistent between the sample plate and the extraction grid. As a result, ions with higher initial kinetic energy will move further away from the sample plate in comparison to those with lower kinetic energies. After the delay, the ions are accelerated through the flight tube, where the high energy ions will experience less of a potential difference than the low energy ions. This allows ions of the same mass to eventually reach identical velocities as they travel towards the detector. Alternatively, the reflectron mode can be used to reduce effects of variations among initial energy distribution for ions generated. In reflectron mode, a series of parallel mirrors with a voltage gradient are used to slow, and turn ions onto a second flight path towards the detector [36]. This allows ions with greater kinetic energy to penetrate deeper and travel a further distance prior to redirecting towards the detector (Figure 1.1). As a result, ions of the same mass with varying initial kinetic energy will arrive at the detector simultaneously, hence improving the mass resolution obtained.

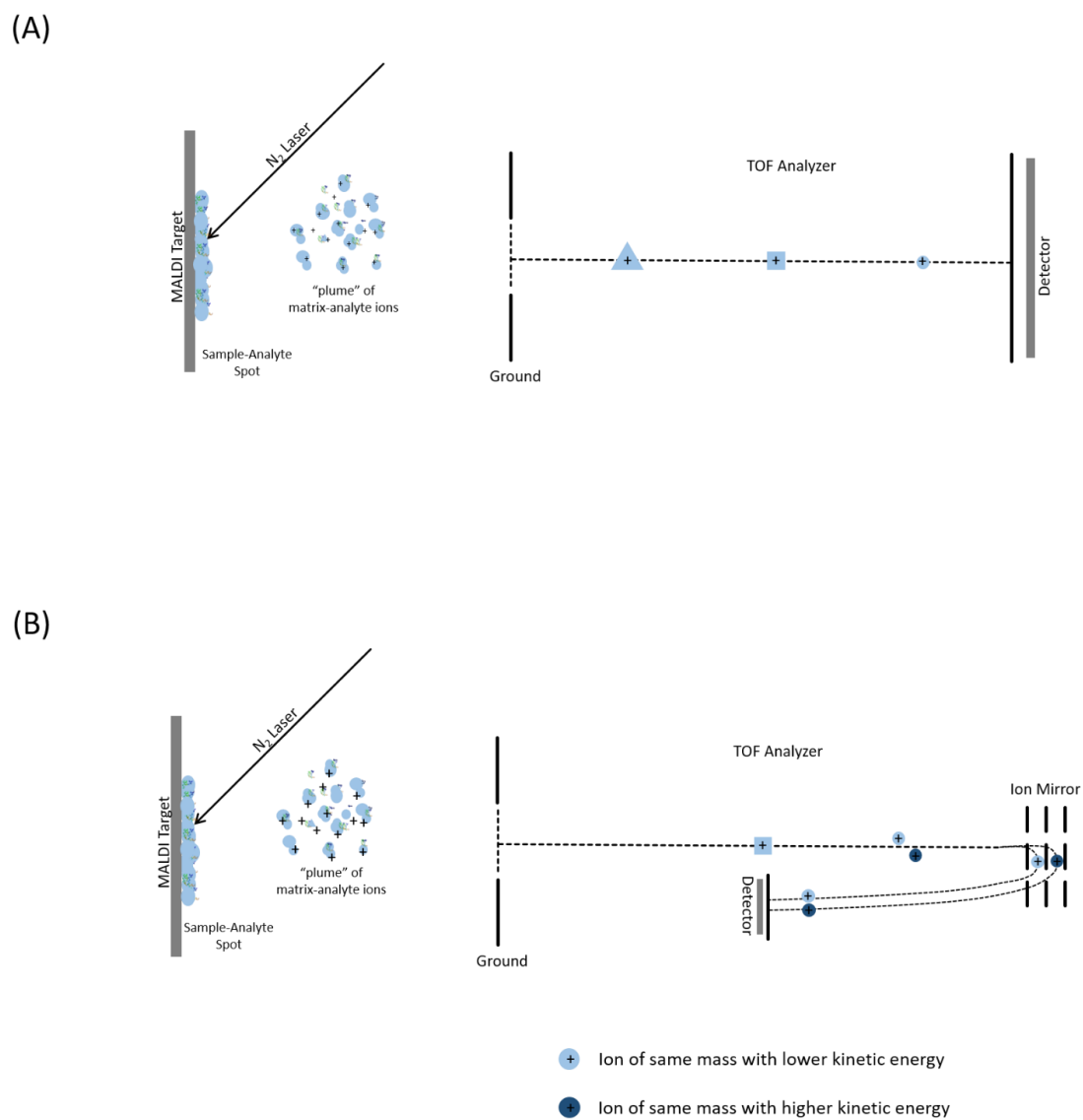


**Figure 1.1** Schematics for both linear (A) and reflectron (B) modes of MALDI TOF mass analyzers.

### *1.3.1.2 Applications of TOF Analyzer*

TOF analyzers are now one of the most commonly used mass analyzers for MALDI MS. In theory, TOF possesses an unlimited mass range since ion trapping is not applied, and linear flight paths are used. However, in practice the detector restricts detection efficiencies to within a few hundred kDa mass range. Even with the confines of the detector, TOF analyzers provide a high practical mass range in comparison to other available mass analyzers [36]. TOF also has high levels of detection sensitivity, and remains the fastest MS analyzer available. This analyzer possesses good levels of mass accuracy, and its construction is comparatively inexpensive to other analyzers.

The high mass range TOF analyzers are capable of, in conjunction with the high signal resolution, sensitivity, and mass accuracy, these analyzers provide the ideal parameters for protein analysis. When used in MALDI MS systems, the soft ionization method provides data regarding the molecular mass of polypeptides, while the MS/MS capabilities offer an additional dimension of analysis. Upon selection of a precursor ion, the amino acid sequence, and post translational modifications of protein samples can be identified. However, advantages of TOF analyzers are strongly limited by the capabilities of the detector employed.

### *1.3.1.3 Detectors*

All mass spectrometers aside from orbitraps and fourier-transform ion cyclotron resonance (analyzer acts as a detector as well) requires a detector [43]. The detectors record the ion intensities of each  $m/z$  value, and records the data electronically in the form of a mass spectrum [44]. Depending on the type of detector used, the resulting signals are produced by either generating secondary electrons, which are then further amplified, or by inducing a current using a moving charge [36]. Commonly used detectors for MS include, Faraday cup, electron multiplier (EM), and photomultiplier (or scintillation counter). The role of the detector is to be able to identify the abundance of ions present per  $m/z$ . The information obtained is then converted for computer based data storage, and processing in order to convey the data in the form of a spectra [45]. With continued development in the realm of ionization and separation for MS analysis, the demand for advancements in detection technology has become more critical. Although improvements in existing detection capabilities have been observed, these changes have been minimal in comparison to the developments made in the technology for mass analyzers. Ideally, MS detectors need to be consistent with ion-detection efficiency, possess minimal to no noise, capable of simultaneous detection of multiple ions, possesses a wide mass and dynamic range, short recovery time, and a high saturation level [44]. Ion detection efficiency, and level of noise present for detectors are limiting factors in obtaining high mass accuracy and sensitivity in MS measurements. The level of noise present can be a result of multiple sources, noise can be generated within the detector itself, or from supporting electronic sources. Techniques capable of minimizing effects of noise are, signal filtering, and time averaging. Although,



no single detector stands superior in all characteristics, choice of detector employed is determined by the needs of the analyzer. Detector selection for TOF mass analyzers prioritize a broad mass range, mass accuracy, minimal recovery time, and capabilities of simultaneous ion detection. Due to rapid operations of TOF mass analyzers, detectors used must be capable of simultaneous detection of multiple ions, and a short recovery time.

### *1.3.2 Soft Ionization Methods*

#### *1.3.2.1 Electrospray Ionization (ESI)*

In response to the rising demand of biological applications for mass spectrometry, “soft” ionization methods were developed. Electrospray ionization (ESI) was first conceptualized in the 1960s by Malcolm Dole, but it wasn’t until 20 years later that ESI was first applied for biomolecule analysis by John Fenn [33]. In ESI, there are three major steps in order to generate gas-phase ions, solvent introduction, solvent evaporation, and finally development of charged gaseous ions [46]. ESI is an atmospheric technique where sample solutions flow continuously (nL / min to  $\mu\text{L}/\text{min}$ ) through a metal capillary needle held at an electric potential [46-50]. As an electric field is imposed on to the liquid sample, an enrichment of like charged ions occur near the cone. This potential difference between the capillary and the surrounding environment causes a dispersion of charged sample droplets in the form of a fine mist. The droplets then travel downfield towards the opposing electrode. During this process, exposure to the inert gas in the environment promotes solvent evaporation. As the solvent evaporates, the growing charge density results in an

increase in repulsion between the charges. The buildup of repulsion is eventually enough to overcome surface tension of the droplet, and coulomb fission occurs. This process continues with the parent droplets leading to secondary fissions, which eventually generates charged gas-phase ions. These ions are then introduced into the mass analyzer for separation and detection.

ESI generally produces multiply charged ions, therefore it is able to enhance the capabilities of mass spectrometers with limited mass range to be applicable in the analysis of larger analytes. However, in order for successful detection of larger molecules, the instrument must possess high resolving powers to differentiate between peaks of multiply charged ions. ESI MS has minimal tolerance for contaminants such as salts or detergents which can cause adduct formation with proteins or compete with target analytes for ionization [46]. Therefore, ESI MS is typically coupled with on-line liquid chromatography (LC) to separate components within a complex mixture prior to MS analysis.

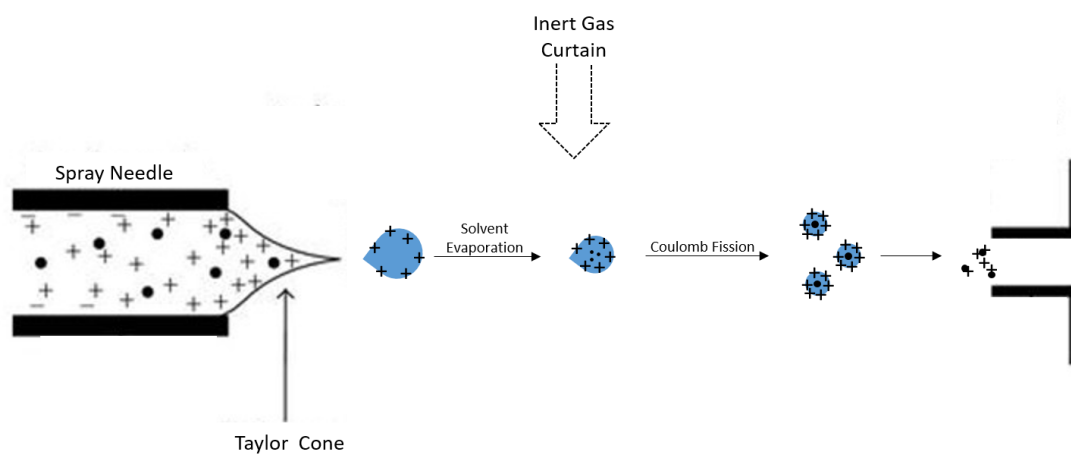


**Figure 1.2** Illustration of an ESI ion source in positive mode. An electric field is imposed on the sample liquid, resulting in a build-up of positive ions near the cone. The potential difference between the capillary and the environment results in a dispersion of positively charged sample liquid in the form of a mist. As the solvent evaporates, the charge repulsion within each droplet builds up and eventually causes coulomb fission to occur.

### *1.3.2.2 Matrix-Assisted Laser Desorption/Ionization (MALDI)*

Matrix-assisted laser desorption/ionization (MALDI) was first introduced by Franz Hillenkamp and Michael Karas in 1988 [36]. Over the past 30 years, MALDI has developed into a technique that is applicable to various scientific fields, including chemistry, biochemistry, biology, and even in clinical settings. While ESI converts liquid phase analytes to gas phase ions for analysis, MALDI converts solid phase analytes to gas ions. This technique generates primarily singly charged molecules, and has a higher tolerance against contaminants in comparison to ESI. This makes MALDI MS a valuable tool for untargeted research of complex biological systems.

In the MALDI MS process, analyte molecules are embedded in the crystalline structure of a small organic compound called the matrix. This mixture is then deposited onto a MALDI target plate. Once dried, the sample is introduced into the mass spectrometer, where the sample-matrix mixture is irradiated by a UV laser pulse (typically of wavelengths 337 nm and 355 nm). The laser causes heat production at the target plate, resulting in localized sublimation and ultimately ionization of the sample-matrix mixture releasing the molecules into the gas phase [51]. Both ions and neutral molecules are generated from this process, but only the ions are accelerated by the electric field towards the analyzer for separation followed by detection.

MALDI matrix selection is extremely important in order for successful detection of target analytes. Although guidelines are available for the most common matrices, definitive

selection of a suitable matrix is still a process of trial-and-error as a result of the uncertainties with the mechanism of the ionization process. Ionization of target samples with MALDI is a two part process, first the matrix must be ionized, and this is followed by an ion-molecule reaction to generate charged analyte ions [36, 52-53]. Several models have been proposed in attempts to elucidate the phenomenon, but it is highly unlikely to generate a model that can encompass the range of parameters that may affect the ionization environment. Among the proposed mechanisms, the most widely accepted hypothesis involves a gas-phase transfer of protons from matrix to analyte. In this model, matrix ions are generated in the primary ion formation, resulting in an expanding matrix “plume”. A secondary ionization then occurs as a proton transfer takes place between the matrix and analyte thereby desorbing and ionizing the analyte molecules [54].

Since its conception, MALDI MS has become a well established technique in the analysis of a wide range of samples, including proteins, peptides, oligonucleotides, polysaccharides, lipids, synthetic polymers, and inorganics. Among its applications, MALDI MS has been most prominent in the analysis of peptides and proteins since they have a much higher proton affinity ( $10^{-3} - 10^{-4}$ ) in comparison to analytes like carbohydrates ( $10^{-7} - 10^{-8}$ ) [55-59].

## 1.4 Application of MALDI Mass Spectrometry

### *1.4.1 Role of MALDI Matrices*

Overall, there is a general consensus in the significance of MALDI matrices in the entire ionization process, however controversy exists in the ionization mechanism. A suitable mechanism should be able to explain the presence and abundance of all the ions generated, but so far none of the proposed mechanisms are capable. It is also extremely difficult to generate one hypothesis which can encompass the range of experimental and instrumental conditions which may affect the ionization of the matrix-analyte mixture. The controversy primarily surrounds the initial ionization of the matrix molecule. However, there are higher levels of acceptance regarding the proposed mechanism in which secondary ionization generates charged analyte ions. During this secondary ionization process, proton transfer occurs between the matrix and the analyte [51, 53]. The matrix acts as both a proton donor and acceptor facilitating the generation of ions in both positive and negative modes, respectively. During this process, energy resulting from this transfer is also received by the analyte. The level of energy that is transferred directly influences the degree of in source fragmentation that occurs [60]. Different matrices transfer different degrees of energy during this process, matrices that provide a greater energy transfer are considered “hot” matrices, while lesser energy transfer indicates the matrix is “cold” [42]. The matrix also plays a protective role in shielding the analyte from the initial laser irradiation, and therefore minimizes undesirable fragmentation making MALDI a “soft” method of ionization.

### *1.4.2 MALDI Matrices and Deposition Methods*

Several criteria must be met for MALDI matrices to effectively ionize the target samples. Most commonly used matrices are solid, organic acids. However, continuous investigation into effective, novel materials have shown success in use of liquid matrices, and solid micro/nano particles. Matrices must also be readily soluble in commonly used sample preparatory solvents (eg. acetonitrile, ethanol, methanol etc.), relatively stable in a vacuum environment, provide a homogenous matrix-analyte deposit, and possesses strong UV absorbing capabilities at the laser wavelength.

The three most commonly used matrices are, 2, 5-dihydroxybenzoic acid (DHB),  $\alpha$ -cyano-4-hydroxycinnamic acid (CHCA), and sinapinic acid (SA). The latter two are predominantly used for peptide and protein analysis respectively [61]. The structures of each have been shown in Figure 1.3. DHB has a molecular weight of 154.12 g/mol, and it is capable of absorbing UV wavelengths of 266 nm, 337 nm, and 355 nm. Among the three standard matrices, DHB produces less background signals from matrix clusters. Therefore, this matrix is suitable for analysis of the lower  $m/z$  range, where signals from matrix clusters are often observed. DHB is considered a “cold” matrix, therefore minimal loss of neutral groups attached to the protein backbone during the ionization process occurs [62]. As a result, DHB is commonly used for the study of proteins with post translational modifications (PTMs), phosphopeptides, and glycoproteins.

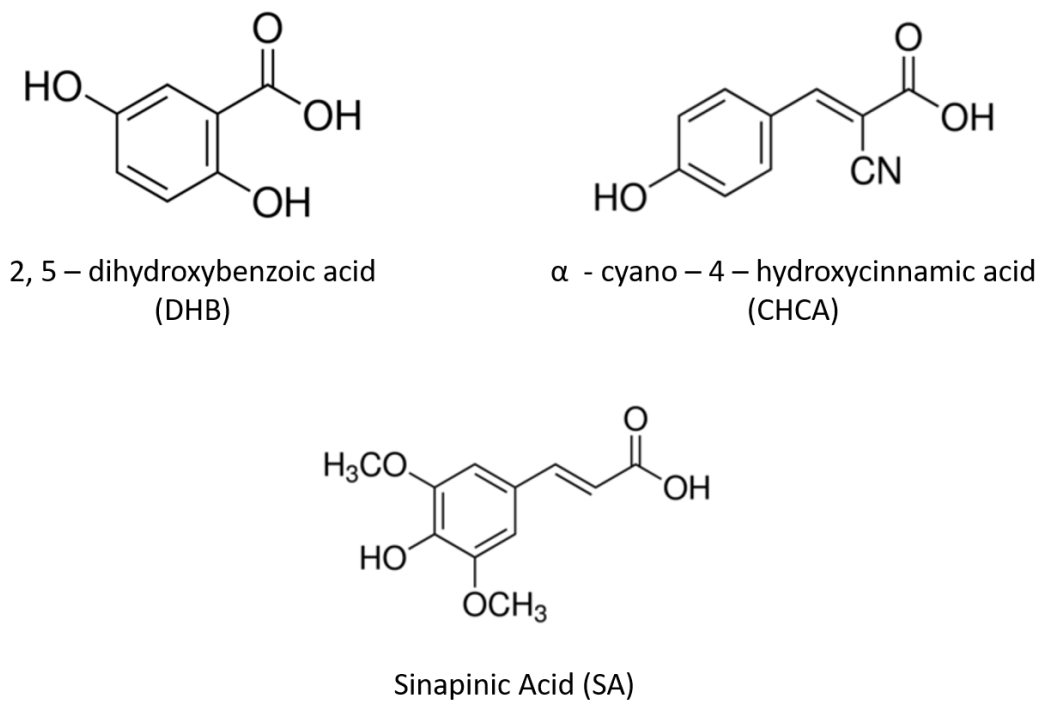


**Figure 1.3** The structure of three commonly used matrices in MALDI MS have been shown. All three matrices are small, organic acids consisting of an aromatic ring. Each matrix possesses UV absorbing capabilities in the 337 nm, and 355 nm wavelengths.



CHCA has a molecular weight of 188.16 g/mol, and it is widely used to facilitate ionization of peptides or small proteins with a molecular mass of < 10,000 Da. CHCA matrix generates a homogenous matrix-analyte deposition, which contributes to a high shot-to-shot reproducibility making it very effective in peptide mass fingerprinting. This matrix absorbs UV at both 337 nm and 355 nm wavelengths, and is readily soluble in polar solvents. Successful application of CHCA has also been reported for lipid and nucleotide analysis, but it is important to note that this matrix generates numerous peaks within the 100 - 400 m/z region . CHCA is also effective in the detection of low concentration protein digests using MALDI-TOF MS.

SA has a molecular weight of 224.21 g/mol, and is mostly used in the positive mode of analysis. Like DHB, it is considered a “cold” matrix, and capable of absorbing UV wavelengths of 266 nm, 337 nm, and 355 nm. SA can be applied to peptide analysis, but generally it excels in the detection of intact proteins because of the lesser degree of in-source fragmentation observed [63]. Continuous development of potential MALDI matrices have generate several alternative compounds which have shown to be effective in facilitating ionization in MALDI MS. These compounds, dihydroxyacetone phosphate (DHAP), 1, 5 – diaminonaphthalene (DAN), 2, 4, 6 – trihydroxyacetophenone (THAP), and 2 – (4 – hydroxyphenylazo)benzoic acid (HABA) along with the primary analytes they target have been listed in Table 1.2.

**Table 1.2** Alternative matrices developed for MALDI MS analysis, and the target analyte of interest each matrix is most successfully used for have been listed. Unfortunately, as a result of the uncertainties with the ionization mechanism, these are all simply guidelines when choosing a matrices for experiments. The guidelines help to narrow down the selection, however trial-and-error is required to determine the optimal selection for the target analyte.

	<b>DHAP</b>	<b>DAN</b>	<b>THAP</b>	<b>HABA</b>
<b>Glycoproteins</b>			X	X
<b>Complex Protein Profiling</b>	X			
<b>Gangliosides</b>		X		
<b>Oligonucleotides</b>			X	
<b>Glycolipids</b>				X
<b>Synthetic Polymers</b>				X

Sample preparation methods are another factor that greatly effects signal detection. Standard MALDI MS samples utilize the dried-droplet method that was first introduced by Hillenkamp and Karas. To facilitate co-crystallization, matrix and samples solutions are first premixed in a 1:1 ratio. This mixture is then spotted (0.5  $\mu\text{L}$  – 1  $\mu\text{L}$ ) onto a MALDI target plate. Once dried, the sample plate can be inserted into the vacuum system for analysis. Alternatively, two-layer, three-layer, and sandwich deposition methods are also available. Many variations of the first two layered techniques exists. Generally, it involves spotting the matrix, analyte, or matrix-analyte mixture in succession. Sandwich methods normally involve the sample solution to be “sandwiched” between two layers of matrix deposits. Overall, matrix molecules must be present in excess for efficient ionization to occur.

## **1.5 Introduction of MALDI Mass Spectrometry Imaging (MALDI MSI)**

### *1.5.1 Theory of MALDI MSI*

#### *1.5.1.1 Ionization of Analytes from Intact Tissue Sections*

Three ionization techniques used in MSI analysis of intact tissue samples are secondary ion mass spectrometry (SIMS), desorption electrospray ionization (DESI), and MALDI. SIMS utilizes an ion beam directed at the sample surface in order to induce the release of secondary analyte ions for analysis. Although this technique provides images of the

greatest spatial resolution, it is a hard ionization method and therefore mostly used for analytes in the lower mass range (<1000 Da) [64]. Alternatively, DESI was introduced by Dr. Graham Cooks' research group as a soft ionization method capable of applications within atmospheric conditions [65]. DESI was developed based on the principles of ESI and desorption ionization techniques. Ionization occurs as charged droplets are directly applied onto the sample surface. The charged droplets coat the sample allowing for analyte extraction. Continuous spray application results in momentum transfer from droplet collisions and subsequently desorbs analyte ions from the sample surface towards the mass spectrometer. Development of DESI provides an ionization technique for MSI analysis of small molecules, lipids, and peptides (< 2000 Da) [66-67].

Development of MALDI MSI by Dr. Richard Caprioli's research group provided an alternative soft ionization method for MSI analysis. The molecular specificity and wide mass range of MALDI-TOF MS has made this technique a powerful tool for imaging intact biological samples [68-69]. In comparison to the aforementioned ionization methods for MSI, MALDI provides the greatest applicable mass range making this technique most suitable for simultaneous MSI analysis of proteins and peptides. MALDI MSI uses fixed UV laser pulses to extract analyte information from matrix coated tissue sections. This method of analysis is non-destructive, the ionization process ablates only the matrix layer, leaving the underlying tissue intact for alternative forms of analysis post imaging. Due to the complexity of the tissue surface, matrix selection becomes increasingly important to facilitate the ionization of desired components within the tissue section, while minimizing undesirable signal detection from the tissue background or matrix. Parameters such as  $m/z$  range, raster size, laser intensity, shots/spot, and region of interest (ROI) must be optimized

for each sample. Once determined, laser pulses ablate each spot as it travels throughout the designated ROI. These ablations generate analyte ions per spot. The data is then collected, and processed to represent each pixel within an image of the ROI. A general schematic has been provided in Figure 1.4.

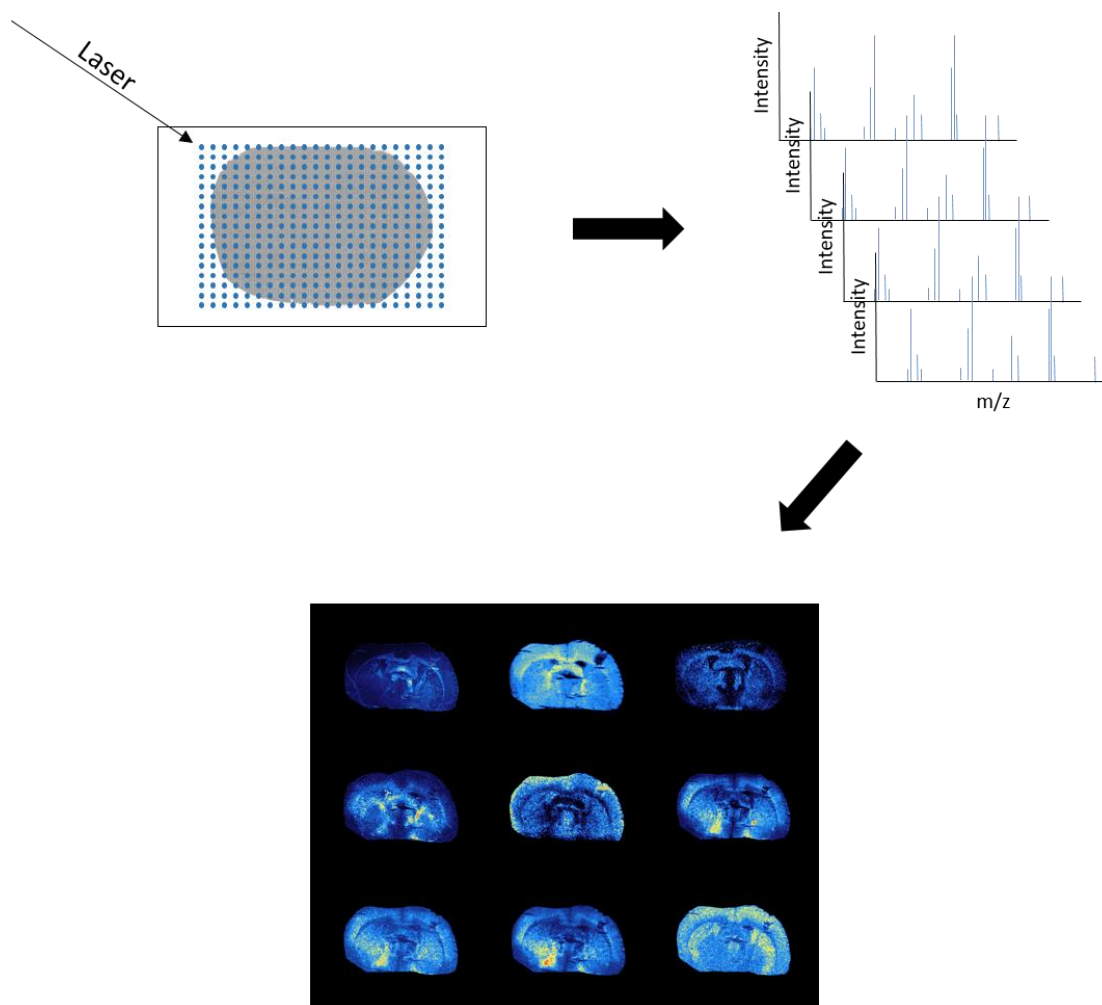


**Figure 1.4** A schematic of the MALDI MSI workflow. Once the MALDI MSI parameters are selected, the laser moves along the ROI ablating spot after spot. Information is then collected for the molecules present within each ablated spot. This information can then be collectively used to generate a tissue image.

### *1.5.1.2 Signal Detection Sensitivity versus Image Spatial Resolution*

In MALDI-TOF MSI analysis, both sensitivity and spatial resolution contribute significantly to the quality of the image generated. Detection sensitivity measures the instrument's ability to detect the lowest abundance analyte within a sample, while spatial resolution describes the ability to resolve two peaks of similar  $m/z$  values [70]. The measurement of sensitivity is directly related to the detection limit of the technique, in presence of comparable S/N, the greater the detection sensitivity the lower the detection limit. Therefore, when analyzing proteins and peptides, high levels of sensitivity are desired in order to overcome issues of lipid abundance within tissue sections. However, the degree of detection sensitivity acquired is inversely correlated with the level of resolution attained. The ability to clearly identify two components of a mixture with similar  $m/z$  is extremely beneficial, especially when analyzing biological samples.

To improve detection sensitivity, a larger number of ions must be sent to the detector in a shorter time frame. This helps to enhance the signal-to-noise (S/N) ratio, and increase the number of ions detected [36]. Although this may aid to improve sensitivity of detection, increasing the volume of space for which ions may travel through to the detector, negatively impacts the resolving power of the instrument. In order to improve the resolving capabilities, the spatial distribution of the ions must be accounted for. A greater volume of space contains more ions, but ions of the same  $m/z$  with variations in starting energy and spatial distribution will contribute to differences in arrival times. This in turn decreases resolution attained. In extreme cases where parameters are greatly optimized for sensitivity,

the extremely low resolving capabilities will lead to a decrease in S/N as well. Therefore, in all experiments, a compromise must be made between sensitivity and resolution in order to find the optimal ratio to provide the necessary information that will answer the question at hand.

## *1.5.2 Applications of MALDI MSI*

### *1.5.2.1 Tissue Collection and Storage*

Appropriate tissue handling and treatment techniques are crucial in obtaining successful MALDI MSI results. This involves identifying suitable tissue extraction, sectioning, and sample preparation techniques. These techniques will differ depending on the sample, and question under analysis. Therefore, an evaluation is required prior to analysis of every new sample. Two tissue collection techniques are available for MALDI MSI, fresh frozen and formalin-fixed paraffin embedded (FFPE) tissue.

With fresh frozen tissue, the greatest issue resides in the ability to homogeneously freeze the tissue section immediately after extraction to maintain integrity and shape. Immediate freezing helps to minimize protein degradation, which occurs immediately post-mortem through enzymatic proteolysis. Homogeneous freezing can be accomplished through use of liquid nitrogen, or dry ice. A homogeneous freeze minimizes development of ice crystals within the tissue section, these crystals can then increase chances of tissue fractures upon sectioning [71]. The tissue can be lightly wrapped with aluminum foil prior to submersion



in liquid nitrogen, or buried in dry ice to promote a “gentle” freeze application. This can help to prevent tissue deformities, and the formation of fractures during the freezing process. Once retrieved, the tissue needs to be stored in  $-80\text{ }^{\circ}\text{C}$  to minimize degradation and chances of ice crystal formation.

Alternatively, recent developments in MALDI MSI allow for the analysis of FFPE tissue. When tissues are treated with formalin, inter- and intra-molecular crosslinking occurs between primary amino or thiol groups and arginine, cysteine, tryptophan, lysine, and histidine residues [72-73]. This crosslinking provides stability and helps to preserve tissue structure. Therefore, FFPE samples are commonly collected in batches to develop tissue banks since FFPE tissue can remain stable for decades at room temperature [74]. Although tissue integrity can be preserved with this method, when analyzing proteins, paraffin is not compatible with MALDI MSI. Presence of paraffin can result in significant ion suppression effects, therefore removal must be accomplished through xylene washes prior to analysis [75]. In addition to paraffin removal, on-tissue digestion is often used to help facilitate protein and peptide identification among crosslinked proteins [76]. This process helps to preserve the spatial distribution of resulting peptides for identification.

FFPE tissue retrieval method provides a sample of high stability in comparison to fresh frozen tissue. However, sample preparatory steps required for successful MALDI MSI analysis of FFPE tissue is extremely extensive. The paraffin removal process may not always be 100% successful resulting in ion suppression of lower abundance analytes. Additionally, the ability to simultaneously detect multiple analytes within tissue samples is hindered as a result of degradation of lipids within FFPE tissue sections since the only

molecules preserved are the crosslinked proteins [76]. Therefore, fresh frozen tissue is often selected in order to preserve the native distribution of analytes within tissue sections, and to be able to study multiple analytes per sample acquired.

#### *1.5.2.2 Tissue Sectioning and Mounting*

Selection of tissue sectioning methods is dependent on the extraction technique used. For fresh frozen tissue, the tissues are secured onto the holder using water which is flash frozen with dry ice. As the tissue samples are secured onto the holder, it is important to minimize embedment of the sample area in water. Embedding the sample in water can result in a decrease in signal detected as a result of ion suppression effects [77]. Once secured, the holder can then be placed into the cryotome set to a temperature of -20 to -25 °C for sectioning. If the temperature is set too low, chances of tears and tissue fractures occur, but if the temperature is too high, tissue deformation may occur. Variations in temperature exists between runs resulting from changes in the temperature and humidity of the environment. Therefore, if sectioning is performed in an unregulated environment, temperature settings must be adjusted accordingly. The degree of blade sharpness also plays a critical role in the quality of sample sections obtained. Ideally, a fresh blade is used per sample run to minimize variables that could contribute to lack of reproducibility. Tissue thickness varies between 10 – 35  $\mu\text{m}$  [69]. The optimal tissue thickness is inversely correlated with the molecular weight of the target analyte in order to facilitate extraction of larger analytes from the tissue section.

Once sectioned, tissue is mounted onto indium tin oxide (ITO) coated glass slides. Two mounting methods are available, flip mounting and thaw mounting. Flip mounting is when the ITO glass slide is pressed on top the sectioned tissue sample, therefore resulting in the tissue inversely mounted onto the slide. This mounting method reduces chances of tissue tearing and deformation, but an increase in noise is detected for these samples. Therefore, if low abundance analytes are in question, this technique would not be favorable. Alternatively, the thaw mounting method generates data with a cleaner baseline. Thaw mounting requires the use of thin brushes to maneuver the tissue section onto the glass slide. Once desired placement is obtained, the tissue can be thawed onto the ITO glass slide by placing a finger underneath the slide. Once mounted, the tissue sections must be treated and analyzed immediately.

For FFPE tissue, sectioning is accomplished using a microtome at room temperature. As the tissue is sectioned, it is transferred to a water bath of 37 °C, and mounted onto an ITO coated glass slide. In order to ensure tissue adhesion to the glass surface, presence of water must be completely removed. This can be accomplished through incubation of the slide at 30 – 37 °C for 1 - 2 minutes. Once mounted, the tissue can be stored at room temperature for several months prior to analysis.

### *1.5.2.3 Matrix Application Methodology*

MALDI MSI requires the presence of a UV absorbing matrix to be coated on top of the tissue sections in order to help facilitate the soft ionization process. The matrix deposited

plays a vital role in the quality of images obtained. Crucial parameters that require optimization are, uniformity, concentration, and matrix selection. Uniformity of the matrix layer along the entire tissue section is extremely important for consistent signal detection in order to obtain an accurate spatial comparison of analytes across the entire ROI. If uneven application occurs, the concentration of matrix will vary among different areas of the tissue resulting in differences in the signal intensity detected. Concentration of matrix used is also extremely important, there is a set window for the optimal matrix concentration per sample analyzed. If the concentration falls below this range, the analyte to matrix ratio will be insufficient to maximize signal detection, but if the concentration is greater than this range, the matrix will act to suppress desired analyte signals. Therefore, optimization of the matrix concentration is required per sample analyzed. Matrix compatibility with target analytes must also be considered. Not only does the matrix selection have to be suitable to the type of analyte under investigation, the solvents used to solubilize the matrix must also be compatible with the sample. Three methods of matrix application are available, airbrush, automated sprayer, and sublimation.

Airbrush application is a fast and simple method for matrix deposition for MALDI MSI. The matrix selected is dissolved in the appropriate solvent and sprayed using an artisan airbrush onto the tissue section. A major disadvantage of this technique is its poor reproducibility. Huge variations exist between users since the velocity, duration, and direction of the spray is controlled manually. Therefore, the quality of the spray can vary not only between users, but between runs. Although the presence of a solvent facilitates analyte – matrix interactions which increases extraction potential, a significant concern

resides in the possibility of spraying too much solvent resulting in delocalization of analytes on the tissue surface.

Development of automated sprayer systems such as the TM – Sprayer from HTX Technologies, helped to remove variability in spray parameter. This improved the reproducibility between runs, and minimized user-to-user variations when depositing matrix. Automated sprayers provided a platform for users to have full control over desired spray parameters such as velocity, flow rate, number of passes, spray temperature, and spray pattern. The robotically controlled nozzle then applies the matrix using the preset parameters, which allows for the density of matrix applied to be calculated. The ability to control flow rate helped to facilitate the degree of analyte extraction without significantly compromising spatial resolution of images acquired. The capabilities of automated sprayers in regulating parameters to optimize for extraction potential, makes this method ideal when studying low abundance analytes such as, proteins and peptides.

Among the three techniques, sublimation is the only solvent free application method. With sublimation, the matrix is placed in the bottom of the reservoir, while the tissue mounted slide is taped directly above. Ice is added to the reservoir above the slide, and heat is applied below the matrix reservoir with the entire system under vacuum. The matrix goes directly from the solid state to the gaseous state. As the matrix particles rise, the ice above cools the region around the slide resulting in the matrix particles returning to solid state, and subliming onto the slide. This form of matrix application generates a uniform coating with a small matrix crystal size. This solvent free technique eradicates the potential of analyte delocalization, therefore generating images of high spatial resolution. However, the

absence of solvent also removes the analyte – matrix interaction period, resulting in poor extraction efficiency. Therefore, sublimation is ideal for generating images of high spatial resolution for easily extracted or high abundant analytes.

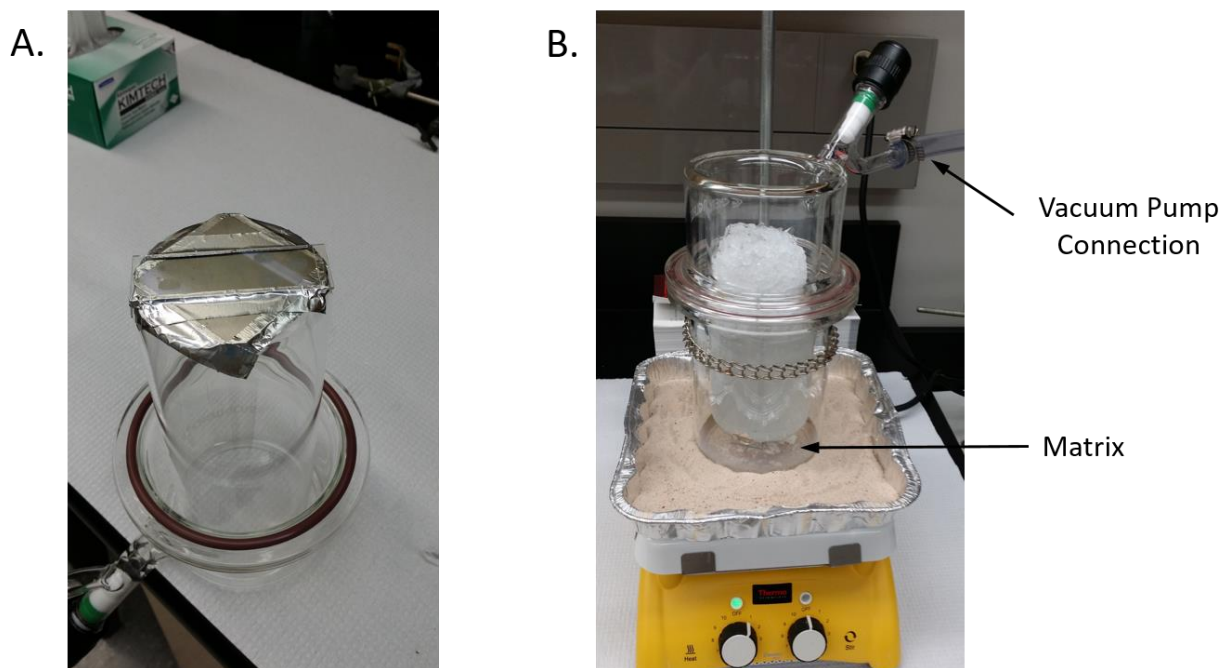


**Figure 1.5** Sublimation was accomplished by adhering the tissue mounted ITO slide onto the top half of the glass apparatus. This was placed onto the container with the pre-weighed dry matrix, and the apparatus was then connected to the vacuum pump. Once under vacuum, the glass apparatus was placed on the heated sand surface.

#### *1.5.2.4 Sample Rehydration Methodology*

As a final step in the sample preparation procedure prior to MALDI MSI analysis, rehydration is employed to help increase the opportunity for analyte – matrix interactions. This protocol aims to improve analyte extraction in order to increase detection capabilities. Rehydration is typically achieved using an acidic solvent within a closed chamber. A filter paper soaked in the acidic solvent is placed at the base of the chamber, while the tissue mounted slide is taped onto a metal heat sink attached to the top of the chamber directly above the solvent. This chamber is sealed and placed in 70 – 85 °C incubator for 3 - 5 minutes. Optimizations for incubation temperature and time vary depending on the matrix used. This step has been found to improve signal detection for all analytes under investigation.



## 1.6 References

- [1] Biro, J. C.; *Theor Biol Med Model* **2006**, *3*, 15.
- [2] Whitford, D., *Proteins: Structure and Function*. Wiley: 2013.
- [3] Pelley, J. W., 2 - Structure and Properties of Biologic Molecules. In *Elsevier's Integrated Biochemistry*, Mosby: Philadelphia, 2007; pp 7-18.
- [4] Janin, J.; *Nature* **1979**, *277* (5696), 491-2.
- [5] Wolfenden, R.; Andersson, L.; Cullis, P. M., et al.; *Biochemistry* **1981**, *20* (4), 849-55.
- [6] Kyte, J.; Doolittle, R. F.; *J Mol Biol* **1982**, *157* (1), 105-32.
- [7] Rose, G. D.; Geselowitz, A. R.; Lesser, G. J., et al.; *Science* **1985**, *229* (4716), 834-8.
- [8] Dougherty, D. A.; *J Nutr* **2007**, *137* (6 Suppl 1), 1504S-1508S; discussion 1516S-1517S.
- [9] Danger, G.; Plasson, R.; Pascal, R.; *Chem Soc Rev* **2012**, *41* (16), 5416-29.
- [10] Schermann, J.-P., 4.2 - Amino Acids, Peptides and Proteins. In *Spectroscopy and Modeling of Biomolecular Building Blocks*, Schermann, J.-P., Ed. Elsevier: Amsterdam, 2008; pp 251-296.
- [11] Pelley, J. W., 3 - Protein Structure and Function. In *Elsevier's Integrated Biochemistry*, Pelley, J. W., Ed. Mosby: Philadelphia, 2007; pp 19-28.
- [12] Godbey, W. T., Chapter 2 - Proteins. In *An Introduction to Biotechnology*, Godbey, W. T., Ed. Woodhead Publishing: 2014; pp 9-33.

- [13] Nooren, I. M.; Thornton, J. M.; *Embo J* **2003**, 22 (14), 3486-92.
- [14] Jones, S.; Thornton, J. M.; *Proc Natl Acad Sci U S A* **1996**, 93 (1), 13-20.
- [15] van Meer, G.; Voelker, D. R.; Feigenson, G. W.; *Nat Rev Mol Cell Biol* **2008**, 9 (2), 112-24.
- [16] Holthuis, J. C.; Menon, A. K.; *Nature* **2014**, 510 (7503), 48-57.
- [17] Saliba, A. E.; Vonkova, I.; Gavin, A. C.; *Nat Rev Mol Cell Biol* **2015**, 16 (12), 753-61.
- [18] Sharpe, H. J.; Stevens, T. J.; Munro, S.; *Cell* **2010**, 142 (1), 158-69.
- [19] Lemmon, M. A.; *Nat Rev Mol Cell Biol* **2008**, 9 (2), 99-111.
- [20] Lev, S.; *Nat Rev Mol Cell Biol* **2010**, 11 (10), 739-50.
- [21] Grabon, A.; Khan, D.; Bankaitis, V. A.; *Biochim Biophys Acta* **2015**, 1851 (6), 724-35.
- [22] Domon, B.; Aebersold, R.; *Science* **2006**, 312 (5771), 212-7.
- [23] Heck, A. J.; Van Den Heuvel, R. H.; *Mass Spectrom Rev* **2004**, 23 (5), 368-89.
- [24] Staub, A.; Guillarme, D.; Schappler, J., et al.; *J Pharm Biomed Anal* **2011**, 55 (4), 810-22.
- [25] Han, X.; Wei, Q.; Kihara, D.; *Current Protocols in Bioinformatics* **2017**, 60 (1), 1-3.
- [26] Stubbs Ii, M. T., Protein Crystallography A2 - Taylor, John B. In *Comprehensive Medicinal Chemistry II*, Triggler, D. J., Ed. Elsevier: Oxford, 2007; pp 449-472.

- [27] Berg, J. M.; Tymoczko, J. L.; Stryer, L., *Three-Dimensional Protein Structure Can Be Determined by NMR Spectroscopy and X-Ray Crystallography*. 5th ed.; W. H. Freeman: Ney York, 2002.
- [28] Wüthrich, K.; *Nat Struct Biol* **2001**, *8*, 923.
- [29] Kluger, R.; Alagic, A.; *Bioorganic Chemistry* **2004**, *32* (6), 451-472.
- [30] Kenworthy, A. K.; *Methods* **2001**, *24* (3), 289-296.
- [31] Kukar, T.; Eckenrode, S.; Gu, Y., et al.; *Anal Biochem* **2002**, *306* (1), 50-54.
- [32] Thomson, J. J., *Rays of positive electricity and their applications to chemical analysis*. CreateSpace Independent Publishing Platform: 1913; p 118.
- [33] Griffiths, J.; *Anal Chem* **2008**, *80* (15), 5678-83.
- [34] El-Aneed, A.; Cohen, A.; Banoub, J.; *Applied Spectroscopy Reviews* **2009**, *44* (3), 210-230.
- [35] Hart-Smith, G.; Blanksby, S. J., *Mass Analysis, in Mass Spectrometry in Polymer Chemistry*. Wiley-VCH Verlag GmbH & Co. KGaA: Weinheim, Germany, 2011.
- [36] Gross, J. H., *Mass Spectrometry*. 2 ed.; Springer: Heidelberg, 2010.
- [37] Clarke, W., Chapter 1 - Mass spectrometry in the clinical laboratory: determining the need and avoiding pitfalls. In *Mass Spectrometry for the Clinical Laboratory*, Nair, H.; Clarke, W., Eds. Academic Press: San Diego, 2017; pp 1-15.
- [38] Schermann, J.-P., 3 - Experimental Methods. In *Spectroscopy and Modeling of Biomolecular Building Blocks*, Elsevier: Amsterdam, 2008; pp 129-207.
- [39] Loo, J. A., The Tools of Proteomics. In *Advances in Protein Chemistry*, Smith, R. D.; Veenstra, T. D., Eds. Academic Press: 2003; Vol. 65, pp 25-56.

- [40] Campana, J. E.; *Instrumentation Science & Technology* **1987**, *16* (1), 1-14.
- [41] Mamyrin, B. A.; *Int J Mass Spectrom* **2001**, *206* (3), 251-266.
- [42] Luo, G.; Marginean, I.; Vertes, A.; *Anal Chem* **2002**, *74* (24), 6185-90.
- [43] Scigelova, M.; Hornshaw, M.; Giannakopoulos, A., et al.; *Mol Cell Proteomics* **2011**, *10* (7), M111 009431.
- [44] Koppelaar, D. W.; Barinaga, C. J.; Denton, M. B., et al.; *Anal Chem* **2005**, *77* (21), 418A - 427A.
- [45] Greaves, J.; Roboz, J., *Mass Spectrometry for the Novice*. CRC Press: 2013.
- [46] Kebarle, P.; Verkerk, U. H.; *Mass Spectrom Rev* **2009**, *28* (6), 898-917.
- [47] Konermann, L.; Ahadi, E.; Rodriguez, A. D., et al.; *Anal Chem* **2013**, *85* (1), 2-9.
- [48] Cech, N. B.; Enke, C. G.; *Mass Spectrom Rev* **2001**, *20* (6), 362-87.
- [49] Van Berkel, G. J.; Kertesz, V.; *Anal Chem* **2007**, *79* (15), 5510-20.
- [50] Ho, C. S.; Lam, C. W.; Chan, M. H., et al.; *Clin Biochem Rev* **2003**, *24* (1), 3-12.
- [51] Chang, W. C.; Huang, L. C.; Wang, Y. S., et al.; *Anal Chim Acta* **2007**, *582* (1), 1-9.
- [52] Lai, Y. H.; Wang, Y. S.; *Mass Spectrom (Tokyo)* **2017**, *6* (Spec Iss 2), S0072.
- [53] Lu, I. C.; Lee, C.; Lee, Y. T., et al.; *Annu Rev Anal Chem (Palo Alto Calif)* **2015**, *8*, 21-39.
- [54] Zenobi, R.; Knochenmuss, R.; *Mass Spectrom Rev* **1999**, *17* (5), 337-366.

- [55] Moser, A.; Range, K.; York, D. M.; *J Phys Chem B* **2010**, *114* (43), 13911-21.
- [56] Knochenmuss, R.; *Analyst* **2006**, *131* (9), 966-86.
- [57] Knochenmuss, R.; Zhigilei, L. V.; *J Mass Spectrom* **2010**, *45* (4), 333-46.
- [58] Tsai, M. T.; Lee, S.; Lu, I. C., et al.; *Rapid Commun Mass Spectrom* **2013**, *27* (9), 955-63.
- [59] Bae, Y. J.; Shin, Y. S.; Moon, J. H., et al.; *J Am Soc Mass Spectrom* **2012**, *23* (8), 1326-35.
- [60] Smolira, A.; Wessely-Szponder, J.; *Appl Biochem Biotechnol* **2015**, *175* (4), 2050-65.
- [61] Signor, L.; Boeri Erba, E.; *J Vis Exp* **2013**, (79).
- [62] Bourcier, S.; Bouchonnet, S.; Hoppilliard, Y.; *Int J Mass Spectrom* **2001**, *210-211*, 59-69.
- [63] Hillenkamp, F.; Peter-Katalinic, J., *MALDI MS: A Practical Guide to Instrumentation, Methods and Applications*. Wiley: 2013.
- [64] Bodzon-Kulakowska, A.; Suder, P.; *Mass Spectrom Rev* **2016**, *35* (1), 147-69.
- [65] Takats, Z.; Wiseman, J. M.; Gologan, B., et al.; *Science* **2004**, *306* (5695), 471-3.
- [66] Wiseman, J. M.; Ifa, D. R.; Zhu, Y., et al.; *Proc Natl Acad Sci U S A* **2008**, *105* (47), 18120-5.
- [67] Bennet, R. V.; Gamage, C. M.; Fernandez, F. M.; *J Vis Exp* **2013**, (77), e50575.
- [68] Seeley, E. H.; Caprioli, R. M.; *Proc Natl Acad Sci U S A* **2008**, *105* (47), 18126-31.

- [69] Walch, A.; Rauser, S.; Deininger, S.-O., et al.; *Histochem Cell Biol* **2008**, *130* (3), 421-434.
- [70] de Hoffmann, E.; Stroobant, V., *Mass Spectrometry: Principles and Applications*. Wiley: 2013.
- [71] Rohner, T. C.; Staab, D.; Stoeckli, M.; *Mech Ageing Dev* **2005**, *126* (1), 177-85.
- [72] Kriegsmann, M.; Seeley, E. H.; Schwarting, A., et al.; *Scand J Rheumatol* **2012**, *41* (4), 305-9.
- [73] Aichler, M.; Walch, A.; *Lab Invest* **2015**, *95* (4), 422-31.
- [74] Maier, S. K.; Hahne, H.; Gholami, A. M., et al.; *Mol Cell Proteomics* **2013**, *12* (10), 2901-10.
- [75] Smith, A.; Piga, I.; Galli, M., et al.; *Int J Mol Sci* **2017**, *18* (12).
- [76] Wisztorski, M.; Franck, J.; Salzet, M., et al., MALDI Direct Analysis and Imaging of Frozen Versus FFPE Tissues: What Strategy for Which Sample? In *Mass Spectrometry Imaging: Principles and Protocols*, Rubakhin, S. S.; Sweedler, J. V., Eds. Humana Press Inc, 999 Riverview Dr, Ste 208, Totowa, Nj 07512-1165 USA: 2010; Vol. 656, pp 303-322.
- [77] Reyzer, M. L.; Hsieh, Y.; Ng, K., et al.; *J Mass Spectrom* **2003**, *38* (10), 1081-92.

## **Chapter 2: Alzheimer's Disease and the Amyloid Cascade Hypothesis**

## 2.1 Introduction to Alzheimer's Disease

Alzheimer's disease (AD) is a progressive, and currently irreversible neurodegenerative disease which affects more than 80% of dementia cases worldwide [1]. This disease can be categorized into two groups, early-onset AD and late-onset AD. Early-onset is regarded as the manifestation of AD symptoms before the age of 60. This familial form of AD is caused by the inheritance of mutated amyloid precursor proteins (APP), and/or presenilin proteins which represents approximately 1-6% of all AD occurrences [2-5]. Alternatively, numerous hypotheses for causation factors have been proposed for late-onset AD. However, the multi-faceted nature of the disease makes it difficult for one theory to encompass all of the contributing factors for disease development. Biologically, neuronal damage resulting from AD pathology occur decades prior to the onset of cognitive and behavioural symptoms [6-8]. During the preclinical stages of the disease, development of amyloid beta ( $A\beta$ ) oligomers, plaques and tau tangles in the brain continue to facilitate neuronal damage through disruption of connections eventually resulting in neuronal death [9]. This damage appears to occur initially in the hippocampus, as a result, the first clinical symptoms observed tend to be the loss of one's memory [10-12]. As the disease continues to progress, the damage eventually spreads throughout the brain, and the symptoms of AD get progressively worse as it impairs mental, behavioral and functional capabilities of those affected.

Manifestation of symptoms result in tremendous emotional and financial strains to both the patient's families and the health care system. With the incidence rate of AD estimated to



affect over 1 million Canadians by 2038, AD research has become a prevalent field of study [13]. Extensive studies in the pathology of AD resulted in constantly changing theories of causation. Initially, disease manifestation was characterized by high levels of amyloid plaques, and therefore emphasis was initially placed studying plaque characterization and development. However, eventually the hypotheses of causation factors shifted to tau phosphorylation and the A $\beta$  peptides as the primary culprits [8]. Challenges in elucidating AD pathology has resulted as a hindrance to the development of diagnostics and treatments for the disease. As a result, increased interest has resided in the ability to develop and explore alternative techniques for the analysis and detection of A $\beta$  proteins in hopes to provide clarity regarding the complex web of factors that contribute to the development of AD.

### *2.1.1 Alzheimer's Disease Pathology*

Genetic, environment, behavioural and developmental components all influence the onset and progression of AD. Therefore, the ability to elucidate definitive cause and effect factors for this multifactorial disease have been challenging [1]. The earliest hypothesis described two hallmarks of AD, the accumulation of amyloid resulting in amyloid plaques, and abnormal hyperphosphorylation of tau leading to neurofibrillary tangles (NFTs) [14-15]. This hypothesis relied on the premise that A $\beta$  accumulated in extracellular space resulting in the development of senile plaques. These plaques then, in turn, led to the formation of NFTs which both contribute to cell loss, and eventually dementia [16]. However, continuous research revealed the lack of correlation between disease manifestation and the

degree of plaque development observed. Additionally, not only was neuronal damage detected in brain regions free from plaques, significant amyloid plaque formation was discovered in cognitively normal individuals as well [17-20]. Furthermore, the formation of amyloid plaques does not occur until much later in AD development, and is therefore unlikely to be the main driving force of disease progression [21]. Consequently, multiple theories and factors were hypothesized based on different causation factors of AD as presented in Figure 2.1. These hypotheses include: the tau hypothesis, inflammation hypothesis and the amyloid cascade hypothesis (ACH) [22]. Each hypothesis encompasses multiple factors that cause the onset of AD symptoms. The tau hypothesis postulates that abnormal increases in hyperphosphorylated tau proteins found in AD patients result in the loss of normal tau functions leading to neuronal dysfunction [23-27]. The inflammation hypothesis focuses upon the inflammation of the central nervous system which leads to oxidative stress followed by neuronal death [28-29]. The ACH indicates that A $\beta$  accumulation is the primary initiator that triggers a cascade of events resulting in neuronal death and dementia exhibited in AD patients [7].

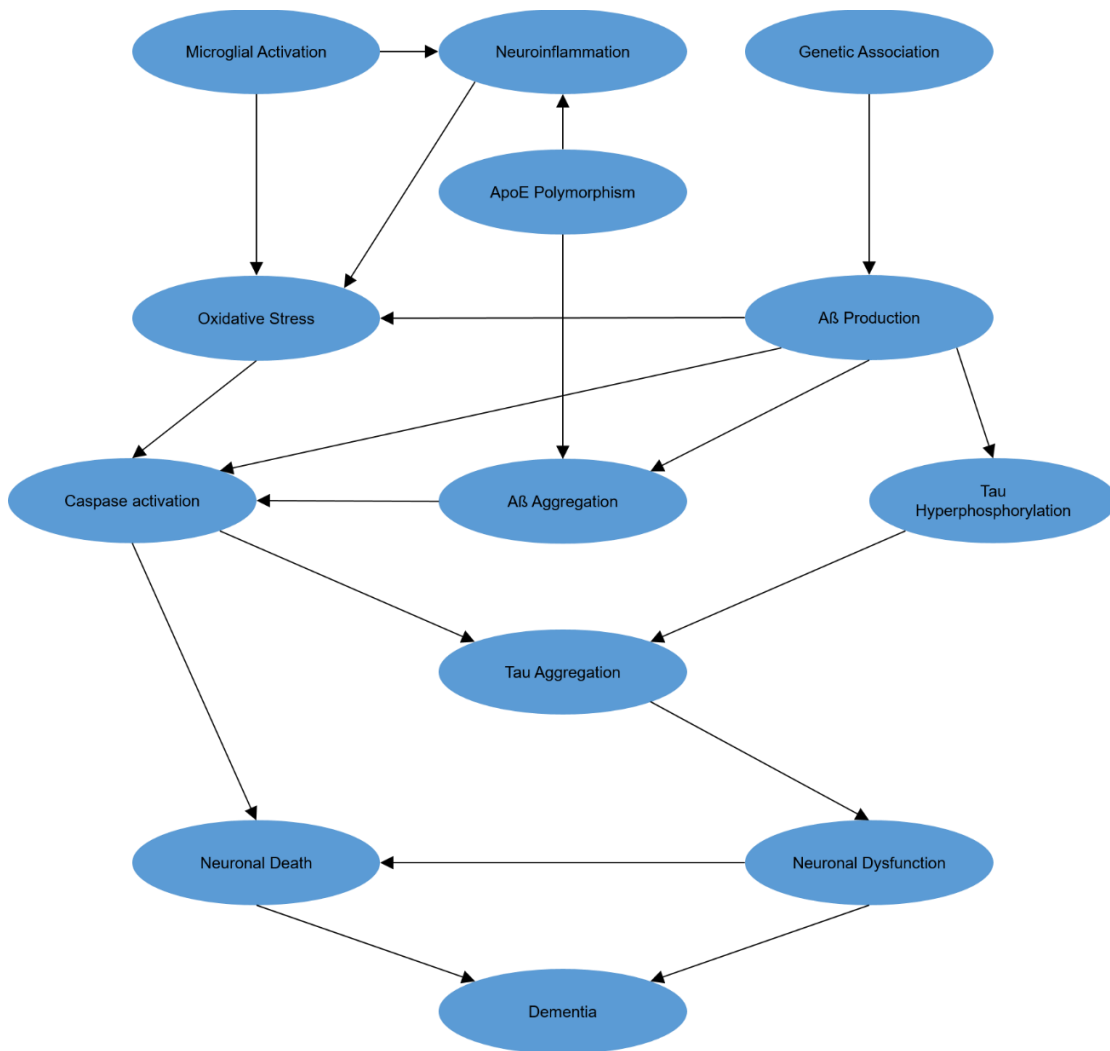


**Figure 2.1** A simplified schematic demonstrating factors that influence AD development and progression modified from Anand et al. [1]. The factors are found to be largely interconnected in causation and effect. All the individual events lead to neuronal death or dysfunction, and the eventual onset of dementia.

### *2.1.2 Amyloid Cascade Hypothesis (ACH)*

Among the proposed hypotheses for AD development and progression, ACH retains focus due to the correlations observed regarding neuronal toxicity, and the presence of soluble A $\beta$  oligomers. The presence of A $\beta$  oligomers were found to induce neuronal damage, and induce memory loss with or without plaque formation [30-31]. In the preliminary phase of ACH development, researchers believed the overproduction, or a decrease in clearance efficiency of A $\beta$  peptides resulted in an accumulation of A $\beta$ <sub>1-40</sub> and A $\beta$ <sub>1-42</sub> [8]. As the concentration of A $\beta$  peptides increases, peptide aggregation occurs which induces a multifaceted neurotoxic cascade of events. This includes the hyperphosphorylation of tau proteins, neuronal loss, cerebrovascular damage, and microglia activation [30].

A $\beta$  production results from proteolytic processing of the amyloid precursor protein (APP). This occurs either through the amyloidogenic, or non-amyloidogenic pathways. In normal conditions, the non-amyloidogenic pathway uses  $\alpha$ -secretases which cleaves APP within the A $\beta$  domain (between Lys16 and Leu17) resulting in the release of sAPP $\alpha$ . However, under pathological conditions, the amyloidogenic pathway uses  $\beta$ -secretases. The  $\beta$  cleavages site is located at the beginning of the A $\beta$  domain, therefore cleavage through  $\beta$ -secretase generates sAPP $\beta$ . The following  $\gamma$ -secretase cleavage then releases A $\beta$  peptides [8, 14, 32]. Continuous A $\beta$  production along with poor A $\beta$  removal induces the damages which eventually results in neuronal death. The development of the ACH throughout the years has made this theory the most well defined, and greatly studied concept for AD pathology.

## 2.2 Amyloid Beta

### 2.2.1 Physical Properties

A $\beta$  plays an important role in biological processes such as signaling, neuronal development and intracellular transport [33]. The amino acid sequence of these peptides contains approximately 50% hydrophobic residues with the majority of these residues concentrated on the latter half of the sequence (Figure 2.2). The hydrophobic stretches in the middle and C-terminus of A $\beta$ <sub>1-42</sub> are the driving forces of the aggregation process [34]. The hydrophobic composition of A $\beta$  creates challenges in sample handling under research conditions. Therefore, strong emphasis must be placed on ensuring sample integrity prior to additional analysis on biological effects within an experimental system.

A $\beta$ <sub>1-40</sub>      DAEFRHDSGY EVHHQKLVFF AEPVGSNKGA IIGLMVGGVV  
 A $\beta$ <sub>1-42</sub>      DAEFRHDSGY EVHHQKLVFF AEPVGSNKGA IIGLMVGGVV IA

**Figure 2.2** Amino acid sequence of pathogenic A $\beta$  peptides 1-40 and 1-42 have been provided. The peptide contains approximately 50% hydrophobic residues (shown in red).

### 2.2.2 A $\beta$ Assemblies

Monomeric A $\beta$  undergo aggregation which results in the formation of low molecular weight oligomers followed by higher molecular weight aggregates. These aggregates develop into spherical oligomers comprised of 12 to 24 monomers. The spherical structure then elongate into protofibrils, and finally insoluble fibrils as seen in Figure 2.3 [35]. These variations in A $\beta$  assemblies then come together to form amyloid plaques. The soluble A $\beta$  oligomers possess a heterogeneous size distribution *in vivo* due to the monomers propensity for spontaneous aggregation [33]. With the help of circular dichroism (CD), infrared spectroscopy and hydrogen/deuterium exchange (HDX), A $\beta$  oligomers were found to possess significant  $\beta$ -sheet secondary structures [36]. The transient nature of A $\beta$  oligomers make it extremely difficult to produce *in vitro* samples of homogenous oligomer composition, making the structural characteristic of A $\beta$  oligomers more challenging to identify [37]. The staple characteristic of these oligomers is the apparent  $\beta$ -sheet structure arranged in parallel and antiparallel fashion [38]. Initially, development of spherical oligomeric aggregates was thought to be required prior to the formation of long protofibrils leading to the formation of fibrils. However, studies indicated protofibril development can potentially occur directly from the monomeric state as well. Uncertainties in A $\beta$  structure, and the developmental pathways elicit continuous developments in analytical methods for the identification and analysis of this protein.

Unlike the dynamic oligomeric form of A $\beta$ , the static structure of the A $\beta$  fibrils has been well characterized. A $\beta_{1-40}$  and A $\beta_{1-42}$  fibrils consist of  $\beta$ -strands which run perpendicular to

the fibril axis [39]. The  $\beta$ -strands run antiparallel in a  $\beta$ -hairpin motif, where the first and second  $\beta$ -strands are connected by a short loop [40-43]. The first  $\beta$ -strand begins after the initial disordered stretch of amino acid residues at the N-terminus (approximately residues 1-14). This strand is followed by a turn which leads into the second  $\beta$ -strand [44-45]. Hydrogen bonding between these strands results in parallel stacking of the protomers forming protofibrils. The protofibrils developed can then twist together to become mature, stable fibrils. The  $\beta$ -sheet structure of amyloid fibrils act efficiently in burying the hydrophobic side chains within. Complete elucidation of the A $\beta$  aggregation pathway for the development of toxic oligomers, and stable fibrils may help to reveal underlying mechanisms of A $\beta$  related neurodegenerative diseases.

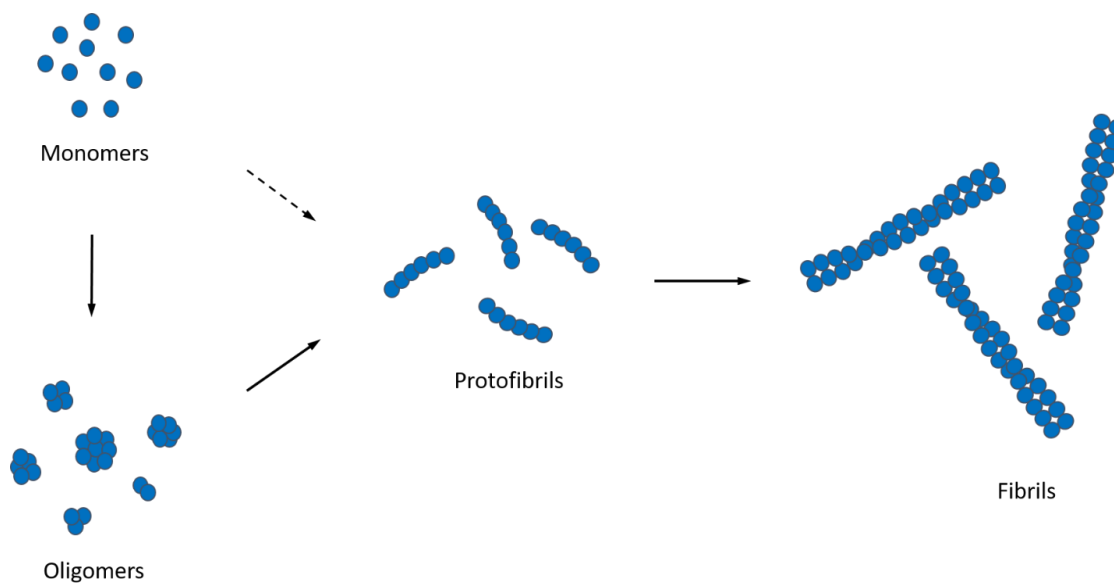


**Figure 2.3** Different stages of A $\beta$  aggregation has been presented in the currently understood aggregation pathway. A $\beta$  monomers aggregate to form a heterogeneous composition of soluble oligomers. These oligomers elongate to form the transitional protofibril structure prior to the development of mature, insoluble fibrils. However, supporting evidence indicate the monomeric form of A $\beta$  can potentially aggregate directly into protofibril formation as well.



### *2.2.3 Biological Functions & Neurotoxicity of Amyloid Beta*

The complexity of AD resulting from the pathogenic interactions between genetics, epigenetics, and the environment makes it challenging to develop therapeutic interventions for AD management. Novel therapeutics are focused on facilitating amyloid oligomer reduction by inhibition of A $\beta$  production, or by improving the efficiency of A $\beta$  degradation through over-expression of A $\beta$  degradation enzymes [33]. Beta ( $\beta$ )- and Gamma ( $\gamma$ )-secretase inhibitors, or modulators have been introduced as a means to prevent the production of A $\beta$  by minimizing the cleavage of APP through the amyloidogenic pathway. The hope was that this process would defer APP cleavage towards the non-amyloidogenic pathway using  $\alpha$ -secretase [46]. Unfortunately, these interventions are still undergoing clinical trials, therefore there are a limited number of approved drug treatments currently available for AD management [33].

Increased understanding of the mechanisms for A $\beta$  toxicity is required to further the development of therapeutic treatments for AD. However, due to the complexity of oligomer formation, there has been several proposed mechanisms for A $\beta$  toxicity [47]. A $\beta$  toxicity has been linked to the disruption of receptors, including the induction of the nerve growth factor (NGF) receptor mediated neurodegeneration and cell death [47-49]. A $\beta$  was also found to bind to membrane proteins such as insulin receptors. Similarities in structure result in A $\beta$  competing with insulin for insulin degrading enzymes resulting in the impairment of glucose metabolism observed in AD [50-51]. Since the plasma membrane regulates the exchange of materials between cells and the environment, the structural integrity of these

membranes is crucial for cellular viability. Extracellular aggregation of A $\beta$  deposits within the hippocampus, amygdala, entorhinal cortex and basal forebrain contribute towards the deteriorating memory, learning and emotional behaviours found in patients suffering from AD [33, 59].

In attempts to isolate therapeutic interventions, the development of various techniques for *in vitro* A $\beta$  analysis have been developed. Researchers aimed to probe the physical and chemical properties of these toxic proteins to identify the origins of its toxicity within biological systems. These techniques include: nuclear magnetic resonance (NMR), X-ray diffraction crystallography, as well as spectroscopy and microscopy based methods. Both NMR and X-ray diffraction crystallography are able to provide 3D structures of amyloidogenic peptides and proteins. NMR is able to monitor protein folding, including the secondary structures, along with the interactions among different regions of the protein [60-62]. Through NMR analysis, amino acid residues 1-14 were found to be unstructured, polar, water soluble residues while segment 15-36 form  $\alpha$ -helical structures [63]. Helical sections of the protein convert to coils upon the loss of a proton for two acidic amino acid residues. This conversion was found to precede the aggregation of A $\beta$ <sub>1-40</sub> [63]. In comparing the physical structure of A $\beta$ <sub>1-40</sub> and A $\beta$ <sub>1-42</sub>, residues 31-34 and 38-41 in A $\beta$ <sub>1-42</sub> was found to form  $\beta$ -hairpin structures resulting in a reduction of the flexibility at the C-terminal [64]. This was speculated to be a factor of the peptides greater propensity for aggregation in comparison to A $\beta$ <sub>1-40</sub>. Currently, gel electrophoresis is commonly used for identification of A $\beta$  aggregation in biological samples [65]. This technique relies on the ability of SDS to bind to proteins of interest, however this binding can also compromise the structural integrity of desired aggregates [66]. Issues regarding low sample throughput,

limitations in resolution, as well as gel smearing can reduce the effectiveness of this technique. Alternatively, atomic force microscopy (AFM), surface plasmon resonance (SPR), absorbance, and fluorescence spectroscopy have been used to study A $\beta$  composition with some success [67-68]. Each technique possesses its own set of limitations. AFM is most suitable for studying large, stable amyloid fibrils, while SPR is generally used to investigate the interaction of A $\beta$  aggregates. Both absorbance and fluorescence spectroscopy present restrictions in the ability to differentiate between aggregates of differing sizes.

## 2.3 Amyloid Beta Imaging

Techniques for A $\beta$  imaging within intact tissue sections have evolved greatly in the past two decades in response to the increasing demands within both research and commercial fields. Localization of A $\beta$  proteins within intact brain sections can help to elucidate AD progression and associate effects patients experience. Traditionally, histological stains using Congo Red or Thioflavins on formalin-fixed paraffin embedded (FFPE) tissue can be used for the identification of amyloid in tissue samples [69-70]. Alternatively, monoclonal mouse antibodies can be used to tag, and locate pre-amyloid and amyloid deposits with immunohistochemistry (IHC). However, issues reside with background staining caused by serum cross reactivity, or poor antibody specificity [71-72].

Through the introduction of mass spectrometry imaging (MSI), comprehensive analysis of the spatial distribution for molecular components eliminates the need for chemical staining, or antibody labelling. Over the last 10 years, continuous developments in matrix-assisted laser desorption/ionization mass spectrometry imaging (MALDI MSI) has been beneficial for the spatial profiling of amyloid plaques. However, currently MALDI MSI analysis of A $\beta$  has been limited to the detection of fibrillary A $\beta$  and amyloid plaques, both of which possess very stable, sedentary structures of considerable size [73-76]. The ability to identify soluble oligomeric forms of A $\beta$  through MALDI MSI is still required. Chapter 3 aims to present MALDI MS as a method of analysis for soluble A $\beta$  oligomeric samples.

## 2.4 Overview of Thesis

The main goal of this thesis is to improve methods for protein and peptide detection in MALDI MSI. A picture says a thousand words, we hope to apply this technique for the analysis of proteins and peptides in order to provide additional insight on disease development and progression. In the past few years, MALDI MSI has become a prominent tool in the study of intact biological samples. This method provides a new platform to not only identify and characterize target molecules within tissue samples, but also to investigate the significance of the distribution for these compounds. This thesis focuses on the analysis of amyloid beta ( $A\beta$ ) proteins which are found to be strongly correlated with Alzheimer's disease (AD) progression. The developments accomplished to improve detection sensitivity of MALDI MSI in the analysis of proteins and peptides will be able to provide a wealth of information to propel our understanding of disease onset and pathology, as well as to further the understanding of drug transport in order to aid in drug design.

The thesis begins with an overview of MALDI MS and the technical elements of this technique, followed by details regarding the application of MALDI MSI. Difficulties of  $A\beta$  analysis, and the significance of this protein in regards to AD are outlined. Chapter 3 focuses on the development of a sample preparation protocol in the MALDI MSI detection for a small peptide. The ability of MALDI MSI in the detection and analysis of lipids and metabolites have been well reported in the last decade of MALDI MSI development. However, the capabilities of proteins and peptides detection using this technique are still

fairly limited. Therefore, we begin our study of MALDI MSI by investigating a dipeptide, ZP1609. Optimization and modifications to sample preparation protocols were employed in order to detect ZP1609 within intact mouse brain sections. In chapter 4, the focus then shifts to the study of the A $\beta$  peptide. Variations in sample preparation techniques, and the ability for MALDI MS detection of different A $\beta$  fragments were reported. MALDI MSI developments outlined in chapter 3 were then applied to the analysis of A $\beta$  in chapter 5. Issues of poor signal resolution, and detection sensitivity were encountered. Solid-phase extraction using magnetic beads was attempted to enhance signal detection capabilities of MALDI MSI.

## 2.5 References

- [1] Anand, R.; Gill, K. D.; Mahdi, A. A.; *Neuropharmacology* **2014**, *76 Pt A*, 27-50.
- [2] Zhu, X. C.; Tan, L.; Wang, H. F., et al.; *Ann Transl Med* **2015**, *3* (3), 38.
- [3] Rossor, M. N.; Fox, N. C.; Mummery, C. J., et al.; *Lancet Neurol* **2010**, *9* (8), 793-806.
- [4] Sassi, C.; Guerreiro, R.; Gibbs, R., et al.; *Neurobiol Aging* **2014**, *35* (10), 2422 e13-6.
- [5] Selkoe, D. J.; Hardy, J.; *EMBO Mol Med* **2016**, *8* (6), 595-608.
- [6] Hardy, J.; Selkoe, D. J.; *Science* **2002**, *297* (5580), 353-356.
- [7] Pimplikar, S. W.; *Int J Biochem Cell Biol* **2009**, *41* (6), 1261-8.
- [8] Barage, S. H.; Sonawane, K. D.; *Neuropeptides* **2015**, *52*, 1-18.
- [9] Murphy, M. P.; LeVine, H.; *Journal of Alzheimers Disease* **2010**, *19* (1), 311-323.
- [10] Halliday, G.; *The Lancet Neurology* **2017**, *16* (11), 862-864.
- [11] Mu, Y.; Gage, F. H.; *Mol Neurodegener* **2011**, *6*, 85.
- [12] Cass, S. P.; *Curr Sports Med Rep* **2017**, *16* (1), 19-22.
- [13] Chang, F.; Patel, T.; Schulz, M. E.; *Can Pharm J (Ott)* **2015**, *148* (4), 193-9.
- [14] Kumar, A.; Singh, A.; Ekavali; *Pharmacol Rep* **2015**, *67* (2), 195-203.
- [15] Sengupta, U.; Nilson, A. N.; Kayed, R.; *EBioMedicine* **2016**, *6*, 42-49.
- [16] Hardy, J. A.; Higgins, G. A.; *Science* **1992**, *256* (5054), 184-5.
- [17] Sloane, J. A.; Pietropaolo, M. F.; Rosene, D. L., et al.; *Acta Neuropathol* **1997**, *94* (5), 471-8.
- [18] Erten-Lyons, D.; Woltjer, R. L.; Dodge, H., et al.; *Neurology* **2009**, *72* (4), 354-60.
- [19] Nordberg, A.; *Eur J Nucl Med Mol Imaging* **2008**, *35 Suppl 1*, S46-50.

- [20] Villemagne, V. L.; Fodero-Tavoletti, M. T.; Pike, K. E., et al.; *Mol Neurobiol* **2008**, *38* (1), 1-15.
- [21] Dal Pra, I.; Chiarini, A.; Gui, L., et al.; *Neuroscientist* **2015**, *21* (1), 9-29.
- [22] Kurz, A.; Pernecky, R.; *Prog Neuropsychopharmacol Biol Psychiatry* **2011**, *35* (2), 373-9.
- [23] Goedert, M.; Jakes, R.; *Biochim Biophys Acta* **2005**, *1739* (2-3), 240-50.
- [24] Roy, S.; Zhang, B.; Lee, V. M., et al.; *Acta Neuropathol* **2005**, *109* (1), 5-13.
- [25] Kuret, J.; Congdon, E. E.; Li, G., et al.; *Microsc Res Tech* **2005**, *67* (3-4), 141-55.
- [26] Mazanetz, M. P.; Fischer, P. M.; *Nat Rev Drug Discov* **2007**, *6* (6), 464-79.
- [27] Forman, M. S.; Trojanowski, J. Q.; Lee, V. M.; *Nat Med* **2004**, *10* (10), 1055-63.
- [28] Eikelenboom, P.; Veerhuis, R.; Scheper, W., et al.; *J Neural Transm (Vienna)* **2006**, *113* (11), 1685-95.
- [29] Griffin, W. S.; *Am J Clin Nutr* **2006**, *83* (2), 470S-474S.
- [30] Lesne, S.; Kotilinek, L.; Ashe, K. H.; *Neuroscience* **2008**, *151* (3), 745-9.
- [31] Gandy, S.; Simon, A. J.; Steele, J. W., et al.; *Ann Neurol* **2010**, *68* (2), 220-30.
- [32] Lansdall, C. J.; *Bioscience Horizons* **2014**, *7*, 1-11.
- [33] Chen, G. F.; Xu, T. H.; Yan, Y., et al.; *Acta Pharmacol Sin* **2017**, *38* (9), 1205-1235.
- [34] Kim, W.; Hecht, M. H.; *Proc Natl Acad Sci U S A* **2006**, *103* (43), 15824-9.
- [35] Glabe, C. G.; *J Biol Chem* **2008**, *283* (44), 29639-43.
- [36] Kaye, R.; Head, E.; Thompson, J. L., et al.; *Science* **2003**, *300* (5618), 486-9.
- [37] Oddo, S.; Caccamo, A.; Shepherd, J. D., et al.; *Neuron* **2003**, *39* (3), 409-21.
- [38] Yu, L.; Edalji, R.; Harlan, J. E., et al.; *Biochemistry* **2009**, *48* (9), 1870-7.
- [39] Sunde, M.; Blake, C. C.; *Q Rev Biophys* **1998**, *31* (1), 1-39.
- [40] Pan, J.; Han, J.; Borchers, C. H., et al.; *Biochemistry* **2012**, *51* (17), 3694-703.



- [41] Benzinger, T. L.; Gregory, D. M.; Burkoth, T. S., et al.; *Proc Natl Acad Sci U S A* **1998**, *95* (23), 13407-12.
- [42] Benzinger, T. L.; Gregory, D. M.; Burkoth, T. S., et al.; *Biochemistry* **2000**, *39* (12), 3491-9.
- [43] Petkova, A. T.; Ishii, Y.; Balbach, J. J., et al.; *Proc Natl Acad Sci U S A* **2002**, *99* (26), 16742-7.
- [44] Luhrs, T.; Ritter, C.; Adrian, M., et al.; *Proc Natl Acad Sci U S A* **2005**, *102* (48), 17342-7.
- [45] Balbach, J. J.; Petkova, A. T.; Oyler, N. A., et al.; *Biophys J* **2002**, *83* (2), 1205-16.
- [46] Godyn, J.; Jonczyk, J.; Panek, D., et al.; *Pharmacol Rep* **2016**, *68* (1), 127-38.
- [47] Kaye, R.; Lasagna-Reeves, C. A.; *J Alzheimers Dis* **2013**, *33 Suppl 1*, S67-78.
- [48] Snyder, E. M.; Nong, Y.; Almeida, C. G., et al.; *Nat Neurosci* **2005**, *8* (8), 1051-8.
- [49] Kagan, B. L.; Azimov, R.; Azimova, R.; *J Membr Biol* **2004**, *202* (1), 1-10.
- [50] Verdier, Y.; Zarandi, M.; Penke, B.; *J Pept Sci* **2004**, *10* (5), 229-48.
- [51] Xie, L.; Helmerhorst, E.; Taddei, K., et al.; *J Neurosci* **2002**, *22* (10), RC221.
- [52] Arispe, N.; Rojas, E.; Pollard, H. B.; *Proc Natl Acad Sci U S A* **1993**, *90* (2), 567-71.
- [53] Arispe, N.; Pollard, H. B.; Rojas, E.; *Proc Natl Acad Sci U S A* **1993**, *90* (22), 10573-7.
- [54] D'Andrea, M. R.; Nagele, R. G.; Wang, H. Y., et al.; *Histopathology* **2001**, *38* (2), 120-34.
- [55] Gouras, G. K.; Tsai, J.; Naslund, J., et al.; *Am J Pathol* **2000**, *156* (1), 15-20.
- [56] Gyure, K. A.; Durham, R.; Stewart, W. F., et al.; *Arch Pathol Lab Med* **2001**, *125* (4), 489-92.
- [57] Jin, S.; Kedia, N.; Illes-Toth, E., et al.; *J Biol Chem* **2016**, *291* (37), 19590-606.
- [58] Yang, A. J.; Chandswangbhuvana, D.; Shu, T., et al.; *J Biol Chem* **1999**, *274* (29), 20650-6.

- [59] Greenwald, J.; Riek, R.; *Structure* **2010**, *18* (10), 1244-60.
- [60] Tomaselli, S.; Esposito, V.; Vangone, P., et al.; *ChemBiochem* **2006**, *7* (2), 257-67.
- [61] Sung, Y. H.; Eliezer, D.; *Protein Sci* **2006**, *15* (5), 1162-74.
- [62] Esposito, G.; Corazza, A.; Viglino, P., et al.; *Biochim Biophys Acta* **2005**, *1753* (1), 76-84.
- [63] Coles, M.; Bicknell, W.; Watson, A. A., et al.; *Biochemistry* **1998**, *37* (31), 11064-77.
- [64] Sgourakis, N. G.; Yan, Y.; McCallum, S. A., et al.; *J Mol Biol* **2007**, *368* (5), 1448-57.
- [65] Bitan, G.; Fradinger, E. A.; Spring, S. M., et al.; *Amyloid-Journal of Protein Folding Disorders* **2005**, *12* (2), 88-95.
- [66] Bitan, G.; Lomakin, A.; Teplow, D. B.; *Journal of Biological Chemistry* **2001**, *276* (37), 35176-35184.
- [67] Amaro, M.; Kubiak-Ossowska, K.; Birch, D. J., et al.; *Methods and Applications in Fluorescence* **2013**, *1* (1), 1-13.
- [68] Lindberg, D. J.; Wrann, M. S.; Gatty, M. G., et al.; *Biochem Biophys Res Commun* **2015**, *458* (2), 418-423.
- [69] Khurana, R.; Coleman, C.; Ionescu-Zanetti, C., et al.; *J Struct Biol* **2005**, *151* (3), 229-38.
- [70] Jin, L. W.; Claborn, K. A.; Kurimoto, M., et al.; *Proc Natl Acad Sci U S A* **2003**, *100* (26), 15294-8.
- [71] Picken, M. M.; Herrera, G. A.; *Arch Pathol Lab Med* **2007**, *131* (6), 850-1.
- [72] Linke, R. P.; Oos, R.; Wiegel, N. M., et al.; *Acta Histochem* **2006**, *108* (3), 197-208.
- [73] Kaya, I.; Brinet, D.; Michno, W., et al.; *ACS Chem Neurosci* **2017**, *8* (2), 347-355.
- [74] Michno, W.; Kaya, I.; Nyström, S., et al.; *Anal Chem* **2018**.
- [75] Kaya, I.; Brinet, D.; Michno, W., et al.; *ACS Chem Neurosci* **2017**, *8* (12), 2778-2790.

[76] Kaya, I.; Zetterberg, H.; Blennow, K., et al.; *ACS Chem Neurosci* **2018**.

**Chapter 3: Matrix-Assisted Laser Desorption/Ionization  
Mass Spectrometry Imaging of Intraperitoneally  
Injected Danegaptide (ZP1609) for Treatment of  
Stroke-Reperfusion Injury in Mice**

## 3.1 Introduction

### 3.1.1 MALDI MSI Analysis of Small Peptides

Visualization of biological systems provide a platform to unravel and understand the complexities of cells, disease pathology and drug pathways. The molecular specificity of mass spectrometry imaging (MSI) and the “soft” ionization source, has made matrix-assisted laser desorption/ionization (MALDI) MSI a powerful, emerging tool for imaging intact biological tissue samples [1-3]. The specificity and sensitivity mass spectrometry provides allows it to be used as a new technology for directly mapping and imaging intact biological tissue sections [4-6]. Current imaging techniques for biological specimens have contributed greatly in the study of biological systems, and the practice of medicine, but a common limitation resides in the inability for untargeted monitoring of multiple analytes simultaneously without introduction of labels or structural modifications to the system [7]. MALDI MSI can overcome this limitation by monitoring thousands of molecules within one experiment in order to study the spatial arrangement within tissue sections [8-9]. This technique is capable of localizing proteins, peptides, lipids, metabolites and small molecules *in situ* [10-11]. The data acquired can help shape our understanding of biological functions and diseases in order to improve current methods of treatment and prevention.

### *3.1.2 Biological Significance of Danegaptide (ZP1609)*

It is estimated that over 600,000 Canadians will be suffering from the effects of stroke by the year 2038 [12]. Stroke occurs when there is restricted blood flow to the brain resulting in loss of oxygen and neuronal cell death [13-14]. These infarctions result in debilitating effects, such as mobility limitations, chronic pain, vision problems, and excessive fatigue which impact the lives of not only the patients, but also puts extensive strain on the caregivers [15]. Antiarrhythmic drugs like rotigaptide (ZP123) were originally described to protect against cardiac ischemia-reperfusion injury as it exhibited protection in ischemic conditions [16-19]. Further development of ZP123 produced ZP1609 which exhibited similar effects as its parent compound, but it has the additional advantage of improved oral bioavailability making it a stronger candidate clinically [20-22]. When assessing the protective properties of ZP1609 in pre-clinical models of stroke-reperfusion injury, results demonstrated a decrease in infarct size when ZP1609 was administered prior to the reperfusion phase following ischemic conditions [14, 21, 23-24]. However, a current limitation to using ZP1609 as a neuroprotective agent for stroke, is a clear understanding on the ability of the dipeptide to target the brain itself. Blood brain barrier (BBB) permeability is essential for potential drug candidates in drug discovery programs. The BBB is designed to protect the central nervous system from toxins and pathogens, but this characteristic also acts to restrict the delivery of drugs to the brain [25-27]. Visualization of drug distribution can be achieved through radiolabeling drug derivatives, but this method is susceptible to false positives and is expensive to execute [28]. More importantly, the labels can potentially change the property of a small drug molecule. MALDI MSI provides

a label-free method capable of visualizing distribution of drug molecules within tissue sections. The ability to visualize BBB permeability of ZP1609 will give a better understanding of drug transport, toxicity, and help to predict potential off-target effects to advance development. This method is effective, yet requires experimental optimization, such as matrix selection and tissue washing to successfully detect the analytes of interest.

ZP1609 has a monoisotopic mass of 291.12 Da, consisting of a benzamide group attached to amino acid residues proline and glycine (Figure 3.1). Investigation of the BBB permeability of ZP1609 using MALDI MSI can help advance our understanding of the neuroprotective properties of this compound against ischemic stroke. With MALDI MS, the matrix helps to transfer the laser energy for the “soft” ionization of analyte molecules and facilitate their detection, but even so, fragmentation still occurs especially for small peptides like ZP1609. Ideally, MALDI MS is capable of the direct analysis of ZP1609 from the complex background of biological tissues while simultaneously searching for possible fragments and adducts of ZP1609. Within this work, we demonstrate MALDI MSI capabilities in the direct detection of an intraperitoneally (IP) injected small peptide, ZP1609 within intact tissue sections as well as provide visual confirmation of the dipeptide’s successful penetration of the BBB.

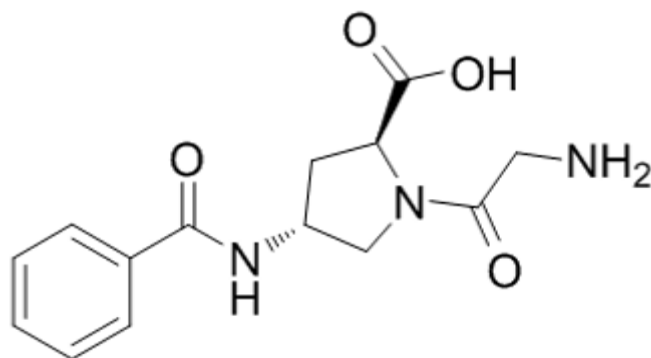


**Figure 3.1** ZP1609 dipeptide has a monoisotopic mass of 291.12 Da. This dipeptide consists of a benzamide group attached to proline and glycine amino acid residues.



## 3.2 Experimental

### 3.2.1 Apparatus

All MALDI MS sample analyses were performed on a Sciex TOF TOF 5800 MALDI mass spectrometer equipped with a 1 kHz OptiBeam™ On-Axis Nd:YAG laser system (Ontario, Canada). The TOF TOF Series Explorer and Data Explorer were used for data acquisition and processing respectively. The Sciex TOF TOF Imaging software was used for region selection and image data collection. All MALDI MSI data was processed and analyzed using MathWorks MATLAB MSiReader software.

Matrix sublimation was accomplished using a glass sublimator built in-house. Spray matrix application was applied using HTX Technologies automated TM Sprayer system (Chapel Hill, NC). CryoStar NX50 from ThermoFisher Scientific (Ontario, Canada) was used for all tissue slicing. Syringes and Needles used for sample preparation were purchased from Dyna Medical (Ontario, Canada), and Becton-Dickinson & Co (Franklin Lakes, NJ) respectively. Rehydration chambers were created with Fisherbrand Petri Dishes from Fisher Scientific (Ontario, Canada) and rehydration was achieved using a Robbins Scientific Micro Hybridization Incubator Model 2000 (San Diego, CA). Deionized water used throughout these experiments were obtained from a Millipore Milli-Q A10 Water Purification System (Bedford, MA).

### *3.2.2 Samples and Reagents*

All ZP1609 standards were supplied by Dr. Christian Naus from the University of British Columbia. Reagent grade acetonitrile (ACN), ammonium hydroxide, ethanol, and methanol were purchased from Caledon (Ontario, Canada). HPLC grade trifluoroacetic acid (TFA) was purchased from Fischer Scientific Ltd. (Hampton, NH). 2, 5 – dihydroxybenzoic acid (DHB), sinapinic acid (SA), chloroform, ammonium citrate dibasic, and acetic acid were purchased from Sigma Aldrich (St. Louis, MO). Phosphoric acid was obtained from EM Science (Darmstadt, Germany), and trifluoroacetic acid (TFA) was purchased from Fischer Scientific (Ottawa, ON, Canada).

### *3.2.3 Treatment Conditions for Tissue Samples*

All procedures were approved by the Animal Care Committee of the University of British Columbia. Wildtype C57Bl/6 mice from the Jackson laboratory (Maine, USA) aged 3-4 months were used. Transient Middle Cerebral Artery Occlusion (tMCAO) was performed according to the protocols of Lee et al. and Maniskas et al. [29-30]. Briefly, the mice were anesthetized with sodium pentobarbital (65 mg/kg IP) and given an opiate, buprenorphine (0.1 mg/kg). A local analgesic, bupivacaine (0.1 mL at 0.25%), was administered at the incision site prior to surgery. The mouse's head was immobilized in a stereotaxic frame to allow exposure and blockage of the middle cerebral artery. The mouse brain was subjected to anoxic conditions for 1 hour followed by reperfusion of the blood supply. Following

injections of treatment compounds at designated time intervals, the mice were anesthetized using a lethal dose of sodium pentobarbital (120 mg/kg IP) and transcardially perfused with phosphate-buffered saline (PBS). The brains were removed and frozen at - 80 °C.

The treatment paradigm was as follows: 1) Sham – saline brains; saline was IP injected and brains were removed 1 hour after injection. 2) Sham – ZP1609 brains; ZP1609 was IP injected and brains were removed 1 hour after injection. 3) Stroke – saline brains; tMCAO with reperfusion after 1 hour; saline was injected 10 minutes before reperfusion IP and brains were removed 1 hour later. 4) Stroke – ZP1609 brains; tMCAO subjected brains with reperfusion after 1 hour and ZP1609 was IP injected 10 minutes before reperfusion. Brains were removed 1 hour later. 5) Stroke – saline brains; tMCAO subjected brains with 12 hours delayed extraction brains; saline was injected 10 minutes before reperfusion by IV, followed by IP injections every consecutive hour for 3 hour. The brains were removed after 12 hours. 6) Stroke – ZP1609 brains; tMCAO subjected brains with 12 hours delayed extraction; ZP1609 IV injected 10 minutes before reperfusion followed by IP injections every consecutive hour for 3 hours. Brains were removed after 12 hours.

### *3.2.4 Tissue Preparation for MALDI MSI Analysis*

Tissue samples were mounted onto the tissue holder of the cryostat with water, and coronal sections were obtained to 14 µm thicknesses at - 25 °C. Each tissue section was approximately 5.5 – 9 mm by 7 – 9 mm in size. Once sliced, the sections were thaw

mounted onto indium tin oxide (ITO) coated glass slides and placed in a desiccator for 10 minutes.

A six step wash first using, 70% ethanol, and 100% ethanol was employed. This was followed by a mixture of 60% ethanol, 30% chloroform, and 10% acetic acid. Finally, another 100% ethanol, water, and 100% ethanol was used. The wash steps fix the tissue sections, as well as removes unwanted contaminants, salts and lipids. Upon tissue acidification, the water wash was replaced with 0.2% TFA. The tissue was incubated in this solvent at room temperature for 2.5 minutes.

### *3.2.5 MALDI MSI Analysis*

DHB matrix was prepared to 20  $\mu\text{g}/\mu\text{L}$  in 20% EtOH, 15% 100 mM ammonium citrate, and 1% phosphoric acid. When sublimated, 210 mg of DHB was used and sublimated at a temperature of 130  $^{\circ}\text{C}$  for a duration of 4 minutes. DHB was also applied onto sample sections using the automated TM sprayer from HTX Technologies (Chapel Hill, NC). Complete sample coverage was obtained using 8 passes at a velocity of 1200 mm/min, and a flow rate of 0.05 mL/min. A final matrix density of  $3.33 \times 10^{-2}$  mg/mm<sup>2</sup> was achieved. A final rehydration step was performed using a 5% acetic acid solution. The sample slide was placed in the rehydration chamber at 70  $^{\circ}\text{C}$  for 3.5 minutes.

The MALDI MS sample analyzed in the positive ion, reflectron mode. A total sum of 600 shots/spot, and 30 shots/spot for spectral and imaging data acquisition respectively with a

1 kHz OptiBeam On-Axis Nd:YAG laser system. The open source MSiReader software was used for imaging data manipulations and analysis.

### **3.3 Results and Discussion**

#### *3.3.1 Identification of Danegaptide Peaks*

We first determined the sensitivity of MALDI MS for the detection of intact dipeptide, fragments, and adducts. Of the common matrices, 2,5-dihydroxybenzoic acid (DHB) has been found to be more susceptible to in-source decay, therefore making detection of ZP1609 fragments, along with corresponding salts and adduct formations possible [31-32]. Images for the intact peptide, along with confirmed fragments, salt ions, and adducts help to validate the data in order to show MALDI MSI capabilities in targeting analysis of small peptides in complex biological samples. Identification of ZP1609 standards was achieved using MALDI MS peaks of fragment ions, salt ions, and adducts listed in Table 3.1. As a result of the presence of salts within the complex samples, Na<sup>+</sup> and K<sup>+</sup> ions were commonly detected within the sample. Cleavage of glycine and proline also generated detectable peaks within the targeted  $m/z$  range of 100 – 550.

**Table 3.1** Peaks identified through MALDI MS analysis of standard ZP1609 samples were recorded. These peaks include dipeptide fragmentation as well as any salt ions, and adducts formations detected within the  $m/z$  range of 100 – 550.

<b>Description</b>	<b>Ion <math>m/z</math></b>
[Glycine – H + Na +K] <sup>+</sup>	135.96
[Proline – H + 2Na] <sup>+</sup>	160.03
[M – C <sub>2</sub> H <sub>4</sub> NO + 2H] <sup>+</sup>	235.11
[M – CO <sub>2</sub> + H <sub>3</sub> O] <sup>+</sup>	266.14
[M – CO <sub>2</sub> + K] <sup>+</sup>	286.14
[M+H] <sup>+</sup>	292.13
[M + 2H] <sup>+</sup>	293.14
[M + Na] <sup>+</sup>	314.13
[M + K] <sup>+</sup>	330.13

### 3.3.2 *Effects of Variation in Matrix Selection*

The sensitivity of detection for the target  $m/z$  range of 100 – 550 for standard matrices sinapinic acid (SA), and 2,5 – dihydroxybenzoic acid (DHB) was then assessed for MALDI MSI within intact mouse brain tissue sections. Although  $\alpha$ -cyano-4-hydroxycinnamic acid (CHCA) has been shown to be effective for low mass peptide analysis, CHCA generates an abundance of matrix background signals of high signal intensity within the 100 – 500 range and thus CHCA peak intensities suppressed the ZP1609 signal. Although SA is normally used for analysis of small proteins, both DHB and SA matrices have been found to be highly effective for MALDI MSI analysis, therefore both matrices were tested for ZP1609 analysis [33-34]. For matrix comparisons, brain tissue samples from the experimental group with IP injected ZP1609 were coated with either SA or DHB and profiling data were collected (Figure 3.2). Among these two matrices, DHB was found to provide the greatest detection sensitivity of the target analytes with minimal interference from background. The majority of peaks observed with SA resulted from the matrix itself, while use of DHB allowed for detection of  $[M + H]^+$  peaks.

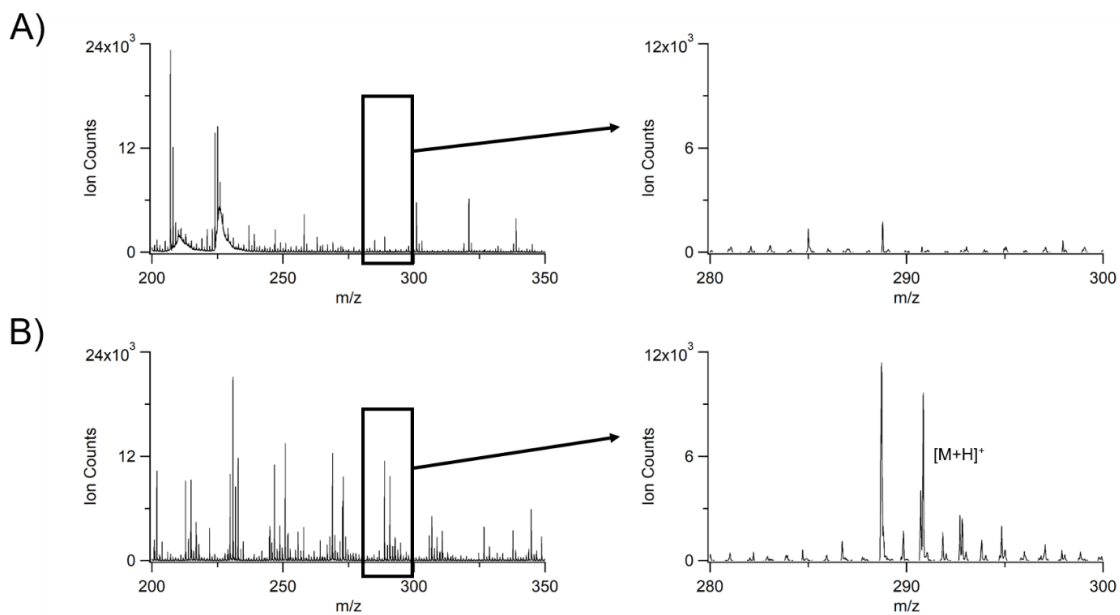


**Figure 3.2** ZP1609 signal detection capabilities of SA (A), and DHB (B) were compared to select the most suitable matrix for image application. SA generated little to no analyte signals in comparison to DHB. This was further proven when data was collected with focus on the targeted  $m/z$  region 280 – 300. The  $[M + H]^+$  peak at  $m/z$  292.13 was identified when DHB was used for analysis.



### *3.3.3 Effects of Tissue Washing in Signal Detection*

Following determination of matrix and target  $m/z$  for analysis, optimization of MALDI imaging parameters was explored. Standard sample preparation protocols for MALDI MSI of proteins and peptides for fresh frozen tissue sections include, tissue extraction, mounting, fixation, wash, matrix application and rehydration [7]. Salts and lipids cause a signal suppression effect on the targeted proteins and peptides so additional fixation and washing steps are required for the detection of target proteins and peptides in MALDI MSI [35-36]. As a result of these sample preparation procedures, compromises in signal and spatial resolution, as well as delocalization of target analytes are often observed when imaging proteins and peptides. Changes in these imaging parameters together contribute to a reduction in image quality when compared with MALDI MSI of lipids. Even though current sample preparation protocols commonly used in our research group have been devised for lipid imaging generating high resolution lipid images, there is still room for improvement when imaging proteins and peptides which typically requires salt and lipid removal by tissue washing. As such, in this study we assess and optimize sample preparation methods for IP injected dipeptides using ZP1609 as the analyte of interest. With peptides of such a low molecular weight (MW) range, tissue washing procedures must be monitored closely to determine whether sample loss poses as a critical factor for signal detection. Wash protocols vary greatly depending on the target analytes that are being investigated. The six step wash protocol was adopted from the Caprioli research group and was modified to maximize efficiency for our target analyte [36]. The six washes were intended to first fix the tissue with ethanol to prevent further degradation, followed by

removal of lipids and salts. The ethanol, chloroform and acetic acid mixture serves as a means of lipid removal while a water wash removes excess salts from the tissue section. Each step of the wash protocol helps to remove the endogenous contaminants that may hinder desorption and ionization of peptides. Effects of peptide detection following the wash protocol was clearly displayed in Figure 3.3. These wash conditions show significant enhancements in detection sensitivity and the signal-to-noise ratio when investigating the  $[M + H]^+$  peak at 292.13.

#### *3.3.4 Effects of Variation in Methods of Matrix Application*

The most widely used forms of matrix application are sublimation or automated spraying. Sublimation provides a means of matrix application without involvement of solvents thus minimizing the chances of additional adduct formation, as well as eradicating the possibility of delocalization producing an image of high spatial resolution [37]. The compromise that comes with sublimation is the reduction in analyte extraction capabilities resulting from the lack of solvent interactions to aid in the co-mixing of target analytes and matrix. When the two matrix application methods were compared for the detection of the small peptide ZP1609, it was clear the automated sprayer provided greater detection sensitivity as well as better signal-to-noise providing an image of greater structural details (Figure 3.4). Although the rehydration step aids in analyte extraction, when analyzing small, low abundance peptides, sublimation still appears to be inferior to matrix sprayers in analyte extraction efficiency. This deficiency resulted in images of poor signal and spatial resolution in comparison to the sprayer.

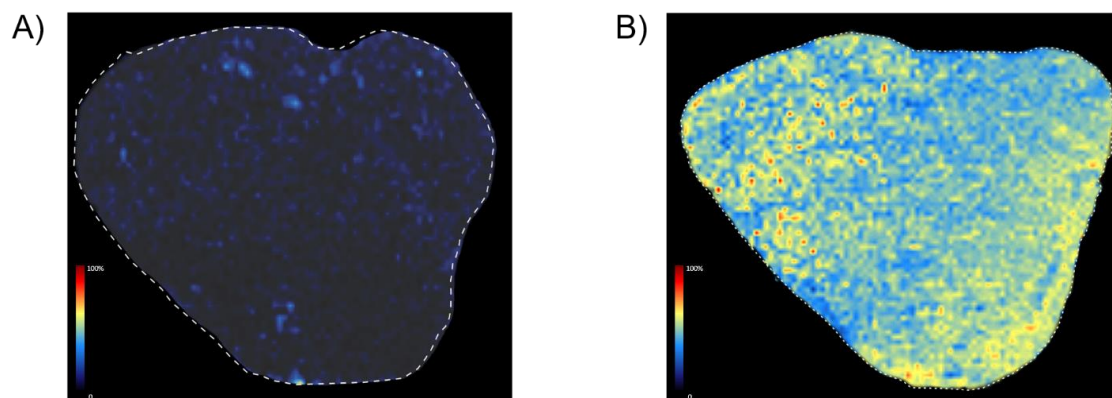


**Figure 3.3** An abundant amount of lipids and salts were present on the surface of the tissue section resulting in signal suppression effects of the  $[M + H]^+$  peak ( $m/z$  292.13) for ZP1609 (A). Upon removal of the excess salts and lipids through the wash protocol, detection of the target analyte was achieved (B).

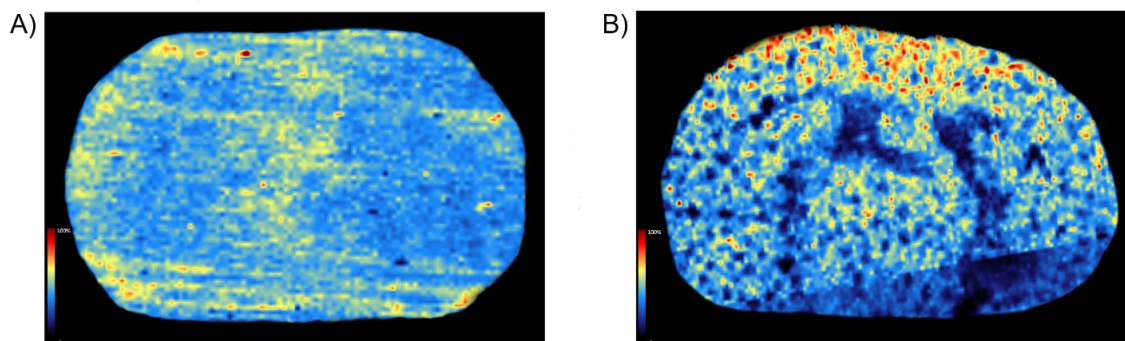


**Figure 3.4** The  $[M + H]^+$  peak of ZP1609 at  $m/z$  292.13 was used to assess extraction capabilities for small MW, low abundance peptides. Sublimation was used as a dry matrix application technique (A), this was compared to a wet application technique through use of an automated sprayer (B). The lack of solvent to facilitate extraction of target analytes resulted in poor signal-to-noise ratio hence compromising detection sensitivity and spatial resolution of the images obtained.

### *3.3.5 Acidification Effects on Signal Detection Sensitivity*

Through optimization of sample preparation protocols, we were able to detect ZP1609, but there was room for improvement in the images obtained. Therefore, increased acidification during the wash protocol was tested for its ability to enhance image resolution for low MW peptides. During the wash protocol, TFA was added to the water wash for excess salt removal. The tissue was washed for an extended period of 2.5 minutes in this TFA solution to allow for sufficient acidification of the tissue sample. This acidification process coupled with rehydration after matrix application using a 5% acetic acid solution resulted in greater signal detection capabilities as well as an image of greater spatial resolution (Figure 3.5). The maximum signal intensities detected per image have been displayed for direct comparison.

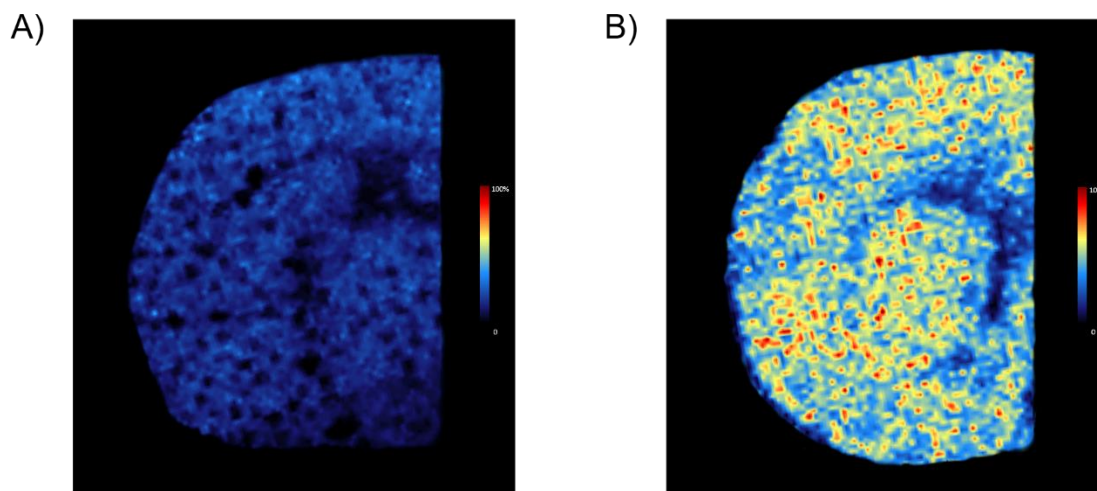


**Figure 3.5** The  $[M + H]^+$  peak of ZP1609 at  $m/z$  292.13 was used to assess the effects of extended acidification in extraction capabilities. To facilitate acidification, the water wash used for salt removal (A) was replaced with 0.2% TFA solution (B). Sensitivity of detection was improved when the tissue washing protocol was modified to include an extended acidification step allowing for higher signal intensity as well as identification of greater structural differentiation within tissue when target  $m/z$  values were assessed.

### 3.3.6 MALDI MSI Analysis of Intraperitoneally Injected ZP1609

Using the above mentioned sample preparations methods, different experimentally treated mice brain samples were compared. Mice underwent four different surgical conditions (sham-saline, sham-ZP1609, stroke-saline, and stroke-ZP1609) in order to determine the efficiency of ZP1609 in penetrating the BBB to reach the brain parenchyma. Several fragment ions were targeted in order to validate the MALDI MSI data obtained was a result of the presence of ZP1609, and not by-products of the protocols. These fragment ions were previously determined when standards of ZP1609 were analyzed. Targeted  $m/z$  values were, 160.03, 266.14, 314.13, and 330.13 and these peaks correlate directly with, [Proline – H + 2Na]<sup>+</sup>, [M – COOH + H<sub>2</sub>O]<sup>+</sup>, [M + Na]<sup>+</sup>, and [M + K]<sup>+</sup> respectively (Figure 3.6). When analysing saline injected tissue in comparison to the ZP1609 injected tissue, it was clear that the targeted peaks were detected with greater signal intensity. The most intense signals were detected from tMCAO subjected mice brains that underwent ZP1609 peptide injection in ischemic conditions followed by reperfusion. ZP1609 was found to exhibit similar protective behaviours as its parent ZP123 by countering the reduction of conductance efficiency under ischemic conditions. Therefore, a greater presence of ZP1609 was expected when treatment groups were subjected to tMCAO conditions. These speculations were supported by the data presented in Figure 3.6. When comparing ZP1609 injected vs. tMCAO & ZP1609 injected tissue sections, a clear increase in signal intensity was observed.

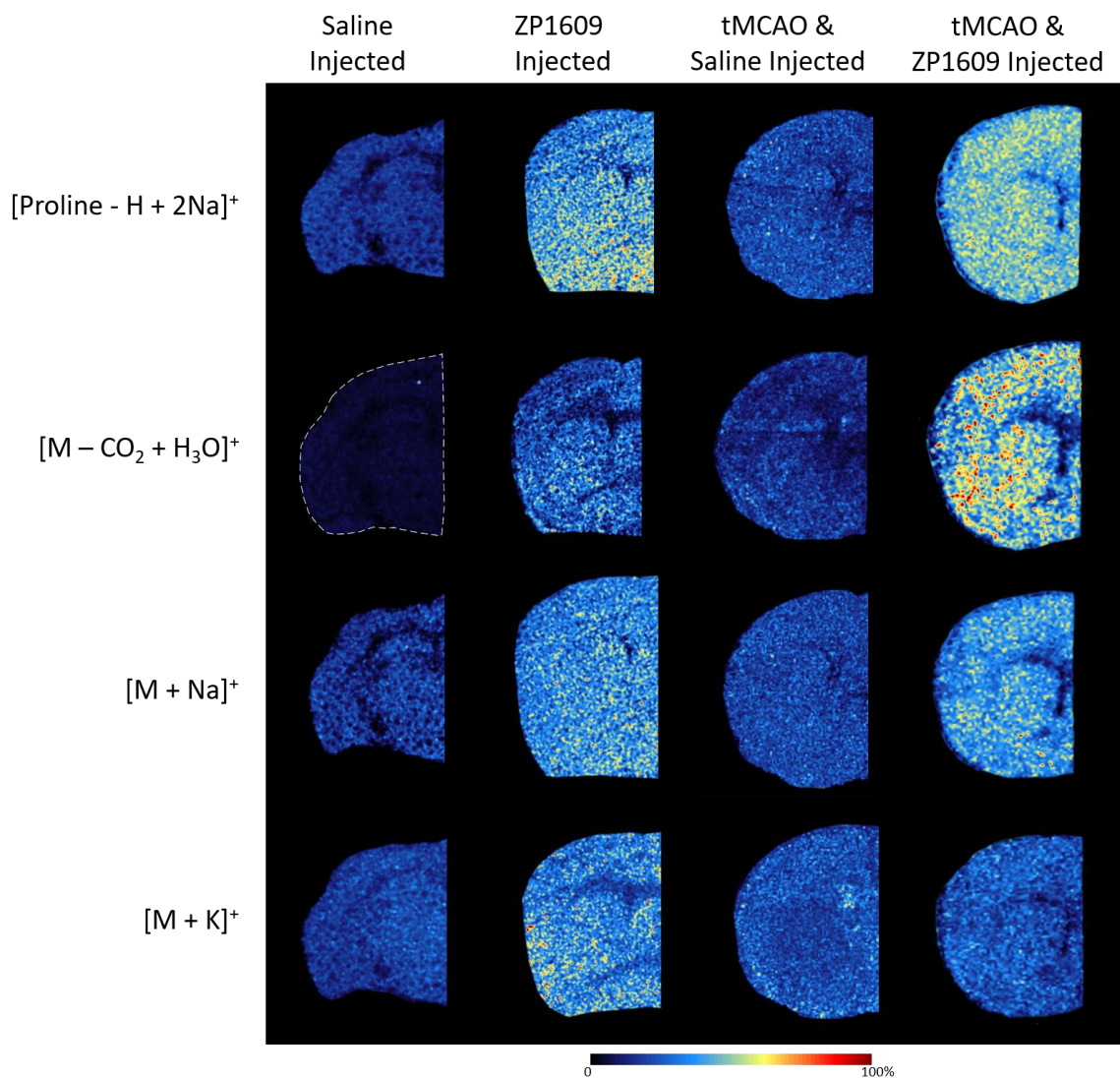


**Figure 3.6** MALDI MSI was able to detect low concentrations of IP injected ZP1609. Analysis of the fragment and salt ions, help reinforce the data suggesting the dipeptide's successful penetration of the blood brain barrier.



With the optimized protocol and added tissue acidification procedure, tissue samples from different treatment groups were analyzed and found MALDI MSI signal detection was sensitive enough to differentiate between treatment groups. Two negative controls were provided, one with saline IP injected in normal conditions, while the other was injected with saline in ischemic conditions followed by reperfusion. The sample preparation protocol was then tested using samples from treatment groups which followed the protocols of current preclinical trials. This protocol differed in multiple ZP1609 injections were administered before reperfusion as well as after in 1 hour intervals. The tissue extraction was then delayed 12 hours following reperfusion in order to provide ample time so ZP1609 can be efficiently transported across the BBB. If ZP1609 is effective in penetrating the BBB, then continuous drug delivery should permeate the brain allowing greater signal intensity to be observed and in turn provide a greater signal-to-noise ratio. The images generated from this sample group possessed greater spatial resolution and signal intensity (Figure 3.7).

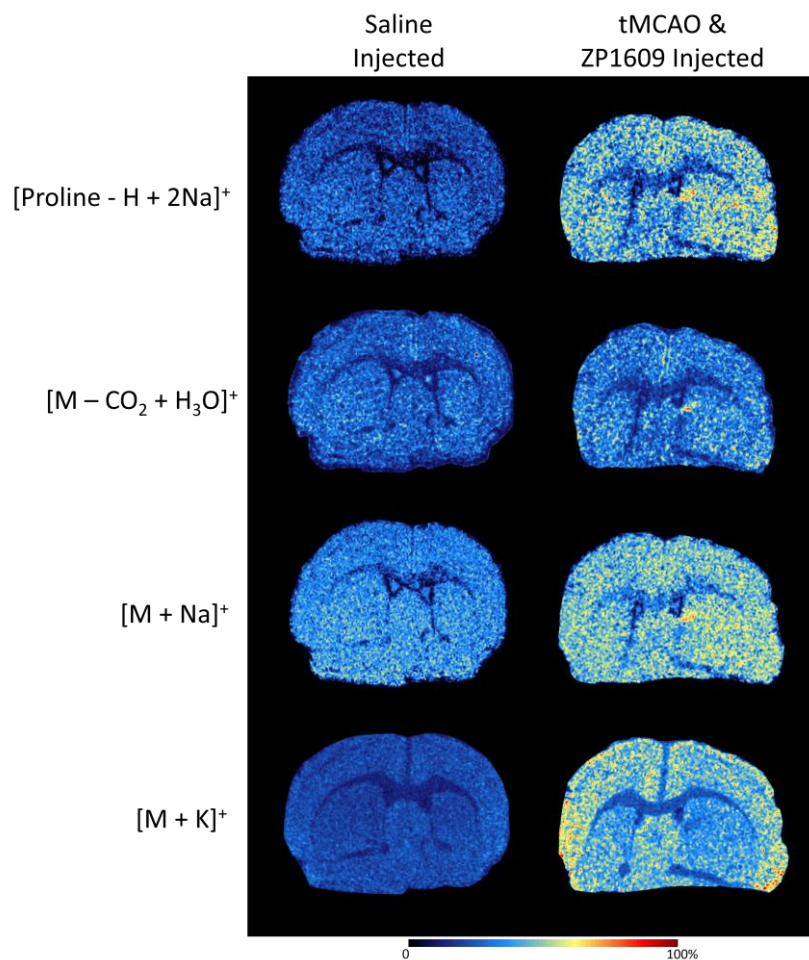


**Figure 3.7** Saline and ZP1609 was administered pre and post reperfusion in one hour intervals for the control and treatment groups respectively. Analysis of target ZP1609 fragment and salt ions generated images of higher spatial resolution and signal intensity. The extended incubation period provided additional time for the dipeptide to permeate the brain tissues resulting in a greater signal detection for each fragment analyzed.

### **3.4 Conclusion**

MALDI MSI shows the benefits of tissue acidification to enhance detection sensitivity and overall image resolution. Analysis of ZP1609 using MALDI MSI shows the specificity of sample preparation parameters required to obtain successful images of small peptides within tissue sections. These parameters require optimization in order to cater to analytes under investigation. Through manipulations of the preparation protocol, we were able to obtain data that uncovers the capabilities of ZP1609 in successful penetration of the BBB. MALDI MSI has shown to be a useful technique for drug detection in intact tissue sections. This demonstrates the ability of the technique to provide important information regarding drug transport to help further develop ZP1609 as a means of pharmaceutical intervention in minimizing effects of stroke-reperfusion injury.

### 3.5 References

- [1] Chughtai, K.; Heeren, R. M.; *Chem Rev* **2010**, *110* (5), 3237-77.
- [2] Seeley, E. H.; Schwamborn, K.; Caprioli, R. M.; *J Biol Chem* **2011**, *286* (29), 25459-66.
- [3] Kherlopian, A. R.; Song, T.; Duan, Q., et al.; *BMC Syst Biol* **2008**, *2*, 74.
- [4] Stoeckli, M.; Chaurand, P.; Hallahan, D. E., et al.; *Nat Med* **2001**, *7* (4), 493-6.
- [5] Urwyler, S. K.; Glaubitz, J.; *Letters in Applied Microbiology* **2015**, *62* (2), 130-137.
- [6] Yang, J.; Caprioli, R. M.; *Anal Chem* **2013**, *85* (5), 2907-12.
- [7] Norris, J. L.; Caprioli, R. M.; *Chem Rev* **2013**, *113* (4), 2309-42.
- [8] Caldwell, R. L.; Caprioli, R. M.; *Mol Cell Proteomics* **2005**, *4* (4), 394-401.
- [9] Rohner, T. C.; Staab, D.; Stoeckli, M.; *Mech Ageing Dev* **2005**, *126* (1), 177-85.
- [10] Liu, X.; Ide, J. L.; Norton, I., et al.; *Scientific Reports* **2013**, *3*, 2859.
- [11] Cobice, D. F.; Goodwin, R. J.; Andren, P. E., et al.; *Br J Pharmacol* **2015**, *172* (13), 3266-83.
- [12] Krueger, H.; Koot, J.; Hall, R. E., et al.; *Stroke* **2015**, *46* (8), 2226-31.
- [13] Goldstein, L. B.; Adams, R.; Alberts, M. J., et al.; *Stroke* **2006**, *37* (6), 1583-633.

- [14] Skyschally, A.; Walter, B.; Schultz Hansen, R., et al.; *Naunyn Schmiedebergs Arch Pharmacol* **2013**, *386* (5), 383-91.
- [15] Ward, A. B.; *Eur J Neurol* **2012**, *19* (1), 21-7.
- [16] Hagen, A.; Dietze, A.; Dhein, S.; *Cardiovasc Res* **2009**, *83* (2), 405-15.
- [17] Jozwiak, J.; Dhein, S.; *Naunyn Schmiedebergs Arch Pharmacol* **2008**, *378* (5), 459-70.
- [18] Kjolbye, A. L.; Haugan, K.; Hennan, J. K., et al.; *Basic Clin Pharmacol Toxicol* **2007**, *101* (4), 215-30.
- [19] Xing, D.; Kjolbye, A. L.; Nielsen, M. S., et al.; *J Cardiovasc Electrophysiol* **2003**, *14* (5), 510-20.
- [20] Butera, J. A.; Larsen, B. D.; Hennan, J. K., et al.; *J Med Chem* **2009**, *52* (4), 908-11.
- [21] Laurent, G.; Leong-Poi, H.; Mangat, I., et al.; *Circ Arrhythm Electrophysiol* **2009**, *2* (2), 171-8.
- [22] De Vuyst, E.; Boengler, K.; Antoons, G., et al.; *Br J Pharmacol* **2011**, *163* (3), 469-83.
- [23] Rossman, E. I.; Liu, K.; Morgan, G. A., et al.; *J Pharmacol Exp Ther* **2009**, *329* (3), 1127-33.
- [24] Haugan, K.; Marcussen, N.; Kjolbye, A. L., et al.; *J Cardiovasc Pharmacol* **2006**, *47* (2), 236-42.
- [25] Chamberlain, M. C.; *Expert Rev Neurother* **2010**, *10* (4), 547-61.
- [26] Pardridge, W. M.; *Drug Discov Today* **2007**, *12* (1-2), 54-61.

- [27] Deli, M. A.; Abraham, C. S.; Kataoka, Y., et al.; *Cell Mol Neurobiol* **2005**, *25* (1), 59-127.
- [28] Solon, E. G.; Balani, S. K.; Lee, F. W.; *Curr Drug Metab* **2002**, *3* (5), 451-62.
- [29] Lee, B.; Clarke, D.; Al Ahmad, A., et al.; *J Clin Invest* **2011**, *121* (8), 3005-23.
- [30] Maniskas, M.; Bix, G.; Fraser, J.; *J Neurosci Methods* **2015**, *240*, 22-7.
- [31] Tsugita, A.; Kamo, M.; Kawakami, T., et al.; *J Protein Chem* **1998**, *17* (6), 520-1.
- [32] Brown, R. S.; Carr, B. L.; Lennon, J. J.; *J Am Soc Mass Spectrom* **1996**, *7* (3), 225-32.
- [33] Troxler, H.; Kleinert, P.; Schmutz, M., et al.; *Adv Clin Chem* **2012**, *57*, 1-28.
- [34] Schwartz, S. A.; Caprioli, R. M., Chapter 23 - Molecular imaging by mass spectrometry. In *Medical Applications of Mass Spectrometry*, Vekey, K.; Telekes, A.; Vertes, A., Eds. Elsevier: Amsterdam, 2008; pp 533-554.
- [35] Schwartz, S. A.; Reyzner, M. L.; Caprioli, R. M.; *J Mass Spectrom* **2003**, *38* (7), 699-708.
- [36] Yang, J.; Caprioli, R. M.; *Anal Chem* **2011**, *83* (14), 5728-34.
- [37] Gemperline, E.; Rawson, S.; Li, L.; *Anal Chem* **2014**, *86* (20), 10030-5.

**Chapter 4: Detection of Amyloid Beta Oligomeric  
Composition Using Matrix-Assisted Laser  
Desorption/Ionization Mass Spectrometry (MALDI MS)**

## 4.1 Introduction

Alzheimer's disease (AD) is now considered the most common cause of dementia, and the 6th leading cause of death in the United States with over 5 million North Americans suffering from this disease [1]. The adverse neuropsychiatric and behavioral symptoms patients suffer from pose as a significant strain on our health care system, and give rise to socioeconomic issues. Hallmarks of the disease include extracellular plaques characterized by the accumulation of protein-containing deposits primarily consisting of amyloid beta ( $A\beta$ ) peptides and intracellular neurofibrillary tangles caused by aberrant phosphorylation of tau [2-4]. Previous work found these large fibrillary  $A\beta$  structures within neuritic plaques killed cultured neurons [5]. This and other evidence led to the amyloid cascade hypothesis (ACH) which originally postulated that these insoluble fibrillary aggregates were the primary cause of neurodegeneration in AD patients [6]. Although extensive research has targeted these plaques, poor correlation between neurological deficits and plaque accumulation have been observed in AD patients [7-8].

Recent studies have shifted focus to examine the onset of  $A\beta$  aggregation from the monomeric peptides to the soluble form of  $A\beta$  multimeric complexes, and found evidence linking the accumulation of the  $A\beta$  oligomers to the progression and severity of AD, in particular, with long term hippocampal, age-onset memory failures [2-3, 9-12]. Due to these recent findings, modifications to the amyloid cascade hypothesis have been made to target the role of soluble  $A\beta$  oligomers in disease progression [13-15]. In healthy individuals,  $A\beta$  peptides are degraded within or cleared from the brain [16-17]. Reduction



in the degradation or clearance efficiency results in accumulation of the soluble oligomers that correlate with disease onset and progression. Understanding the mechanisms and effects of A $\beta$  oligomerization in the brain is therefore critical to the development of novel therapeutics for AD. A common experimental approach is the *in vitro* toxicity assay of A $\beta$  oligomers on neuron cell cultures, where cellular viability is quantified to determine the effects of various forms of A $\beta$  and/or potential therapeutics [18-22]. The A $\beta$  samples for the *in vitro* experiments are typically obtained from commercial sources. Numerous protocols have been reported for *in vitro* oligomeric A $\beta_{1-42}$  preparations with the largest variation residing in the monomerization and oligomerization solutions used [23-26]. Surprisingly, to our knowledge, comprehensive studies examining the effect of protocol conditions on the resulting oligomer size distribution are not available in the literature to our knowledge. In addition, it is not a common practice to verify the composition of the A $\beta$  oligomers prior to use, partly due to the limitations in techniques available for fast and simple A $\beta$  multimer characterization.

Currently, the most common means for oligomer quantification is gel electrophoresis [27]. The technique depends on the ability for SDS to bind to proteins of interest. This binding compromises the structural integrity of proteins resulting in dissociation of oligomer composition [28]. Low sample throughput and prevalence of gel smearing are also significant issues which act as limitations in resolution and possess accuracy issues [29]. Another prominent issue gel electrophoresis possesses is the inability to accommodate for a large mass range for multimer analysis. The percent composition of acrylamide within the gel is tailored for the target sample. The larger the peptide or protein under analysis, the lower the amount of acrylamide used in order to facilitate appropriate separation to

obtain distinct bands. For samples containing a wide range of molecular weights, the set acrylamide concentration could not optimally accommodate for both extremes, resulting in either the smaller molecular weight peptides to run off the gel, or poor resolution of the larger peptides. Other techniques available to study A $\beta$  aggregation include atomic force microscopy (AFM), surface plasmon resonance (SPR), absorbance and fluorescence [30-31]. AFM is generally suitable for detection of large A $\beta$  aggregates such as fibrils, but not the soluble small oligomers. SPR is typically used to detect interactions in amyloid-ligand binding, but ligand interaction is not selective enough to differentiate oligomers by size. Likewise, absorbance and fluorescence can detect the bulk presence of oligomers, but lacks the ability to differentiate between small size differences of A $\beta$  oligomers.

Electrospray ionization mass spectrometry (ESI MS) has been widely used as an alternative label free tool for A $\beta$  analysis [32-34]. ESI is capable of transforming the multimeric forms of amyloidogenic peptides from solvated to gaseous ions as intact non-covalent complexes [35]. However, the resulting complex ions can possess a wide range of multiple charges; for example,  $z = 2$  to 10. Oligomers of different sizes can therefore have identical  $m/z$ , making the peak assignment to oligomer sizes a perplexing task [36-37]. To overcome this, researchers turned to the use of ion mobility spectrometry (IMS), which can resolve the multimeric complex ions, not only by  $m/z$ , but also according to size based on their mobility in a drift tube [38-40]. In recent years, the combination of IMS with ESI MS has become an invaluable tool in deciphering the assembly mechanism of A $\beta$  oligomers [28, 39, 41-45]. While IMS-MS is extremely powerful, the resulting two-dimensional data of drift time and  $m/z$  generally require interpretation by IMS specialists. Hence, its applications remain limited in the neuroscience community.

The work described herein focuses on a simpler mode of MS based on matrix assisted laser desorption ionization (MALDI). In contrast to ESI, MALDI generates gaseous ions of peptides and proteins predominately in the singly charge state ( $z = 1$ ). As a result, the measured  $m/z$  values of A $\beta$  oligomers directly represent the mass of the oligomers. To our knowledge, Van Duyne *et al.* presented the first use of MALDI MS to detect oligomers of A $\beta_{1-42}$ , but the use of MALDI MS was not the focus of their work, and only one mass spectrum of the oligomers was presented as a supplementary figure [46]. Also, the adoption of this application has not been observed in the literature. Most importantly, the authors did not present validation experiments to confirm that the observed A $\beta$  complex ion distribution indeed reflect that of original oligomeric A $\beta$  sample solution. In the work described herein, we will examine the validity of MALDI MS in measuring the composition of A $\beta$  multimers. Particularly, we aim to rule out the non-specific associations of A $\beta$  peptides, either during sample preparation or during the MALDI process, which could produce artificial A $\beta$  complexes non-existent in the original sample. To achieve this, we manipulated the size distribution of A $\beta$  oligomer samples using molecular weight cut off filters, and subsequently illustrated the expected changes in the resulting MS data. After validating MALDI MS in measuring A $\beta$  multimeric composition, the method has been applied to examine the A $\beta$  samples prepared using published protocols on monomerization and oligomerization for *in vitro* toxicity assays.

## 4.2 Experimental

### 4.2.1 Apparatus

A $\beta$  samples were filtered using 10 kDa and 30 kDa MWCO filters purchased from Pall Corporation (Ann Arbor, MI), followed by use of Centrifuge 5417c from Eppendorf (Westbury, NY). ThermoFisher Scientific NanoDrop<sup>TM</sup> Spectrophotometer 2000c (Waltham, MA) was used to assess the final filtrate concentration of A $\beta$  samples after filtration. All MALDI MS sample analyses were performed on a Sciex TOF/TOF 5800 MALDI mass spectrometer equipped with a 1 kHz OptiBeam<sup>TM</sup> On-Axis Nd:YAG laser system (Ontario, Canada). All microscopy data was acquired using a Nikon Eclipse Ni-E microscope with fluorescent filters and a DS-Qi<sub>2</sub> monochrome microscope camera. ImageJ software was used to process and analyze the data collected. Statistical comparisons between experimental groups were performed using the GraphPad Prism software. A two-way ANOVA with Tukey's HSD test was applied.

### 4.2.2 Samples and Reagents

All A $\beta$  peptides were purchased from Bachem (King of Prussia, PA). Ethanol, methanol, and acetonitrile (ACN) were purchased from Caledon (Ontario, Canada), and hexafluoro-2-propanol (HFIP), dimethyl sulfoxide (DMSO), Sinapinic acid (SA), trypsin, amphotericin B solution, 7% poly-L-ornithine from Sigma Aldrich (St. Louis, MO). Phosphate buffered saline (PBS) was purchased from Quality Biologicals (Gaithersburg,

MD). Ham's F-12 nutrients mixture, B27 supplement, N2 supplement, penicillin/streptomycin, glutamax, and 4'-6-diamidino-2-phenylindole (DAPI) were purchased from Life Technologies (Grand Island, NY). Formic acid, ammonium hydroxide was obtained from EM Science (Darmstadt, Germany), and trifluoroacetic acid (TFA) was purchased from Fischer Scientific (Ottawa, ON, Canada). Neurons were isolated from Wistar rats purchased from Charles River (Montreal, QC, Canada), Hank's balanced salt solution (HBSS) and neural basal media from Wisent (St. Jean-Baptiste, QC, Canada), Trypsin inhibitor from Roche Life Sciences (Indianapolis, IN) and propidium iodide (PI) was purchased from Biotium (Hayward, CA).

#### *4.2.3 Amyloid Beta Sample Preparation*

A $\beta$  peptides were suspended in one of the lyophilization solvents (NH<sub>4</sub>OH, TFA, HCO<sub>2</sub>H, or HFIP) at a concentration of 1 mM to facilitate monomerization. To prepare for short term storage, the sample was fractionated in 10  $\mu$ L aliquots and lyophilized for 1 hour at -100 °C and stored at -80 °C. To prepare for use, each aliquot of lyophilized powder was resuspended in 10  $\mu$ L of DMSO and sonicated in a 37 °C water bath for 10 minutes. The sample was then brought to a concentration of 150  $\mu$ M with the selected incubation solvent (F12, PBS, or H<sub>2</sub>O) and vortexed. The solution was incubated at 4°C for 24 hours to facilitate oligomerization.

#### *4.2.4 Molecular Weight Cut-Off Filtration*

A $\beta$  samples monomerized in NH<sub>4</sub>OH followed by resuspension in either PBS, or H<sub>2</sub>O were used for MWCO Filtration assessments. Aliquots of 70  $\mu$ L were pipetted into each filter and centrifuged 4 times in 30 second intervals at 14 000 rpm with Centrifuge 5417c from Eppendorf (Westbury, NY). Once filtered, 1  $\mu$ L of each sample filtrate was pipette onto the NanoDrop<sup>TM</sup> spectrophotometer. The A280 protein/peptide analysis software was used to assess the concentration of each filtrate through monitoring the absorbance at wavelength ( $\lambda$ ) 280 nm. MWCO Filters at 10 kDa and 30 kDa were purchased from Pall Corporation (Ann Arbor, MI).

#### *4.2.5 Amyloid Beta Toxicity for Embryonic Rat Cortical Neuron Cultures*

A $\beta$  samples lyophilized in NH<sub>4</sub>OH and resuspended in DMSO and F12 medium to 150  $\mu$ M was used. An A $\beta$ <sub>1-42</sub> sample was prepared and incubated for 24 hours while a second sample was prepared at the time of use providing the oligomer and monomer conditions respectively. Three different environmental conditions were provided for each cell population (n = 4) with 10  $\mu$ L additions of pre-incubated A $\beta$ <sub>1-42</sub> (monomer), and post incubation A $\beta$ <sub>1-42</sub> (oligomer). One set of cultures were left without any environmental alterations to provide a baseline (control) of the natural decrease in cellular viability over time. The cells were incubated for 6, 24, 36, and 48 hours. PI staining was applied through addition of 10  $\mu$ L of PI 45 minutes prior to fixation. The cells were fixed with 500  $\mu$ L of 4% formaldehyde followed by 400  $\mu$ L of 2% formaldehyde. The fixing agent was removed

with 3 consecutive 1x PBS washes. Fine tweezers were used to plate the cells fixed on 12 mm round cover slips. The cells were counter-stained with DAPI for nuclear visualization and imaged were acquired at 20x magnification. Five images were acquired for each cell culture in order to obtain the average cell deaths vs. total cells per culture.

#### *4.2.6 MALDI MS Analysis*

SA matrix was prepared to 10  $\mu\text{g}/\mu\text{L}$  in 50% ACN and 0.05% TFA. The A $\beta$  sample and SA matrix were deposited as sandwiched layers, where 0.75  $\mu\text{L}$  of the A $\beta$  solution was spotted between two layers of SA (0.75  $\mu\text{L}$ ). The spots were washed twice with 1  $\mu\text{L}$  water prior to analysis. The TOF TOF Series Explorer in positive ion linear mode and Data Explorer were used for data acquisition and processing respectively.

### **4.3 Results and Discussion**

#### *4.3.1 MALDI MS Detection of A $\beta_{1-42}$ and A $\beta_{1-40}$ Oligomer Composition*

We began our studies by reproducing the detection of A $\beta$  oligomers with MALDI MS based on the conditions reported by Van Duyne [46]. Briefly, hexafluoro-2-propanol (HFIP) and F12 medium were respectively the monomerization and oligomerization buffers. Sinapinic acid (SA) was the MALDI matrix, and the same spotting was used with a modification of including a washing step. Effects of different TFA concentrations in the matrix solution was assessed, and we concluded that a reduction in TFA concentrations was most beneficial

in the detection of oligomers within the sample. This coincides with previous studies indicating low pH disruptions in the formation of non-covalent complexes [47-48]. The instrument's acquisition parameters were set to optimize for detection sensitivity.

Additional to studying oligomers from A $\beta$ <sub>1-42</sub>, we also included the commonly studied A $\beta$ <sub>1-40</sub>. Similar results confirming the successful detection of A $\beta$  oligomers of various sizes were observed for both A $\beta$ <sub>1-40</sub> and A $\beta$ <sub>1-42</sub>. The mass spectra from A $\beta$ <sub>1-40</sub> and A $\beta$ <sub>1-42</sub> oligomers are shown as Figure 4.1. The monomeric A $\beta$ <sub>1-40</sub> and A $\beta$ <sub>1-42</sub> peptides have a molecular weight of 4329.86 Da and 4514.10 Da respectively. Doubly charged monomers and trimers were not observed, the mass spectrum therefore displayed signals from singly charged ions from monomers up to 7-mer and 11-mer when the full mass range up to 50 kDa was acquired for A $\beta$ <sub>1-42</sub> and A $\beta$ <sub>1-40</sub> respectively. Compared to the prior report on MALDI MS results of A $\beta$  oligomers [46], the same overall trend in oligomer size distribution was detected. Specifically, the monomer and dimer signals were the strongest with the dimer peak slightly higher in intensity. The signals dropped off in a similar decay fashion for larger complexes, although higher peak intensities from the larger oligomers were shown. Differences in sensitivity could be attributed to the different MALDI mass spectrometers used. The MALDI results also generally agree with those reported by gel electrophoresis, where substantial quantities of multimers relative to the monomer were typically detected, as bands of similar size and darkness. The sensitivity was however much higher for MALDI MS, as it required only 0.5  $\mu$ g per run, compared to the typical 190 – 100  $\mu$ g per run in gel electrophoresis. When compared to ESI MS, rather different looking mass spectra were reported with similar samples. A dominant peak corresponding to the



monomer, with a  $-3$  charge state, is typical in the ESI spectra of  $A\beta_{1-42}$ . The sum of all oligomeric peaks were only a minor part of the total response [42].

#### *4.3.2 Validation of MALDI MS Detection Capabilities*

To prepare for MALDI MS analysis, sample solutions were mixed with laser absorbing matrices, deposited as microliter-volume droplets on target plates, and allowed to dry. Hence, a common concern in the MALDI MS characterization of complexes is the possibility of artificial non-specific associations during drying. In the literature, numerous examples of MALDI MS application on complexes of biomolecules were reported and reviewed [47, 49-50]. The consensus is that the technique is capable of detecting certain non-covalent multimeric complexes under optimized conditions. However, there is not one universally optimal protocol. Therefore, it is important to experimentally verify that the  $A\beta$  non-covalent complexes detected by MALDI MS herein were not an artifact caused by non-specific associations that occurred either during sample spot drying or within the mass spectrometer in gas phase.

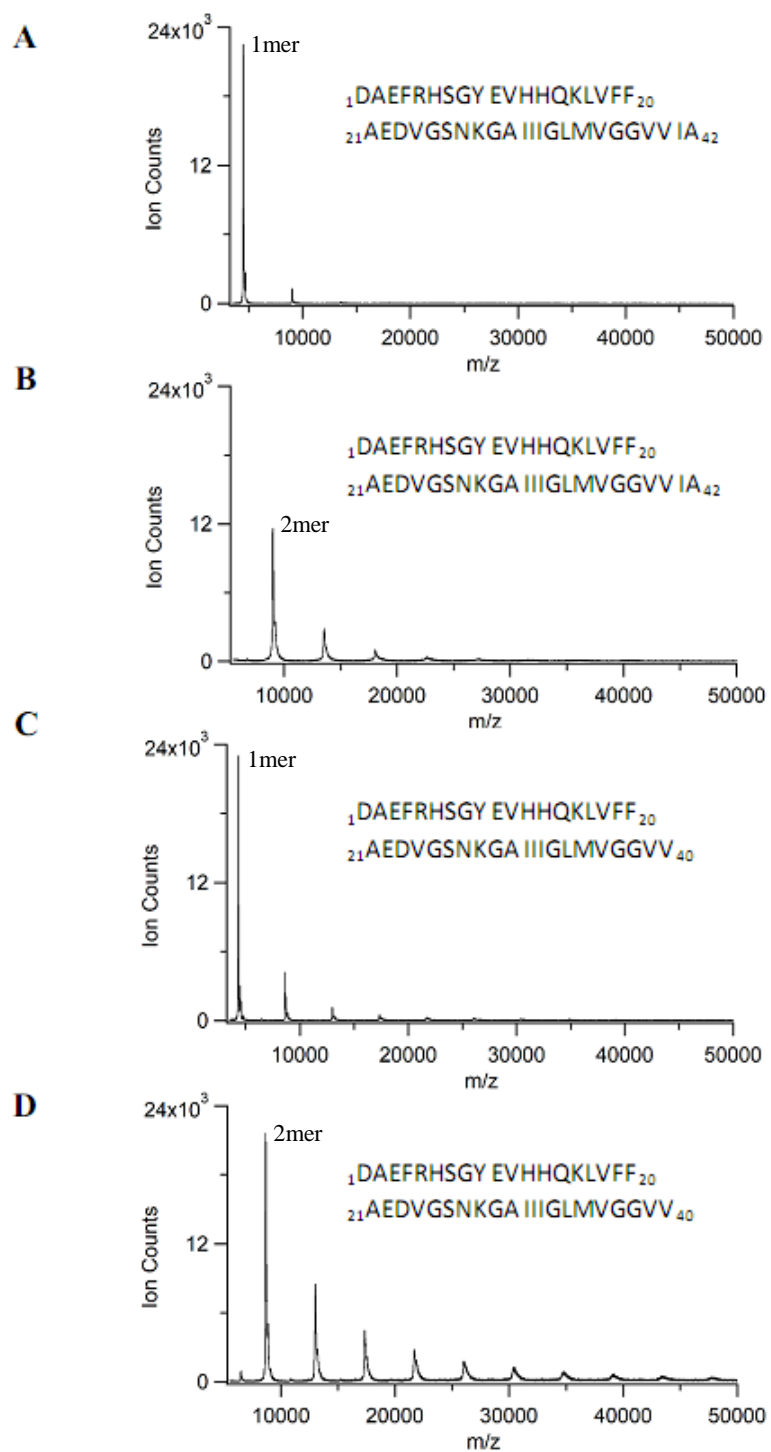


**Figure 4.1** Mass spectra of oligomers prepared from A $\beta$ <sub>1-42</sub> (A-B) and A $\beta$ <sub>1-40</sub> (C-D) displayed singly charged ions upon analysis of the full mass range (A, C). Exclusion of the monomer (B, D) resulted in oligomers up to 50 kDa in mass observed.

#### *4.3.2.1 Analysis of A $\beta$ Fragments with Various Propensities for Oligomerization*

To achieve this, modified A $\beta_{1-40}$  samples with different oligomerization propensities used in toxicity experiments were investigated. Oligomerization of wild-type A $\beta_{1-40}$  sample was compared to a scrambled A $\beta_{1-40}$  sequence, and (Gln<sup>22</sup>) A $\beta_{1-40}$  (Figure 4.2). Scrambled A $\beta_{1-40}$  samples are used in AD research as inactive controls, and therefore does not have an affinity for oligomerization [51]. In contrast, (Gln<sup>22</sup>) A $\beta_{1-40}$  (E22Q) is a mutation which replaces Glu<sup>22</sup> with Gln<sup>22</sup>, this mutation of A $\beta$  was found to aggregate more readily in comparison to the wild-type peptide [52-55]. The resulting MS data presented in Figure 4.2 reflect the reported variation in oligomerization affinities. Focus was placed starting from the expected  $m/z$  of the dimer in order to focus comparison on oligomer composition within samples. Through comparison of these three peptide samples, minimal oligomerization limited to presence of a dimeric peak was detected for scrambled A $\beta_{1-40}$  peptide, while the E22Q mutation clearly presented a much higher propensity for oligomerization in comparison to the wild-type.

#### 4.3.2.2 Molecular Weight Cut-Off Filtration Analysis

Additional validation was achieved through manipulation of the A $\beta$ <sub>1-40</sub> oligomer composition by passing them through molecular weight cut-off (MWCO) filters at either 10 kDa or 30 kDa cut-off points. The 10 kDa cut-off filter should in theory remove complexes larger than dimers (8659.72 Da). The resulting mass spectrum indeed revealed the expected reduction in signals from the large oligomers (Figure 4.3). A moderate suppression of the dimer signal was also observed. In comparison, when the A $\beta$ <sub>1-40</sub> oligomers were filtered at the 30 kDa cut-off point, the monomer to dimer and trimer ratios were largely unchanged. Signal reduction was observed for tetramer ( $m/z$  17,320.44) and larger species. Taking into account of non-specific adsorption and imprecision in filter cut-off points, the collective MS results were found to be in agreement with the expected changes in oligomer composition resulting from the MWCO treatments.

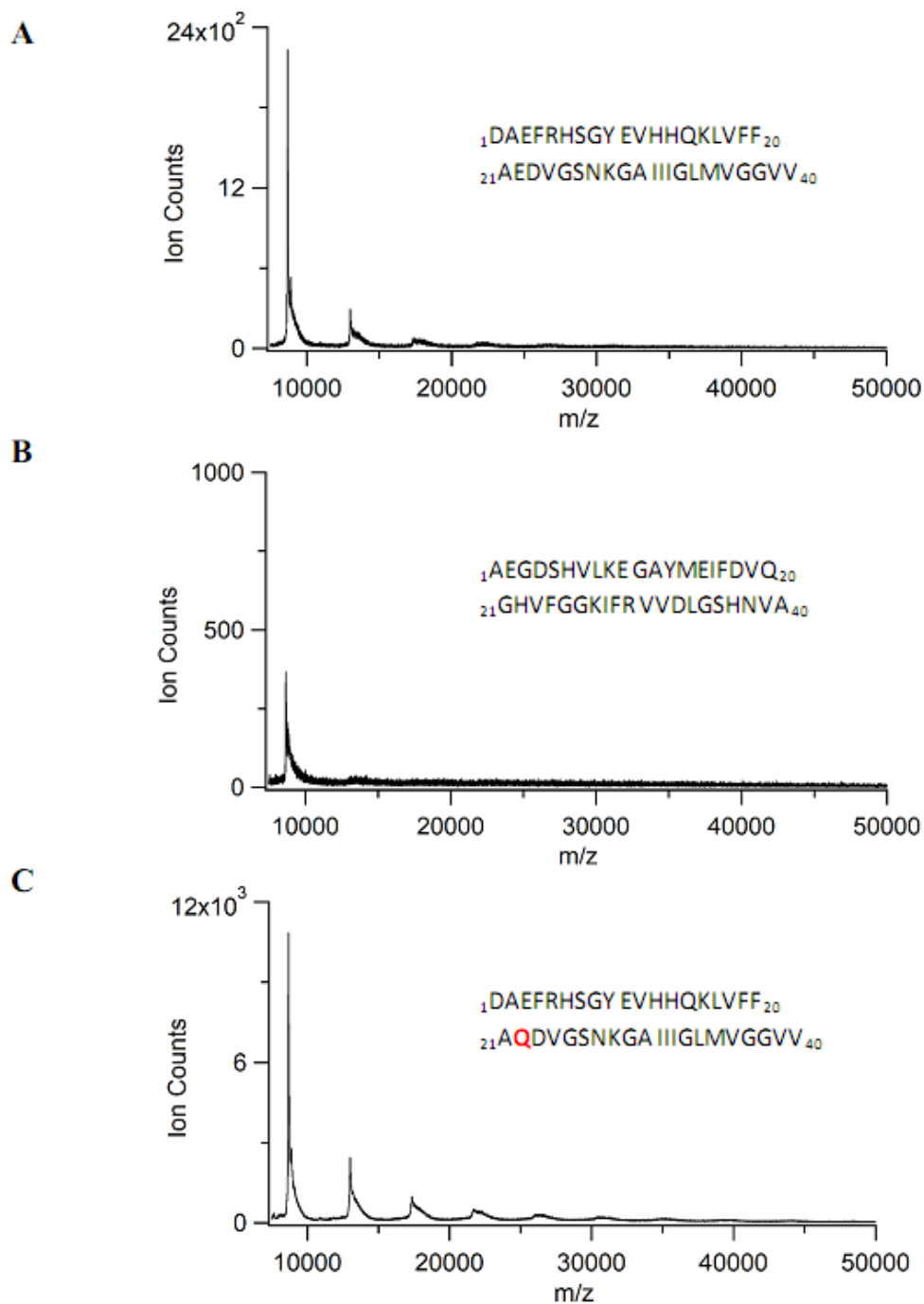


**Figure 4.2** Oligomerization of wild-type A $\beta_{1-40}$  (A) was compared to scrambled A $\beta_{1-40}$  (B), and mutated (Gln<sup>22</sup>) A $\beta_{1-40}$  (C). Through comparison, modifying Glu<sup>22</sup> with Gln<sup>22</sup> in the peptide sequence resulted in an A $\beta_{1-40}$  peptide which aggregates much more readily while the scrambled version of the peptide produced minimal to no oligomerization.

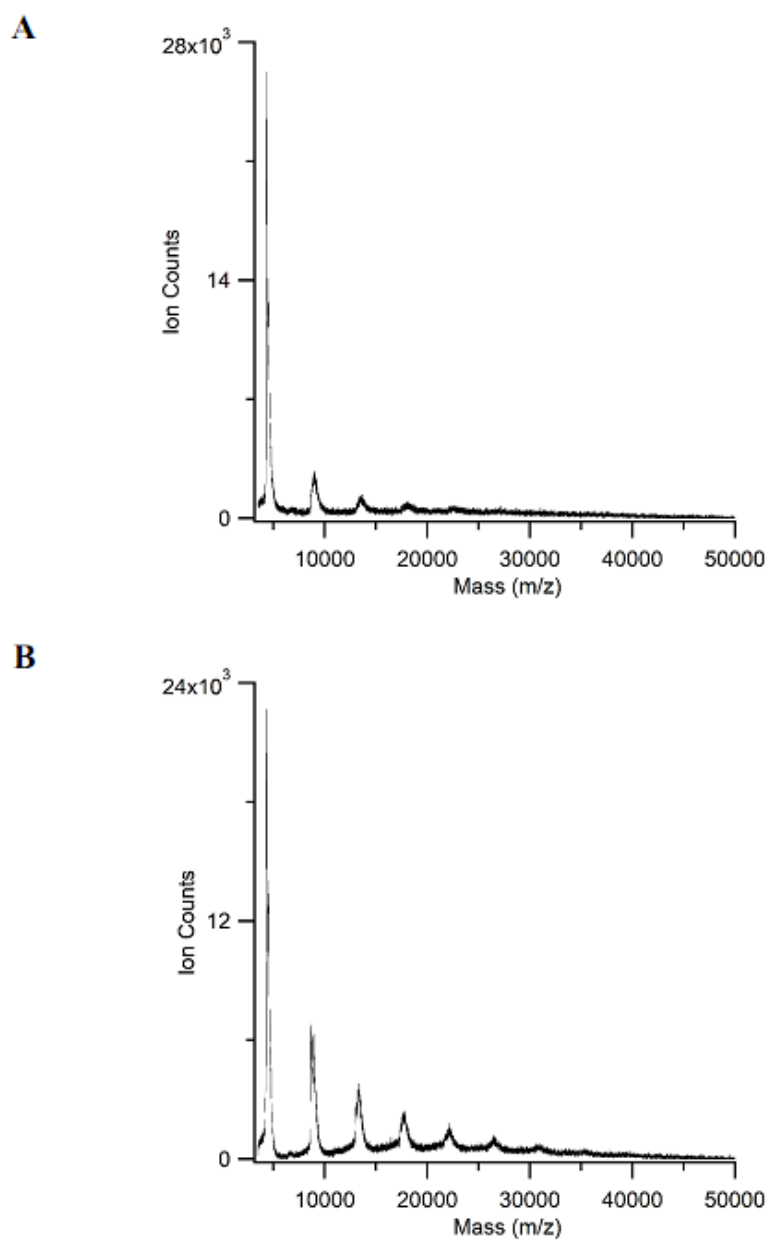


**Figure 4.3** Mass spectra of oligomerized A $\beta$ <sub>1-40</sub> after passing through 10 kDa (A) and 30 kDa (B) filters. Prior to filtration, oligomeric peaks up to 50 kDa were observed. After filtration, peaks detected correlate directly with the filter size used.

The effects of reduction in sample concentration following MWCO treatments were addressed through determination of final filtrate concentration followed by serial dilutions of standard A $\beta$ <sub>1-40</sub> samples. The filtrate concentration was found to be approximately three times lower than stock concentrations. Respective dilution of stock samples were analyzed and a full range of oligomers were detected (Figure 4.4). This allowed us to draw the important conclusion that, despite the harsh, non-native, nature of MALDI MS, it is capable of revealing the oligomeric composition of A $\beta$  complexes in solution. The results in Figure 4.3 did not support any significant levels of non-specific associations of A $\beta$ . The A $\beta$  complexes detected by MALDI closely agreed with expected oligomeric compositions of the solution samples. Finally, the intensity of the MALDI MS signals of these oligomers corresponded to their concentration at least in a semi-quantitative fashion. It is however noteworthy that the detection of very large A $\beta$  oligomers, if present, is limited by the sensitivity of the MS.

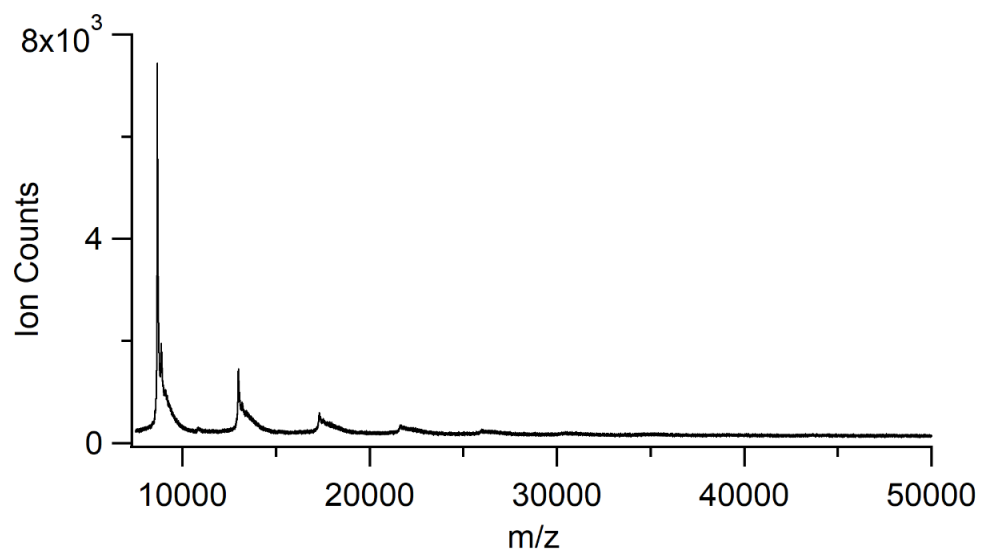


**Figure 4.4** Oligomer samples of  $A\beta_{1-40}$  were prepared and diluted to 50  $\mu\text{M}$  concentrations. Oligomer detection was not compromised from dilutions indicating loss of sample during filtration process would not result in results obtained.



### 4.3.3 Effects of Variations Among Amyloid Beta Preparatory Protocols

Having established MALDI MS to be a technique that can gauge the composition of A $\beta$  oligomers, we aim to further demonstrate its capability as a quality control methodology that monitors the on-set of *in vitro* A $\beta$  oligomerization. As previously mentioned, there are several published protocols of *in vitro* preparation of A $\beta$  oligomers [56-62]. All of them involve the two major steps of; firstly, solubilizing the lyophilized A $\beta$  as presumably monomers; and secondly, incubating the samples for oligomer formation. However, a noticeable difference among published protocols is the choice of solvents or solutions in facilitating these two monomerization and oligomerization steps. Yet the assessment of possible differences in the resulting samples has not been reported to our knowledge. Hence, we conducted the investigation with MALDI MS, first looking at the effect of the monomerization condition followed by that of the oligomerization condition.

#### 4.3.3.1 Monomerization Solvents

The purpose of the monomerization step is to break up previously formed A $\beta$  clusters, and in turn, to promote the formation of  $\beta$  sheets upon oligomerization. A $\beta$  has a high affinity for oligomerization as a result of the hydrophobic amino acid composition. When in aqueous environments, aggregation provides the stability needed therefore making the initial monomerization a crucial step preceding oligomerization. The A $\beta$  clusters must be broken apart prior to the formation of the desired  $\beta$  sheets of the oligomer structure. The

commonly used solvents or solutions are, hexafluoro-2-propanol (HFIP), HCO<sub>2</sub>H, and trifluoroacetic acid (TFA). Acidic solvents provide the low pH which disrupts the quaternary structure of non-covalent complexes. HFIP, HCO<sub>2</sub>H, and TFA are believed to remove A $\beta$  non-specific aggregates and fibrils within a sample [63]. In addition, we also included NH<sub>4</sub>OH in this studies, which was believed to promote monomerization of A $\beta$  and thus others have recently adopted its use [24-25, 59-60]. To begin our assessment, four A $\beta$  samples were prepared with each of these four solvents and lyophilized. MALDI MS analysis was then performed on the resulting “monomerized” A $\beta$  samples. To enhance the sensitivity in the detection of the non-covalent complexes, the spectra were re-acquired beginning at 6500 Da for the purpose of reducing the suppressing effects from the saturating signals of the monomer. The mass spectra shown in Figure 4.5 were each normalized to its monomer intensity. The results revealed that significant amounts of multimers were present in the “monomerized” samples prepared from all three of the most commonly used protocols (HFIP, HCO<sub>2</sub>H, and TFA). The oligomeric complexes were most noticeable from samples prepared with HFIP and HCO<sub>2</sub>H. Only the A $\beta$  sample prepared with NH<sub>4</sub>OH resulted in predominantly monomers. This somewhat unexpected finding illustrates the importance of verifying the A $\beta$  composition prior to use.

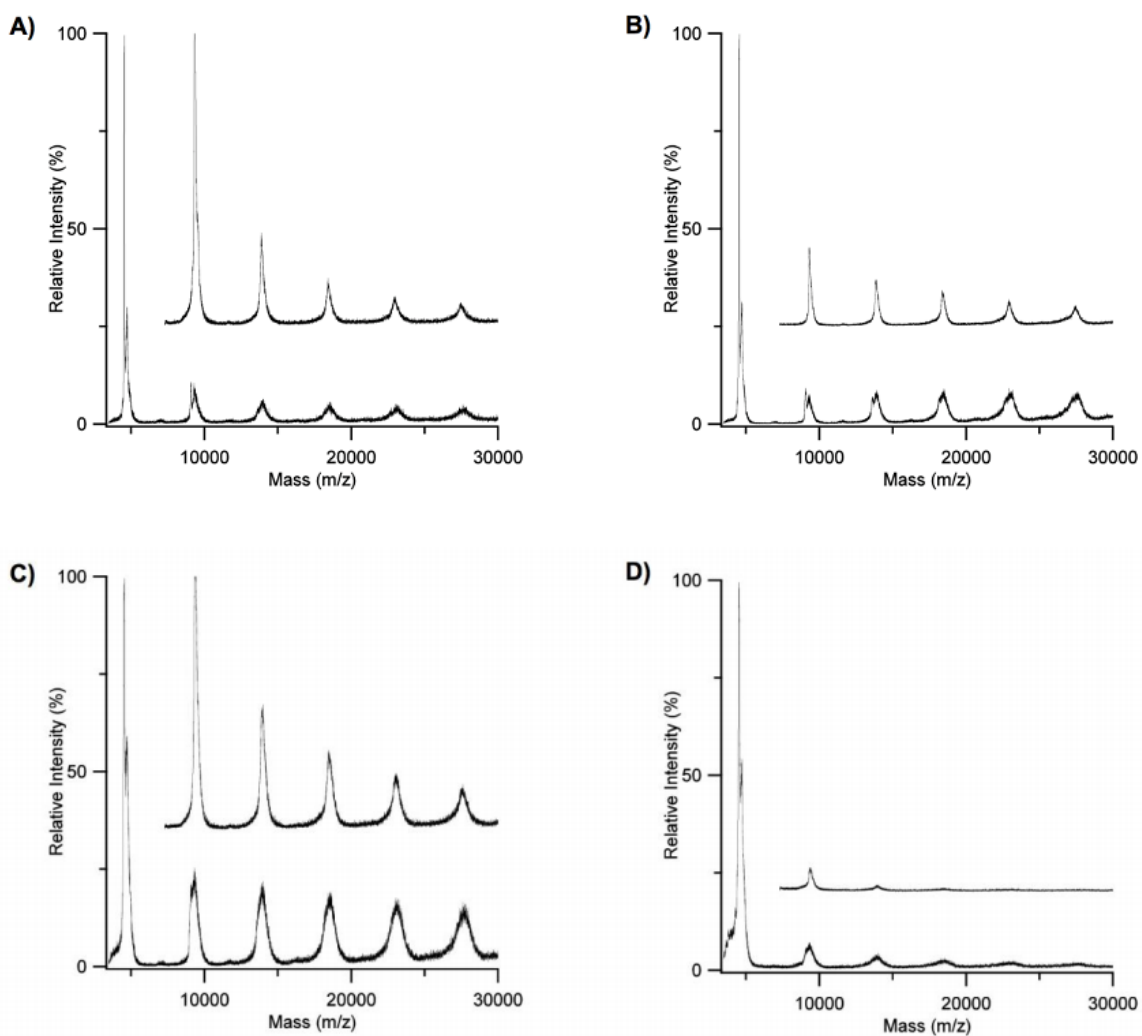


**Figure 4.5** Mass spectra of  $A\beta_{1-40}$  after treatment with four monomerization solutions: HFIP (A), HCO<sub>2</sub>H (B), TFA (C) and NH<sub>4</sub>OH (D). To enhance the sensitivity in the detection of the larger oligomers, the upper spectra were acquired beginning at 6500 Da for the purpose of reducing the suppressing effects from the monomers.

#### *4.3.3.2 Oligomerization Solvents*

The effect of the oligomerization condition on A $\beta$  oligomer composition was examined next. Among the published protocols, PBS and Ham's F12 medium were most widely used in oligomeric A $\beta$  preparation [46, 58, 61, 64]. Additional to these two solutions, we also included the use of deionized water in the comparison. Using these three oligomerization solutions, we performed incubation on each of the four samples monomerized by HFIP, HCO<sub>2</sub>H, TFA and NH<sub>4</sub>OH. Our MALDI MS results revealed a substantial degree of oligomerization across all four samples, in all three oligomerization solutions. The four sets of mass spectra were essentially indistinguishable from one another, and so only the results from the HFIP-monomerized sample are shown as an example (Figure 4.6). HFIP was selected as it was most commonly used in literature. The oligomer distributions from the three oligomerization solutions in Figure 4.6 were not distinctly different from each other. Hence, we concluded that the choice of the oligomerization solvent/solution was not a critical factor to the extent of oligomer formation. We believe that A $\beta$  favors the oligomerized state due to the protein's hydrophobic characteristics, and therefore oligomerization proceeded spontaneously and favorably regardless of the choice of solvent or solution. However, the critical factor resides in the incubation period needed to facilitate the formation of oligomers. When compared with MS results prior to incubation, significantly stronger signals from multimers were observed following incubation.

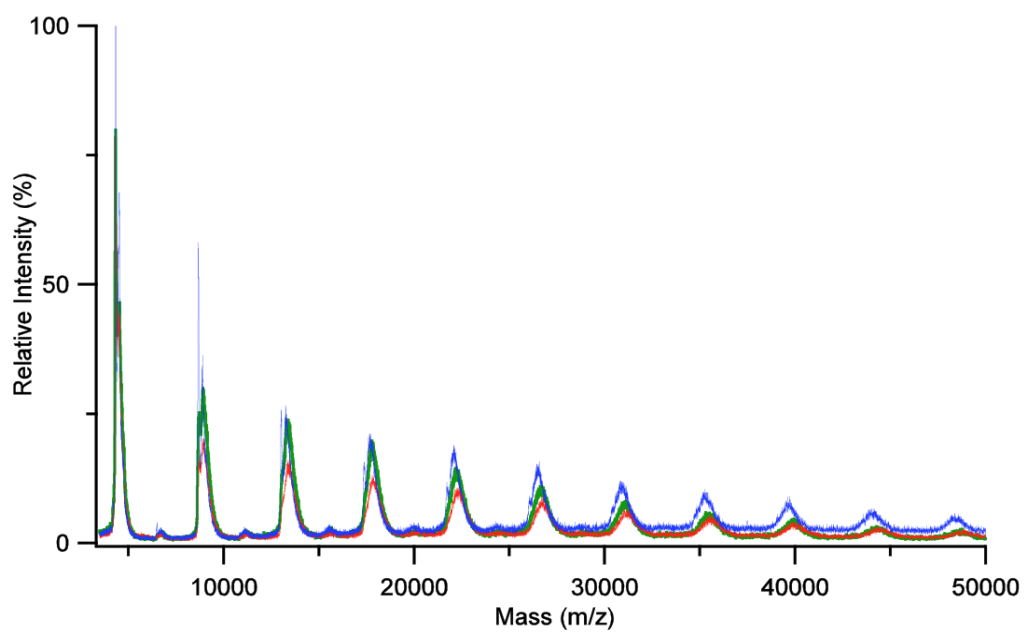


**Figure 4.6** Mass spectra of oligomerized A $\beta$ <sub>1-40</sub> prepared in two oligomerization solutions, PBS (blue) and F12 (green), and in water (red).

#### 4.3.4 *In Vitro* Amyloid Beta Toxicity Assessment

Aside from determining which monomerization or oligomerization conditions work best for A $\beta$ , the more critical message of this work is the importance of experimentally verifying the composition of A $\beta$  multimers prior to use. In this case, all three of the most commonly used monomerization protocols actually resulted in significant amounts of A $\beta$  oligomers; namely a 20-25% dimer to monomer ratio was observed after monomerization, which overlaps with 25-30% ratio observed after oligomerization. Given that the oligomeric form of A $\beta$  is mainly responsible of its deleterious effect on neurons, the use of such false A $\beta$  “monomers” would have led to results conflicting with the literature. To illustrate this point, data from an *in vitro* toxicity assay on embryonic rat cortical neuron cell cultures are presented. The average cell death percentage was determined in 48 hours under the treatment of A $\beta$  oligomers and the verified A $\beta$  monomers prepared by NH<sub>4</sub>OH, and a control of no treatment was also included (Figure 4.7). The results obtained from the monomer treatment were indistinguishable from the control in all time points measured. In contrast, an accelerated rate of cell death was observed upon treatment with A $\beta$  oligomers. At 24 hours, the toxicity of the oligomer sample treatment began to display a notable difference when compared to the monomer sample ( $P = 0.07$ ). As the treatment was extended for 36 hours, the toxicity of the oligomer treatment was significantly higher than that of the control ( $P = 0.002$ ). Once the treatment was carried out for 48 hours, statistically significant differences in toxicity between the oligomeric sample and that of the control and monomeric samples were observed ( $p = 0.03$  and  $0.01$  respectively). In the literature, reports on the effect of A $\beta$  oligomers varied depending on conditions such as cell culture

preparation methods, stains, and dosage. For example, one reported a decrease in cellular viability from 90% to 55% upon exposure to A $\beta$  oligomers while another reported 20% cellular viability after 48 hours [65-66]. Importantly, our results reaffirmed the significant toxicity of the oligomeric form of A $\beta$ , in comparison to the monomeric A $\beta$  and the control, and MALDI MS played an important role of rapid validation of A $\beta$  sample composition for the toxicity experiments.

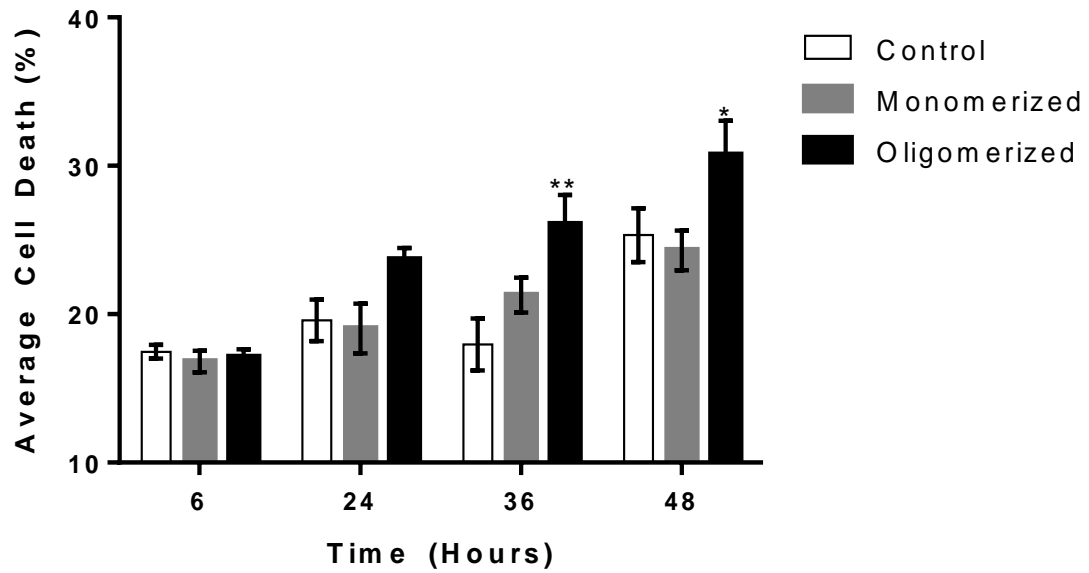


**Figure 4.7** Rat cortical neuron cell death determined under the treatment of  $A\beta_{1-42}$  monomers and oligomers. Results are presented as the mean with S.E.M. (n=4). \*:  $P \leq 0.05$ , \*\*:  $P \leq 0.01$  (two-way ANOVA with Tukey's HSD test).



## 4.4 Conclusion

In this work the capabilities of MALDI MS as a sensitive, fast, and simple method in the detection of *in vitro* A $\beta$  oligomers was demonstrated. The results were validated through use of MWCO filters to ensure the MS data reflects the sample composition in solution. The methodology allowed us to investigate the effect of preparation conditions on the resulting monomeric/multimeric composition, particularly in tracking the onset of oligomerization by monitoring the formation of 2-mer to 10-mer. In terms of applications, MALDI MS allows researchers to quickly characterize their A $\beta$  multimeric composition prior to studying their role in neurodegeneration, and/or evaluating potential neuroprotective agents against A $\beta$ . The importance of quality control on the A $\beta$  composition was demonstrated through an *in vitro* toxic assay on neuron culture, where MALDI MS played a critical role in identifying a fully monomerized sample of A $\beta$ . Finally, the detection of A $\beta$  oligomers with MALDI MS presents an exciting opportunity for *ex vivo* characterization of A $\beta$  extracted from the brain, or direct MALDI MS imaging of multimeric A $\beta$  in brain tissues, although further research and development is required to overcome the potential issue of background interferences and signal suppression.

## 4.5 References

- [1] Murphy, S. L.; Xu, J.; Kochanek, K. D.; National vital statistics reports : from the Centers for Disease Control and Prevention, National Center for Health Statistics, National Vital Statistics System **2013**, 61 (4), 1-117.
- [2] Lauren, J.; Gimbel, D. A.; Nygaard, H. B., et al.; *Nature* **2009**, 457 (7233), 1128-32.
- [3] Wilcox, K. C.; Lacor, P. N.; Pitt, J., et al.; *Cell Mol Neurobiol* **2011**, 31 (6), 939-948.
- [4] Crescenzi, O.; Tomaselli, S.; Guerrini, R., et al.; *European Journal of Biochemistry* **2002**, 269 (22), 5642-5648.
- [5] Gong, Y.; Chang, L.; Viola, K. L., et al.; *Proceedings of the National Academy of Sciences* **2002**, 100 (18), 10417-10422.
- [6] Harman, D.; *Journal of the American Aging Association* **2000**, 23 (3), 147-161.
- [7] Klein, W. L.; Krafft, G. A.; Finch, C. E.; *Trends in Neurosciences* **2001**, 24 (4), 219-224.
- [8] Viola, K. L.; Klein, W. L.; *Acta Neuropathol* **2015**, 129, 183-206.
- [9] Kotilinek, L. A.; Bacskai, B.; Westerman, M., et al.; *Journal of Neuroscience* **2002**, 22 (15), 6331-6335.
- [10] Giordano, C. R.; Terlecky, L. J.; Bollig-Fischer, A., et al.; *Scientific Reports* **2014**, 4 (4983).
- [11] Walsh, D. M.; Klyubin, I.; Fadeeva, J. V., et al.; *Nature* **2002**, 416 (6880), 535-539.
- [12] Ferreira, S. T.; Klein, W. L.; *Neurobiol Learn Mem* **2011**, 96 (4), 529-543.
- [13] Hung, L. W.; Ciccotosto, G. D.; Giannakis, E., et al.; *Journal of Neuroscience* **2008**, 28 (46), 11950-11958.
- [14] Dahlgren, K. N.; Manelli, A. M.; Stine, W. B., Jr., et al.; *J Biol Chem* **2002**, 277 (35), 32046-53.
- [15] Stroud, J. C.; Liu, C.; Teng, P. K., et al.; *Proc Natl Acad Sci U S A* **2012**, 109 (20), 7717-22.

- [16] Hardy, J.; Selkoe, D. J.; *Science* **2002**, *297* (5580), 353-356.
- [17] Trimpin, S.; Deinzer, M. L.; *J Am Soc Mass Spectrom* **2007**, *18* (8), 1533-43.
- [18] Ebenezer, P. J.; Weidner, A. M.; LeVine, H., et al.; *Journal of Alzheimers Disease* **2010**, *22* (3), 839-848.
- [19] Ai, Z. B.; Li, C. Y.; Li, L. T., et al.; *Mol Med Rep* **2015**, *11* (4), 2429-2434.
- [20] Alomari, A. K.; Glusac, E. J.; Choi, J., et al.; *J Cutan Pathol* **2015**, *42* (10), 757-64.
- [21] Cizas, P.; Jekabsone, A.; Borutaite, V., et al.; *Medicina-Lithuania* **2011**, *47* (2), 107-112.
- [22] Kelley, A. R.; Perry, G.; Castellani, R. J., et al.; *ACS Chem Neurosci* **2016**, *7* (3), 261-268.
- [23] Jan, A.; Hartley, D. M.; Lashuel, H. A.; *Nat Protoc* **2010**, *5* (6), 1186-1209.
- [24] Ryan, T. M.; Caine, J.; Mertens, H. D., et al.; *PeerJ* **2013**, *1*, e73.
- [25] Teplow, D. B.; Amyloid, Prions, and Other Protein Aggregates, Pt C **2006**, 413, 20-33.
- [26] Broersen, K.; Jonckheere, W.; Rozenski, J., et al.; *Protein Engineering Design & Selection* **2011**, *24* (9), 743-750.
- [27] Bitan, G.; Fradinger, E. A.; Spring, S. M., et al.; *Amyloid-Journal of Protein Folding Disorders* **2005**, *12* (2), 88-95.
- [28] Pryor, N. E.; Moss, M. A.; Hestekin, C. N.; *Int J Mol Sci* **2012**, *13* (3), 3038-3072.
- [29] Bitan, G.; Lomakin, A.; Teplow, D. B.; *Journal of Biological Chemistry* **2001**, *276* (37), 35176-35184.
- [30] Amaro, M.; Kubiak-Ossowska, K.; Birch, D. J., et al.; *Methods and Applications in Fluorescence* **2013**, *1* (1), 1-13.
- [31] Lindberg, D. J.; Wranne, M. S.; Gatty, M. G., et al.; *Biochem Biophys Res Commun* **2015**, *458* (2), 418-423.
- [32] Bleiholder, C.; Dupuis, N. F.; Wytenbach, T., et al.; *Nature Chemistry* **2011**, *3* (2), 172-177.
- [33] Grasso, G.; Mineo, P.; Rizzarelli, E., et al.; *Int J Mass Spectrom* **2009**, *282* (1-2), 50-55.

- [34] Martineau, E.; de Guzman, J. M.; Rodionova, L., et al.; *J Am Soc Mass Spectrom* **2010**, *21* (9), 1506-1514.
- [35] Vrana, J. A.; Theis, J. D.; Dasari, S., et al.; *Haematologica* **2014**, *99* (7), 1239-1247.
- [36] Smith, A. M.; Jahn, T. R.; Ashcroft, A. E., et al.; *J Mol Biol* **2006**, *364* (1), 9-19.
- [37] Ashcroft, A. E.; *J Am Soc Mass Spectrom* **2010**, *21* (7), 1087-1096.
- [38] Henderson, S. C.; Valentine, S. J.; Counterman, A. E., et al.; *Anal Chem* **1999**, *71* (2), 291-301.
- [39] Hoaglund, C. S.; Valentine, S. J.; Sporleder, C. R., et al.; *Anal Chem* **1998**, *70* (11), 2236-2242.
- [40] Ionut Iurascu, M.; Cozma, C.; Tomczyk, N., et al.; *Anal Bioanal Chem* **2009**, *395* (8), 2509-19.
- [41] Bernstein, S. L.; Dupuis, N. F.; Lazo, N. D., et al.; *Nature Chemistry* **2009**, *1* (4), 326-331.
- [42] Bernstein, S. L.; Wyttenbach, T.; Baumketner, A., et al.; *J Am Chem Soc* **2005**, *127* (7), 2075-2084.
- [43] Baumketner, A.; Bernstein, S. L.; Wyttenbach, T., et al.; *Protein Science* **2006**, *15* (3), 420-428.
- [44] Zheng, X. Y.; Liu, D.; Klarner, F. G., et al.; *Journal of Physical Chemistry B* **2015**, *119* (14), 4831-4841.
- [45] Illes-Toth, E.; Smith, D. P.; *Current Analytical Chemistry* **2013**, *9* (2), 165-180.
- [46] Anker, J. N.; Hall, W. P.; Lambert, M. P., et al.; *Journal of Physical Chemistry C* **2009**, *113* (15), 5891-5894.
- [47] Cuburu, N.; Kweon, M. N.; Song, J. H., et al.; *Vaccine* **2007**, *25* (51), 8598-8610.
- [48] Song, F. H.; *J Am Soc Mass Spectrom* **2007**, *18* (7), 1286-1290.
- [49] Madler, S.; Erba, E. B.; Zenobi, R.; *Applications of Maldi-Tof Spectroscopy* **2013**, *331*, 1-36.
- [50] Farmer, T. B.; Caprioli, R. M.; *Journal of Mass Spectrometry* **1998**, *33* (8), 697-704.

- [51] Ji, Y.; Permanne, B.; Sigurdsson, E. M., et al.; *J Alzheimers Dis* **2001**, 3 (1), 23-30.
- [52] Solito, R.; Corti, F.; Fossati, S., et al.; *Exp Cell Res* **2009**, 315 (3), 385-395.
- [53] Kumar-Singh, S.; Julliams, A.; Nuydens, R., et al.; *Neurobiol Dis* **2002**, 11 (2), 330-340.
- [54] Munoz, F. J.; Opazo, C.; Gil-Gomez, G., et al.; *Journal of Neuroscience* **2002**, 22 (8), 3081-3089.
- [55] Wang, Z. Z.; Natte, R.; Berliner, J. A., et al.; *Stroke* **2000**, 31 (2), 534-538.
- [56] Young, K. F.; Pasternak, S. H.; Rylett, R. J.; *Neurochemistry international* **2009**, 55 (8), 796-801.
- [57] Lambert, M. P.; Viola, K. L.; Chromy, B. A., et al.; *J Neurochem* **2001**, 79 (3), 595-605.
- [58] Barghorn, S.; Nimmrich, V.; Striebinger, A., et al.; *J Neurochem* **2005**, 95 (3), 834-847.
- [59] Rangachari, V.; Moore, B. D.; Reed, D. K., et al.; *Biochemistry* **2007**, 46 (43), 12451-12462.
- [60] Moore, B. D.; Rangachari, V.; Tay, W. M., et al.; *Biochemistry* **2009**, 48 (49), 11796-11806.
- [61] Lambert, M. P.; Barlow, A. K.; Chromy, B. A., et al.; *Proc Natl Acad Sci U S A* **1998**, 95 (11), 6448-6453.
- [62] Risse, E.; Nicoll, A. J.; Taylor, W. A., et al.; *Journal of Biological Chemistry* **2015**, 290 (27), 17020-17028.
- [63] Stine, W. B.; Jungbauer, L.; Yu, C., et al.; *Methods Mol Biol* **2011**, 670, 13-32.
- [64] Chromy, B. A.; Nowak, R. J.; Lambert, M. P., et al.; *Biochemistry* **2003**, 42 (44), 12749-12760.
- [65] Morkuniene, R.; Cizas, P.; Jankeviciute, S., et al.; *J Neurosci Res* **2015**, 93 (3), 475-486.
- [66] Zou, K.; Kim, D.; Kakio, A., et al.; *J Neurochem* **2003**, 87 (3), 609-619.

**Chapter 5: Enhancements in Detection Sensitivity for  
the Amyloid Beta Protein with Matrix-Assisted Laser  
Desorption/Ionization Mass Spectrometry Imaging  
(MALDI MSI)**

## 5.1 Introduction

### *5.1.1 MALDI MSI of Proteins in Intact Tissue Sections*

The development of MALDI matrix application methods has come a long way. From initially pipetting a large droplet of matrix to cover the target sample area, to the development of automated sprayers, these advancements and innovations have made it possible to obtain images of high spatial and signal resolution for lipids, and small molecules [1-6]. This technique can provide information regarding spatial distribution for a wide range of analytes within a single sample, as well as provide a means for untargeted analysis of complex tissue sections [7-11]. Although much progress has been made in the development of MALDI MSI, limitations still exist in the detection sensitivity for low abundance analytes within biological samples. In comparison to lipids and other small molecules, intact proteins are more difficult to extract from tissue sections making imaging of proteins a more challenging task in comparison.

Integration of MALDI MSI into the proteomics field has been hindered by the poor detection sensitivity of low abundant proteins and peptides within the complex molecular composition of each tissue sample [12]. The high concentrations of salts, lipids, and metabolites in comparison cause ion suppression effects, and therefore development of sample preparation methods becomes critical in determining the success or failure of these imaging experiments. Ion suppression results from numerous competing factors that can have a negative effect on the extraction, desorption, and ionization of target analytes within

a sample [13]. There are two types of sample related ion suppression effects with MALDI MS, matrix suppression, and analyte suppression [14]. However, matrix suppression poses as a greater effect when analyzing compounds with a lower  $m/z$ . Therefore, when looking at proteins, understanding sample composition and identifying compounds that could cause ion suppression of your target analyte is of greater importance. Expansion and development of suitable sample preparation techniques along with determination of appropriate instrumental parameters can assist in the detection of intact proteins within tissue samples.

The analysis of  $A\beta_{1-42}$  has been proposed to address the difficulties in the detection and localization of this protein.  $A\beta_{1-42}$  is a small, hydrophobic protein with a mass of 4514.10 Da. The complications in working with  $A\beta$  experimentally is caused by its instability in aqueous conditions which lead to rapid aggregation. Here, focus has been placed on enhancements in detection sensitivity of the intact  $A\beta_{1-42}$  proteins through use of solid-phase extraction techniques. We aim to utilize magnetic C18 beads as a means for  $A\beta$  extraction, while simultaneously retaining the  $A\beta$  distribution within intact brain sections.

### *5.1.2 Magnetic Bead Solid - Phase Extraction*

Solid - phase extraction (SPE) has become one of the most commonly used sample preparation techniques for isolation, and enrichment of target analytes [15]. This technique helps to isolate analytes from complex mixtures which may possess compounds that could prevent the detection and analysis of the target analyte. SPE has gained popularity as a result of its simple execution protocols, and the reduction of solvents needed for sufficient



extraction [16-17]. In comparison to liquid - liquid extraction techniques, SPE delivers a more efficient separation providing higher recovery of analytes [18]. Traditionally, SPE techniques involve a stationary phase, and a mobile phase consisting of the analyte mixture. Efficient analyte isolation or enrichment is dependent on the selection of a suitable stationary phase. The various types of SPE available are: reverse phase, normal phase, and ion exchange [19]. With reverse phase (RP) SPE, the stationary phase is nonpolar while the mobile phase is polar. RP SPE is most suitable when the target analyte is a moderate to nonpolar compound which can be retained on the stationary phase until a nonpolar solvent is used for elution. Normal phase (NP) SPE is the opposite, with the stationary phase being polar while mobile phase is nonpolar, therefore targeting polar analytes. With ion exchange SPE, the main interaction is based on the electrostatic attraction of a compound's charged functional groups with the charged groups bound to the silica surface of the stationary phase.

In this work, we use RP SPE to facilitate extraction of A $\beta$  from the brain tissue surface in order to enhance the sensitivity of MALDI MSI. RP SPE should be highly effective for the hydrophobic A $\beta$  proteins, however traditional SPE columns would not be useful in this instance since the samples of interest are intact brain tissue sections. Instead, the application of loose magnetic beads directly on tissue sections has been proposed. Magnetic beads provide an alternative to chromatography columns, spin columns and pipet tip sample preparation techniques [20-21]. In theory, the beads will extract hydrophobic proteins such as A $\beta$  off from the tissue surface, while the application of the organic matrix solvent will cause the proteins to essentially “elute” off of the beads. This process should improve the efficiency of the co-crystallization process between A $\beta$  and the matrix. In

terms of sample preparation, magnetic beads can be fixed in a stationary position with a magnet, while tissue washing procedures are performed to remove unwanted contaminants. This prevents loss of the protein during preparatory steps prior to analysis, and will also preserve the anatomical location of target analytes allowing for a more rigorous tissue washing approach. Overall, this technique should improve the resulting detection sensitivity of proteins like A $\beta$  within intact tissue for MALDI MSI analysis.

## 5.2 Experimental

### 5.2.1 Apparatus

All MALDI MS sample analyses were performed on a Sciex TOF/TOF 5800 MALDI mass spectrometer equipped with a 1 kHz OptiBeam<sup>TM</sup> On-Axis Nd:YAG laser system (Ontario, Canada). The TOF TOF Series Explorer and Data Explorer were used for data acquisition and processing respectively. The Sciex TOF TOF Imaging software was used for region selection and image data collection. All MALDI MSI data was processed and analyzed using MathWorks MATLAB MSiReader software.

Matrix was applied using HTX Technologies automated TM Sprayer system (Chapel Hill, NC). A CryoStar NX50 from ThermoFisher Scientific (Ontario, Canada) was used for all tissue slicing. Syringes and Needles used for tissue sample preparation A $\beta$  injections were purchased from Dyna Medical (Ontario, Canada), and Becton - Dickinson & Co (Franklin Lakes, NJ) respectively. Rehydration chambers were created with Fisherbrand Petri Dishes from Fisher Scientific (Ontario, Canada), and rehydration was accomplished using a

Robbins Scientific Micro Hybridization Incubator Model 2000 (San Diego, CA). A High Performance BH airbrush was purchased from Iwata (Portland, OR) for all airbrush applications. Deionized water used throughout these experiments were obtained from a Millipore Milli-Q A10 Water Purification System (Bedford, MA).

### *5.2.2 Samples and Reagents*

Reagent grade acetonitrile (ACN), ammonium hydroxide, and methanol were purchased from Caledon (Ontario, Canada). HPLC grade ethanol, acetone, and trifluoroacetic acid (TFA) were purchased from Fischer Scientific Ltd. (Hampton, NH). Ammonium hydrogen phosphate (AP),  $\alpha$ -cyano-4-hydroxycinnamic acid (CHCA),  $\beta$ -casein, chloroform, ammonium citrate dibasic, acetic acid, anhydrous dimethyl sulfoxide (DMSO), and sinapinic acid (SA) were purchased from Sigma-Aldrich (St. Louis, MO). Phosphate buffered saline (PBS) was purchased from Quality Biologicals (Gaithersburg, MD). Ham's F-12 nutrients mixture was purchased from Life Technologies (Grand Island, NY). 4700 calibration mass standards kit was purchased from Applied Biosystems (Foster City, CA). The A $\beta$ <sub>1-42</sub> protein was purchased from Bachem (King of Prussia, PA). C18 beads BcMag, Zip Tips, Dynabeads were purchased from BioClone Inc. (San Diego, CA), Millipore (Billerica, MA), and Life Technologies (Oslo, Norway) respectively. Pentobarbital Sodium Injections were purchased from Bimeda MTC Animal Health Inc. (Ontario, Canada).

### *5.2.3 Amyloid Beta Sample Preparation*

A $\beta$ <sub>1-42</sub> peptides were suspended in NH<sub>4</sub>OH and brought to a concentration of 1 mM to facilitate monomerization. To prepare for short term storage, the sample was fractionated in 10  $\mu$ L aliquots, lyophilized for 1 hour at – 100 °C, and stored at – 80 °C. For each use, an aliquot of lyophilized powder was resuspended in 10  $\mu$ L of anhydrous DMSO, and sonicated in a 37 °C water bath for 10 minutes. The sample was then brought to a concentration of 150  $\mu$ M with Ham's F-12 medium, and vortexed for 30 seconds. The solution was incubated at 4 °C for 24 hours to facilitate oligomerization.

### *5.2.4 Variations in Magnetic Bead Extraction Efficiency*

Three C18 beads were tested for in-vial extraction efficiency (Figure 5.1). C18 Dynabeads were assessed along with BcMag and Zip Tips. The 4700 calibration mixture,  $\beta$  casein digest, and A $\beta$ <sub>1-42</sub> samples were used for the assessments. 10  $\mu$ L of 0.1  $\mu$ g/ $\mu$ L was prepared for each sample. 10  $\mu$ L of each stock bead solution was added to individual eptitubes, and 10  $\mu$ L of each sample was added to corresponding tube and mixed. A binding period of 2 minutes was provided followed by application of magnet to allow for supernatant removal. 10  $\mu$ L of wash solution (0.1% TFA) was added and aspirated with a micropipet. The beads were held constant once again and supernatant removed. After three washes, 6  $\mu$ L of desorption solution (50% ACN) was added. The mixture was aspirated and remained at room temperature for 2 minutes followed by removal of the supernatent. This sample procedure was applied for both BcMag and Dynabeads. The media for Zip Tips

were contained within 10  $\mu$ L pipette tips. In order to test the binding efficiency, the tips were wet with a 50% methanol solution, and equilibrated with a 0.1% TFA solution. Each sample was aspirated 10 times using individual Zip Tips, followed by aspiration of the wash solution (0.1% TFA). The proteins and peptides were then eluted with a 60% acetonitrile solution.

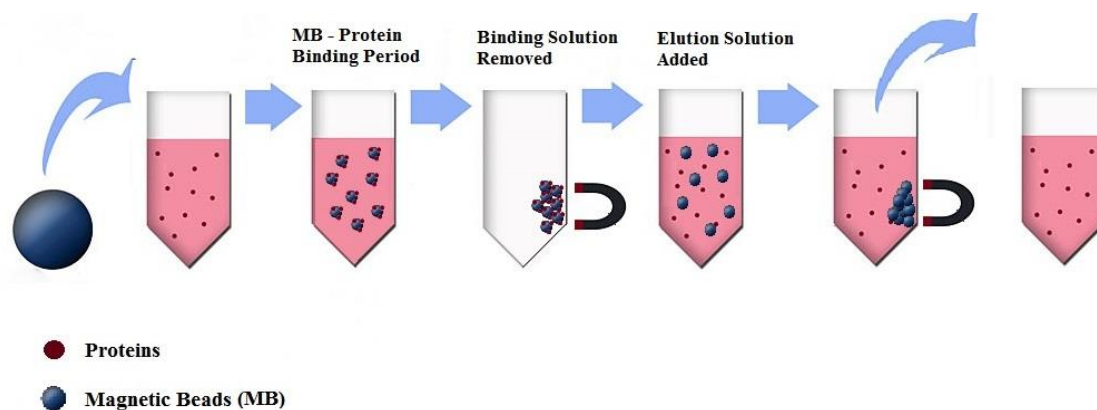


**Figure 5.1** In-vial binding efficiency of BcMag and Dynabead magnetic beads were tested. Magnetic Beads were added into the sample vial, followed by a binding period. After which, the beads were held in place by a magnetic, and the supernatant was removed. The beads were washed three times, followed by addition of an elution buffer to “elute” the target analytes off of the beads. The resulting solution was then spotted on a MALDI MS sample plate and analyzed.

### *5.2.5 Magnetic C18 Dynabeads on Plate Extraction Efficiency*

To test bead compatibility with MALDI MS analysis, 25  $\mu\text{M}$  concentration of  $\text{A}\beta_{1-42}$  was premixed with CHCA, and 0.75  $\mu\text{L}$  was spotted on the plate. A second layer of C18 Dynabeads was spotted on top. 12.5  $\mu\text{g}/\mu\text{L}$  stock solution of Dynabead was diluted 5x, 10x, and 15x with water and 0.75  $\mu\text{L}$  of each dilution was spot on a premixed analyte-matrix spot to assess optimal bead concentration for spot analysis. On plate  $\text{A}\beta$  extraction potential was evaluated by spotting 0.75  $\mu\text{L}$  of 25  $\mu\text{M}$ , 2.5  $\mu\text{M}$ , and 0.25  $\mu\text{M}$   $\text{A}\beta$  on a MALDI plate. Once dried, 0.75  $\mu\text{L}$  of 1.25  $\mu\text{g}/\mu\text{L}$  of Dynabeads were spotted above each sample spot. CHCA was prepared to 5.5  $\mu\text{g}/\mu\text{L}$  in 50% ACN, 6 mM AP, 0.1% TFA, and a final layer of CHCA was then spotted.

### *5.2.6 Sample Preparation for MALDI MSI Analysis*

#### *5.2.6.1 Tissue Extraction and Postmortem Amyloid Beta Injections*

Transgenic and wildtype Fischer (344) rats were used for these experiments. Once deeply anaesthetized, rats were euthanized with a pentobarbital overdose, and brain tissue was extracted using a fresh frozen extraction method [22]. With this method, the rat brain was not perfused with 4% paraformaldehyde prior to  $\text{A}\beta$  injection, therefore the blood flow to the tissue was retained. Immediately after tissue removal, the brain tissue was placed on dry ice and 25  $\mu\text{L}$  of 150  $\mu\text{M}$   $\text{A}\beta$  solution was injected directly into the cerebral cortex. As

the syringe was withdrawn, small amounts of sample solution was continuously released to ensure A $\beta$  is present along the entire sagittal section. This guarantees analyte presence with each coronal tissue section. Once injection was completed, tissue was completely frozen on dry ice and stored in  $-80\text{ }^{\circ}\text{C}$  or sectioned using a cryostat for immediate MALDI MSI analysis.

#### *5.2.6.2 Tissue Mounting and Preparation*

Tissue samples were freeze mounted onto the tissue holder of the cryostat with water and sectioned to  $14\text{ }\mu\text{m}$  thickness at  $-25\text{ }^{\circ}\text{C}$ . Once sectioned, the coronal brain sections were thaw mounted onto ITO glass slides and placed in a desiccator for 10 minutes. A six step tissue fixation, wash and acidification procedure was performed. The samples were first washed by submerging in 70% EtOH solution, followed by 100% EtOH for 30 seconds each. The slide was then removed and placed for 2 minutes in a solution of 60% EtOH, 30% chloroform, and 10% glacial acetic acid. This was followed by a 30 seconds wash of 100% EtOH. Acidification was achieved through submerging the sample within a solution of 0.2% TFA for 2.5 minute. A final wash was done using 100% EtOH to remove residual solvent and water.

#### *5.2.6.3 On Tissue Magnetic Bead Extraction*

The stock Dynabead solution was diluted to  $1.25\text{ }\mu\text{g}/\mu\text{L}$  with Millipore H $_2$ O to make a 3 mL solution. The solution was vortexed for a minute to facilitate dispersion.  $0.75\text{ }\mu\text{L}$  of the



Dynabead solution was pipet onto spiked A $\beta$  samples on top of tissue sections for spot analysis. 1 mL of the Dynabead solution was deposited into the solvent holder of the airbrush. Airbrush application was used to evenly coat the entire tissue section with the Dynabead solution. 4 layers were applied with a 30 seconds wait period in between each layer.

#### *5.2.6.4 Matrix Deposition & Tissue Rehydration*

SA matrix was prepared to 10  $\mu\text{g}/\mu\text{L}$  in 50% ACN, and 0.05% TFA Solution. SA was sprayed onto tissue sections using the TM sprayer. Complete sample coverage was obtained using 4 passes at a velocity of 1200 mm/min and a flow rate of 0.1 mL/min. The temperature and pressure were held constant at 70 °C and 12 psi respectively with a 30 second wait period between layers. A final matrix density of  $1.67 \times 10^{-3} \text{ mg}/\text{mm}^2$  was achieved. When magnetic bead extraction was performed, an additional layer of matrix solvent was sprayed at a reduced flow rate of 0.05 mL/min. Tissue rehydration was performed using a 5% acetic acid solution. A metal heat sink was fixed onto the top half of a petri dish, the sample slide was then fixed onto the heat sink. This portion of the petri dish was placed in a rehydration chamber set to 70 °C for 30 seconds. A filter paper soaked in the 5% acetic acid solution was placed on the bottom half of the petri dish. The top and bottom halves were then sealed together and placed in the rehydration chamber for 3.5 minutes.

### *5.2.7 MALDI MSI Parameters*

The Sciex TOF TOF imaging software was used to select for regions of interest (ROI). Once selected, acquisition parameters were selected for the positive ion mode. Protein and peptide data were acquired in linear and reflectron modes respectively. Images were set up to a raster size of 70  $\mu\text{m}$  and a total of 35 shots was performed at each fixed sample position.

## **5.3 Results and Discussion**

### *5.3.1 Enhancement of Detection Sensitivity Facilitated by C18 Magnetic Bead Extraction*

#### *5.3.1.1 Magnetic Bead Selection*

In vial assessment of variations in binding capabilities among C18 beads from Millipore, BioClone Inc, and Life Technologies was performed. Extraction capabilities of the beads were tested using 0.1  $\mu\text{g}/\mu\text{L}$  samples of  $\beta$ -casein digest, 4700 calibration peptide mixture, and  $\text{A}\beta_{1-42}$ . Through comparison, Dynabeads showed to be superior in the binding and elution capabilities for the scope of samples tested. Of the three beads, BcMag presented the worst retention and elution capabilities for all samples, with poor binding capabilities for the  $\text{A}\beta$  sample resulting in the majority of the analyte residing in the supernatant. BcMag was only capable of recovering three out of five of the peptides within the 4700 calibration mixture. While the ZipTips were great with the recovery of smaller peptides,  $\text{A}\beta$  samples were not able to elute off of the beads, and therefore presented ion counts of

less than 100. In comparison, the Dynabeads were capable of recovering the widest range of samples with the highest recovery for all three samples tested. Therefore, the C18 Dynabeads were selected for further analysis. The magnetic properties of the Dynabeads also provide an additional platform for control over the bead placements.

Upon selection of the C18 Dynabeads, determination of bead concentration was required for uniform coverage without reduction of detected signal intensity. 12.5  $\mu\text{g}/\mu\text{L}$  stock solution of Dynabeads was diluted 5x, 10x, 15x, 20x and spotted onto premixed sample-matrix spots on a MALDI MS plate. The spectral data in Figure 5.2 revealed a 50% decrease in signal intensity when the beads were diluted greater than 10x.

Microscopic images were obtained to visualize bead distribution on sample spots. Uneven bead dispersion was seen when bead concentration was diluted greater than 10x. Poor uniformity in bead coverage greatly affect extraction potential for the target sample throughout the entire section analyzed, and therefore uniform distribution must be taken into account when optimizing the concentration of beads required. Based on the microscopic images presented in Figure 5.3, both 5x and 10x dilutions presented fairly uniform coverage, since signal detection was seen to be relatively similar in intensity, a 1.25  $\mu\text{g}/\mu\text{L}$  concentration of Dynabeads was confirmed to be optimal for further applications.

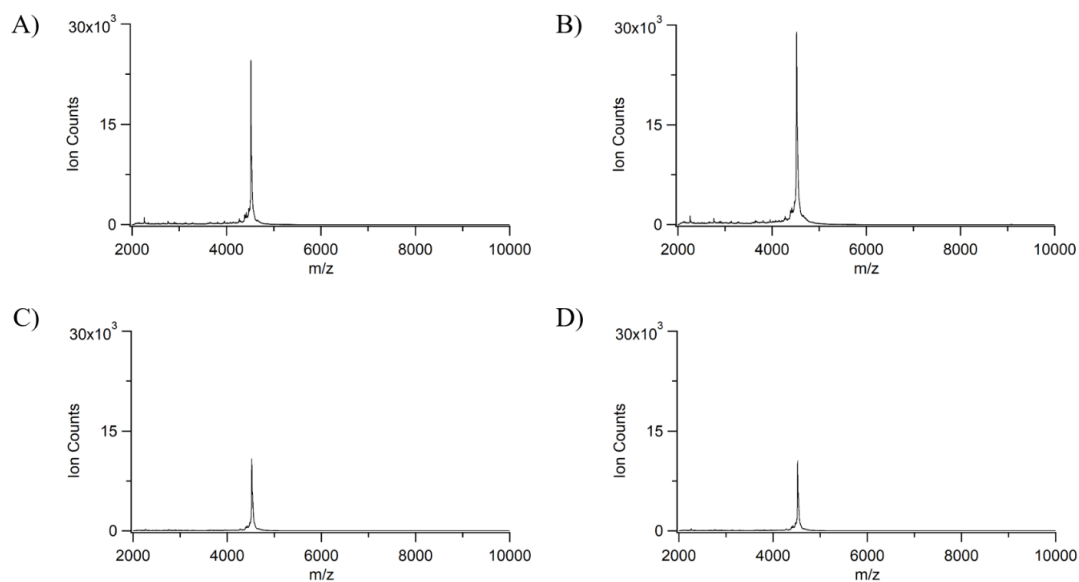


**Figure 5.2** Effects of varying Dynabead concentrations applied per sample spot was assessed. A stock solution of 12.5  $\mu\text{g}/\mu\text{L}$  was diluted 5x (A), 10x (B), 15x (C), and 20x (D).  $\text{A}\beta_{1-42}$  signals obtained was evaluated. A reduction of greater than 50% in signal intensity was observed when bead dilution exceeded 10x, therefore a minimum of 1.25  $\mu\text{g}/\mu\text{L}$  bead concentration per sample spot was determined.

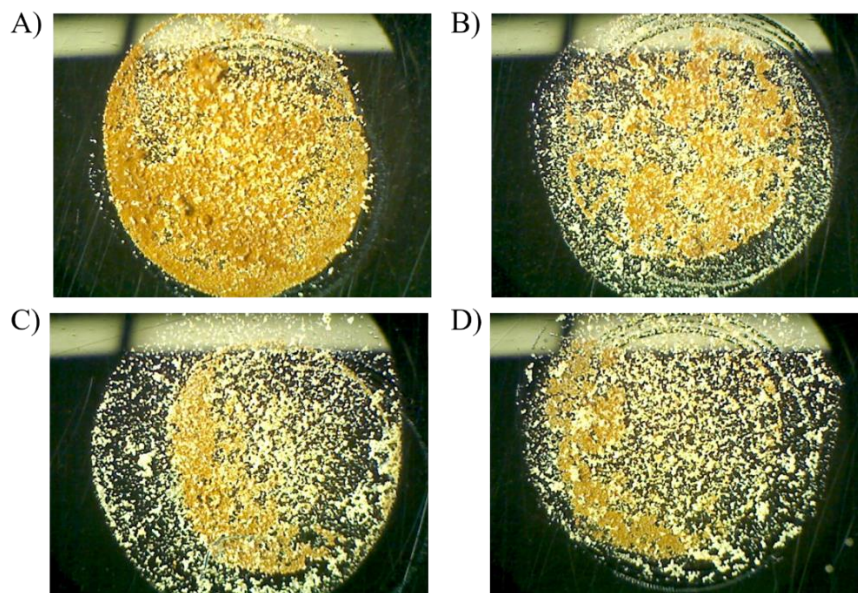


**Figure 5.3** The optimal concentration of C18 Dynabeads was evaluated by visualizing bead coverage on the sample spot. Upon Dilution of the 12.5  $\mu\text{g}/\mu\text{L}$  stock solution 5x (A), 10x (B), 15x (C), and 20x (D), 5x and 10x dilutions provided the most coverage throughout the entire sample section.

### *5.3.1.2 A $\beta$ Signal Enhancement Effects using C18 Magnetic Beads*

C18 Dynabeads utilized the principles of reverse phase chromatography (RPC) to capture hydrophobic proteins and peptides within mixtures. The beads possessed an iron oxide core which was coated with silica. The silica surface was modified with hydrophobic alkyl chains in which target proteins and peptides were bound. Once washed, the bead bound proteins were eluted into a clean solvent for analysis. Enhancement effects of the C18 magnetic beads were tested using 0.25  $\mu\text{M}$ , 2.5  $\mu\text{M}$ , and 25  $\mu\text{M}$  concentration of A $\beta_{1-42}$  proteins. Each of these samples were spotted onto a MALDI MS sample plate in layered format along with 1.25  $\mu\text{M}$  C18 Dynabeads, matrix, and solvent. A final layer of matrix solvent was spotted due to the enhancement effects observed in previous testing. The additional solvent layer was hypothesized to facilitate protein extraction, and the co-crystallization of the matrix – analyte mixture. From Figure 5.4, minor signal enhancement effects were observed for concentrations 2.5  $\mu\text{M}$  and 25  $\mu\text{M}$  sample solutions, while significant enhancement was seen for the detection of the 0.25  $\mu\text{M}$  A $\beta_{1-42}$  sample. A concentration of 0.25  $\mu\text{M}$  was below the instruments detection threshold for A $\beta_{1-42}$ , but with the help of magnetic bead extraction, a well resolved signal was observed.

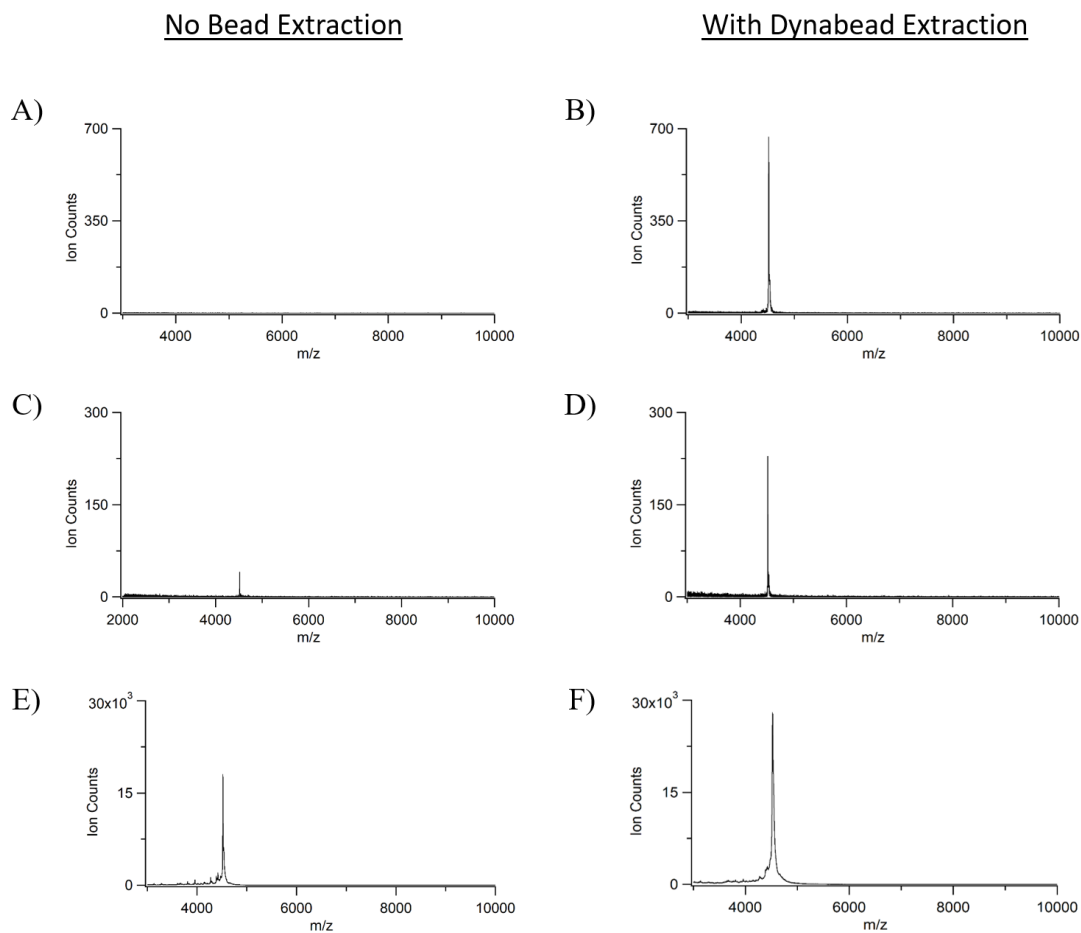


**Figure 5.4** On plate extraction of Dynabeads was assessed using different concentrations of  $A\beta_{1-42}$ , 0.25  $\mu\text{M}$  (A-B), 2.5  $\mu\text{M}$  (C-D), and 25  $\mu\text{M}$  (E-F). MALDI MS spectra was obtained before and after bead extraction protocol was applied in order to compare signal enhancement effects. With Dynabead extraction, signal intensity detected was amplified for each concentration with the most significant being of the lowest, 0.25  $\mu\text{M}$  concentration. On bare plate, an  $A\beta$  concentration of 0.25  $\mu\text{M}$  would have previously gone undetected without the aid of Dynabeads.

Following the enhancements observed through spot analysis of A $\beta$  on the MALDI MS sample plates, the detrimental effects of tissue surface composition on A $\beta$  signal detection was addressed by spotting A $\beta$  samples with the same concentration range of 2.5  $\mu$ M – 25  $\mu$ M on untreated intact tissue sections. Spiked tissue sections were first analysed prior to direct injection of A $\beta$  in order to minimize possible complications such as sample diffusion within the brain. This allows the signal suppression and enhancement effects observed to solely be a result of the tissue background and Dynabeads respectively. Figure 5.5 presents the signal detection capabilities of MALDI MS with and without the Dynabeads. The abundance in molecules on the tissue surface resulted in poor S/N ratios. Without the Dynabeads, the contaminants on the tissue surface strongly suppressed the A $\beta$  signal to nearly undetectable levels. However, the Dynabeads were able to enhance signal detection of the target A $\beta$  protein for all concentrations tested. As expected, although enhancement was observed when Dynabead were used, the effects were severely compromised on tissue in comparison to when previously tested on the bare plate (Figure 5.4). When detected, the A $\beta$  signal was found to be shifted from 4514.10 Da to  $\sim$  5000 Da. This shift is not uncommon when MS experiments are performed on tissue samples [23]. The three-dimensional structure of these samples influence the ion flight time resulting in significantly lower resolution and mass accuracy. These effects become more and more pronounce the larger the target analyte is. Unfortunately, the height difference of the mounted tissue section can be minimized, but not completely eradicated. The tissue was also analyzed prior to any A $\beta$  sample spotting to ensure the peak observed at  $\sim$  5000 Da is representative of the A $\beta$  sample.



The enhancement in signals observed support the prior hypothesis that the beads aid in the extraction of A $\beta$  proteins allowing for improved co-crystallization with the MALDI MS matrix. Significant enhancement effects were most prominent for low A $\beta$  concentrations on bare plate, and on tissue analysis of A $\beta$ . The issue of surface contamination when studying tissue sections can be minimized with additional tissue washing procedures.

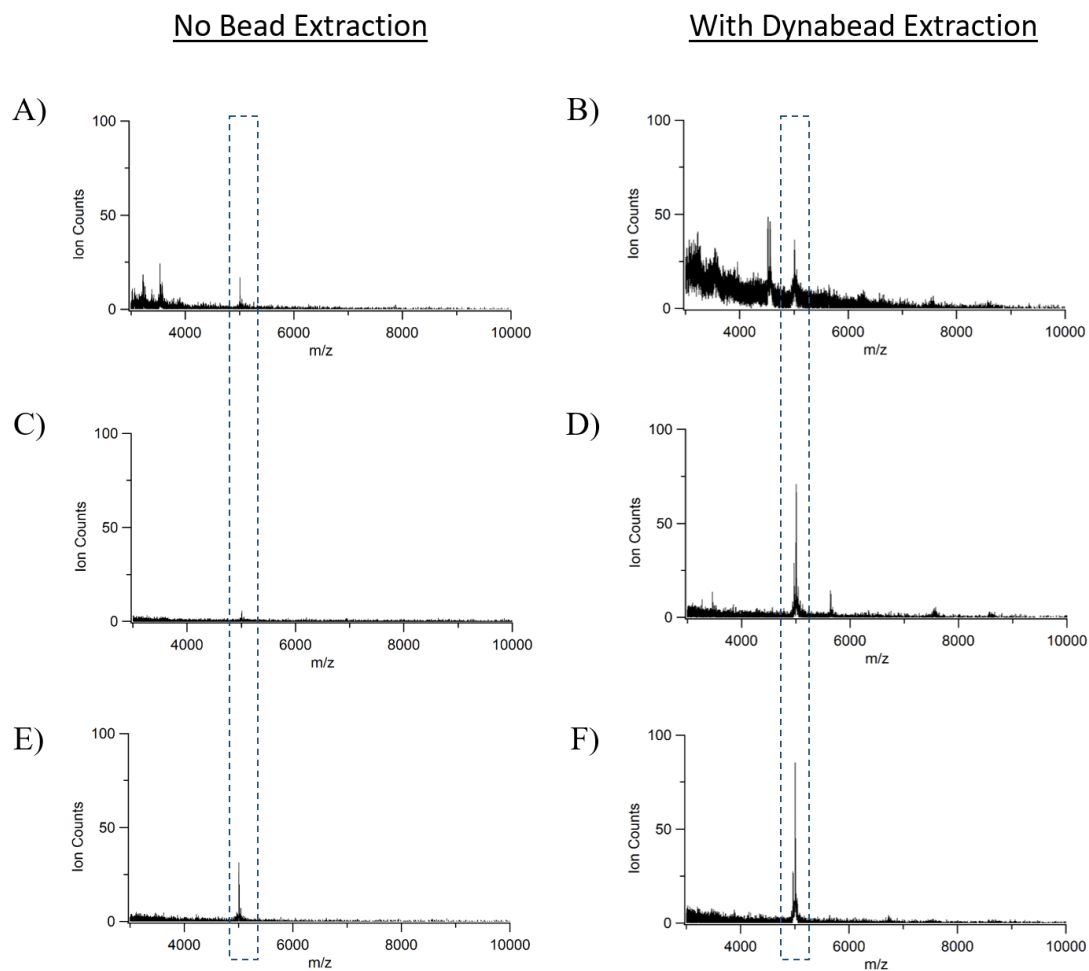


**Figure 5.5** On Tissue extraction capabilities of Dynabeads were assessed with 0.25 μM (A-B), 2.5 μM (C-D), and 25 μM (E-F) concentrations of Aβ<sub>1-42</sub>. With the abundance of molecules on a tissue surface, the MALDI MS spectra displayed poor S/N ratio with a noisy baseline. Signal enhancement effects of Dynabead application was observed for each concentration tested.

### *5.3.2 Signal Enhancement Effects of Magnetic Beads for Amyloid Beta*

#### *Using MALDI MSI*

Successful detection of A $\beta$  fragments and fibrils using MALDI MSI was previously reported, but improvements are still needed to increase image resolution for MALDI MSI, and to be able to detect intact A $\beta$ <sub>1-42</sub> oligomers [24]. To achieve peak magnetic bead extraction efficiency, sample preparatory protocols were first optimized. Salts and lipids were first removed through serial tissue washes, but a balance must be attained to minimize delocalization of target analytes, yet still effectively remove enough endogenous contaminants for the detection of A $\beta$ . The ability to extract proteins from tissue sections was dependent on suitable matrix application protocols. In order to facilitate efficient extraction, a wet matrix application by means of an automated sprayer systems was used. The solvent provides a medium for the extraction of analytes in order to co - crystallize with the matrix for MALDI MS analysis. The spray parameters were tested and modified to offer the ideal compromise allowing for the greatest degree of analyte extraction with minimal levels of delocalization on the tissue surface. The choice of matrix used was also a limiting factor. The matrix must be suitable for a higher mass range to accommodate for the molecular weight of intact proteins, it must be soluble in organic/aqueous solvents, and possess small, unchanging particle size in order to provide a uniform coating on sample sections. Commonly used matrices are CHCA and SA. CHCA is generally applied when studying lower molecular weight proteins (< 5000 Da). SA is generally used for the investigation of proteins of >3500 Da, and therefore makes it more suitable for intact A $\beta$

analysis. Previously, optimization of magnetic bead parameters have been achieved with CHCA due to its abilities to accommodate for a wide range of MW making it ideal for testing bead binding capabilities for a broad range of MW analytes. With the focus now switching to MALDI MSI of tissue sections, sinapinic acid (SA) was tested and revealed comparable results for Dynabead extraction efficiency. The solvent used for SA possessed the same organic : aqueous ratio of 50 : 50 and therefore would not alter elution capabilities.

MALDI MSI data was collected for  $A\beta_{1-42}$  and  $A\beta_{1-40}$  presented in Figure 5.6. Once optimization and development of a suitable sample preparatory techniques in the tissue washing, matrix application, and rehydration protocols were achieved, the images showed dramatic improvements in  $A\beta$  detection.  $A\beta$  proteins were detected at the injection site for both,  $A\beta_{1-40}$  and  $A\beta_{1-42}$  samples using MALDI MSI ( $n = 4$ ,  $n = 2$  respectively). As a result of the high intensity signal at the injection site, anatomical features of the brain tissue were suppressed. Images obtained from wildtype rat brains showed weak levels of  $A\beta$  along the visible length of the corpus callosum within the section, this was a result of the injection site located at the corpus callosum, and the high permeability of this region.

Dynabeads were applied over the entire tissue section with an airbrush. Once dried, additional matrix and solvent layers were applied using the TM sprayer to help facilitate  $A\beta$  extraction from the tissue section. From Figure 5.6, the MALDI MSI data obtained from tissue sections with Dynabead application showed a severe decrease in signal detection with only the injection site from the wildtype tissue with  $A\beta_{1-42}$  injected visible. The spatial resolution of the images were found to be completely compromised, with a significant decrease in signal intensity.

In comparison to former MALDI MS analysis, the images did not correlate with the previous data obtained regarding Dynabead signal extraction. This was speculated to be a result of several contributing factors, including the aforementioned signal suppression effects, and the decrease in signal resolution and mass accuracy experienced when analysis is performed on the three-dimensional tissue sections. When an additional layer of beads were sprayed onto the tissue surface, this enhanced the negative effects of the uneven tissue surfaces. Although expected, the degree of impact this posed for the resulting image surpassed expectations. Additionally, image acquisition requires several hours to complete, within the vacuum system it is possible the beads detached, and fell off during the duration of this time period. Furthermore, additional precautions may be required to prevent potential A $\beta$  sample loss during the tissue washing procedures, and to increase extraction efficiency from the bead to co-crystallize with the matrix applied.

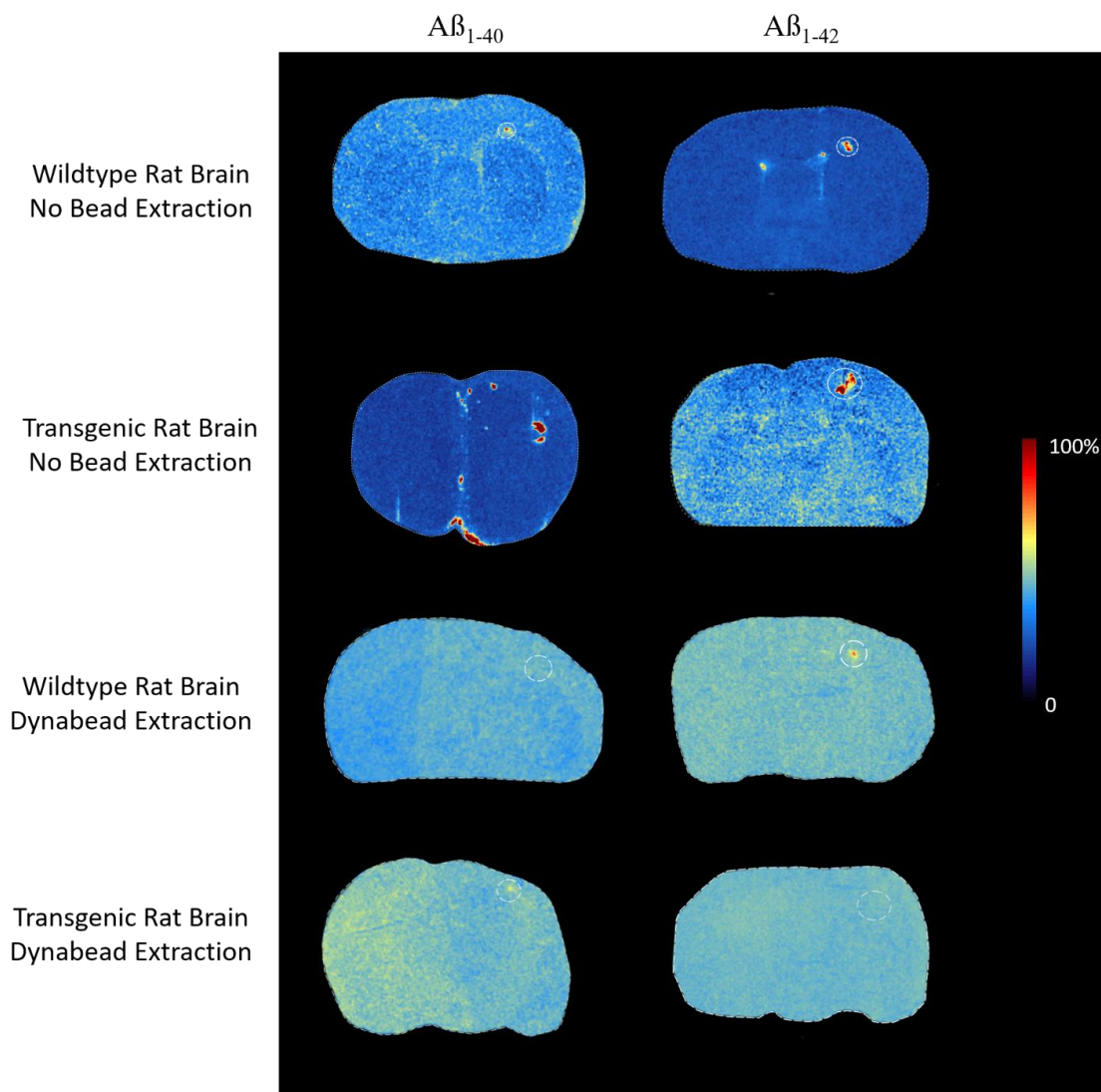


**Figure 5.6** MALDI MSI of  $A\beta_{1-40}$  and  $A\beta_{1-42}$  tissue sections of wildtype and transgenic rats reveals presence of the target protein within the injection sites (circled in the images above). However, upon addition of C18 Dynabeads, enhancement effects were not observed. On the contrary, signal intensity and spatial resolution were both severely compromised.

## 5.4 Conclusion

MALDI MSI has provides a platform for the localization of proteins and peptides within intact tissue sections. However, contaminants on tissue surfaces strongly reduced signal detection capabilities for A $\beta$ . The extraction power of C18 magnetic Dynabeads for A $\beta$  proteins were clearly observed for bare plate and on tissue MALDI MS analysis. When applied to MALDI MSI, a combination of factors including surface uniformity, and extraction efficiency contributed towards the inability to attain additional signal enhancement effects.

Future work should focus on uncovering alternative substrates with A $\beta$  extraction potential, such as magnetic nanoparticles, and use of metal ions. Magnetic nanoparticles would aid in minimizing the negative impact that Dynabeads exhibited on the surface uniformity of samples analyzed. If successful, the magnetic properties of the nanoparticles would be beneficial in retaining spatial resolution when rigorous forms of tissue clean – up are utilized. Application of metal ions as a matrix could potentially eliminate the need for alternative substrates for extraction purposes. Both Zn<sup>2+</sup> and Cu<sup>2+</sup> have been found to bind to histidine residues of A $\beta$  proteins [25-26]. Additionally, both metals have been reported effective as a matrix, either in oxide form (ZnO), or as a modification of standard matrices (Cu-CHCA) [27-28]. If successful, not only will this technique benefit the field of Alzheimer's research, it will help uncover a range of analytes upon tissue sections that may have previously gone unnoticed due to signal suppression effects.

## 5.5 References

- [1] Stoeckli, M.; Chaurand, P.; Hallahan, D. E., et al.; *Nat Med* **2001**, *7* (4), 493-6.
- [2] Stoeckli, M.; Staab, D.; Staufenbiel, M., et al.; *Anal Biochem* **2002**, *311* (1), 33-9.
- [3] Chughtai, K.; Heeren, R. M.; *Chem Rev* **2010**, *110* (5), 3237-77.
- [4] Caldwell, R. L.; Caprioli, R. M.; *Mol Cell Proteomics* **2005**, *4* (4), 394-401.
- [5] Murphy, R. C.; Hankin, J. A.; Barkley, R. M.; *J Lipid Res* **2009**, *50 Suppl*, S317-22.
- [6] Sturtevant, D.; Lee, Y. J.; Chapman, K. D.; *Curr Opin Biotechnol* **2016**, *37*, 53-60.
- [7] Anderson, D. M.; Ablonczy, Z.; Koutalos, Y., et al.; *J Am Soc Mass Spectrom* **2014**, *25* (8), 1394-403.
- [8] Andersson, M.; Andren, P.; Caprioli, R. M., MALDI Imaging and Profiling Mass Spectrometry in Neuroproteomics. In *Neuroproteomics*, Alzate, O., Ed. Boca Raton (FL), 2010.
- [9] Berry, K. A.; Hankin, J. A.; Barkley, R. M., et al.; *Chem Rev* **2011**, *111* (10), 6491-512.
- [10] Chaurand, P.; Cornett, D. S.; Caprioli, R. M.; *Curr Opin Biotechnol* **2006**, *17* (4), 431-6.
- [11] Chaurand, P.; Schwartz, S. A.; Reyzer, M. L., et al.; *Toxicol Pathol* **2005**, *33* (1), 92-101.
- [12] Stauber, J.; MacAleese, L.; Franck, J., et al.; *J Am Soc Mass Spectrom* **2010**, *21* (3), 338-47.



- [13] Taylor, A. J.; Dexter, A.; Bunch, J.; *Anal Chem* **2018**, *90* (9), 5637-5645.
- [14] Lou, X.; van Dongen, J. L.; Vekemans, J. A., et al.; *Rapid Commun Mass Spectrom* **2009**, *23* (19), 3077-82.
- [15] Wierucka, M.; Biziuk, M.; *Trends in Analytical Chemistry* **2014**, *59*, 50-58.
- [16] Plotka-Wasyłka, J.; Szczepanska, N.; de la Guardia, M., et al.; *Trends in Analytical Chemistry* **2015**, *73*, 19-38.
- [17] Plotka-Wasyłka, J.; Owczarek, K.; Namiesnik, J.; *Trends in Analytical Chemistry* **2016**, *85*.
- [18] Hennion, M. C.; *J Chromatogr A* **1999**, *856* (1-2), 3-54.
- [19] Buszewski, B.; *Crit Rev Anal Chem* **2012**, *42* (3), 198-213.
- [20] Gijs, M. A.; Lacharme, F.; Lehmann, U.; *Chem Rev* **2010**, *110* (3), 1518-63.
- [21] Archer, M. J.; Lin, B.; Wang, Z., et al.; *Anal Biochem* **2006**, *355* (2), 285-97.
- [22] Weishaupt, N.; Caughlin, S.; Yeung, K. K., et al.; *Front Neuroanat* **2015**, *9*, 155.
- [23] Rompp, A.; Spengler, B.; *Histochem Cell Biol* **2013**, *139* (6), 759-83.
- [24] Kelley, A. R.; Perry, G.; Bethea, C., et al.; *Open Neurol J* **2016**, *10*, 88-98.
- [25] Frederickson, C. J.; Bush, A. I.; *Biometals* **2001**, *14* (3-4), 353-66.
- [26] Atwood, C. S.; Scarpa, R. C.; Huang, X., et al.; *J Neurochem* **2000**, *75* (3), 1219-33.

- [27] Wu, Z.; Fernandez-Lima, F. A.; Perez, L. M., et al.; *J Am Soc Mass Spectrom* **2009**, *20* (7), 1263-71.
- [28] Watanabe, T.; Kawasaki, H.; Yonezawa, T., et al.; *Journal of Mass Spectrometry* **2008**, *43* (8), 1063-1071.

## **Chapter 6: Conclusions & Future Work**

## 6.1 Conclusions and Future Work

Mass spectrometry (MS) is an incredibly powerful technique that has become an essential tool for the analysis of biological molecules and systems. Through the introduction of soft ionization techniques ESI and MALDI, it became possible for MS to identify intact proteins. MALDI MS offers a means to perform targeted and untargeted identification of the molecular weight, and amino acid sequence for proteins in a complex mixture. Current MALDI MS research has extended past its conventional analysis capabilities, and introduced a new dimension to sample analysis. Development of MALDI MSI provided an alternative platform for protein and peptide detection, where location information within an intact tissue section can be found. This presented the opportunity to utilize MALDI MSI to better understand biological systems, and disease pathology by simultaneously acquiring information regarding multiple analytes within a sample.

Integration of MALDI MSI as a technique for biochemical imaging eradicates the uncertainties that exists with stains and labels used in traditional imaging methodology such as immunohistochemistry (IHC). This is pertinent in furthering research involving the pathology of disease like AD. The uncertainties that reside in disease progression along with the physical and chemical properties of the toxic A $\beta$  protein make it difficult to select stains and labels with high specificity. Unfortunately, A $\beta$ <sub>1-42</sub> is the most relevant factor when discussing AD pathology, but its instability in aqueous conditions and its propensity for aggregation makes A $\beta$  challenging to work with in laboratory settings. Therefore new

technology in the detection of A $\beta$  would be greatly beneficial in the advancements of research in this field.

The ability for MALDI MSI detection of peptides within complex tissue systems was first assessed using a low molecular weight dipeptide, ZP1609. Within tissue sections, the abundance of lipids and metabolites are readily ionizable, and therefore posed as a hindrance for peptide analysis due to ion suppression effects. The importance of tissue washing, acidification, and rehydration protocols was outlined in chapter 3. These tissue preparatory steps facilitated the removal of excess salts and lipids in order to reduce the suppression effects experienced by these contaminants when upon analysis. The addition of an acidification protocol presented significant enhancement effects in both signal detection and spatial resolution of the images acquired. Capabilities of MALDI MS as a fast and sensitive method in the detection of A $\beta$  oligomers was presented in chapter 4 of this thesis. This work presented MALDI MS as a label-free method for researchers to quickly characterize *in vitro* multimeric A $\beta$  composition prior to additional neurodegenerative studies.

Through MALDI MS analysis of A $\beta$ , and the development of successful MALDI MSI tissue preparatory protocols for ZP1609, MALDI MS detection of A $\beta$  spiked on top of the tissue surface was assessed. As expected, the protein presented difficulty ionizing and desorbing off of the tissue section. Along with the challenges of ion suppression from salts and lipids, detection sensitivity of the low abundance A $\beta$  proteins were greatly diminished. Application of solid-phase extraction (SPE) techniques using magnetic beads facilitated the extraction of A $\beta$  samples off of the tissue section. Once the matrix was applied onto the

sample, A $\beta$  was able to successfully elute off of the beads and ionize providing signals of greater intensity. The magnetic beads were able to enhance signal detection of low concentration A $\beta$  samples which were previously undetectable when pipet onto the tissue section. However, when extraction capabilities were tested using MALDI MSI on tissue samples injected with either A $\beta$ <sub>1-42</sub> or A $\beta$ <sub>1-40</sub>, the results differed. The reduction in signal detection and spatial resolution of images acquired after application of the magnetic beads was hypothesized to be a result of the uneven tissue surface. When an additional layer of magnetic beads were applied onto the tissue section, the detrimental effects of the challenges experienced with the uneven surface of three dimensional tissues samples were amplified. Additionally, image acquisition for MALDI MSI requires several hours, the beads were speculated to potentially detach off of the MALDI sample plate during the acquisition process within the vacuum environment.

The ability to perform solid-phase extraction of A $\beta$  prior to MALDI MSI analysis would be greatly beneficial in the *ex vivo* detection of A $\beta$  and understanding its correlations with AD pathology. Not only will these advancements aid AD research, it would be extremely useful in assisting the improvement of MALDI MSI detection sensitivity for all low abundant substances within tissue sections that may have previously gone unnoticed. Therefore, future work would revolve around development of alternative substrates with higher extraction potential, and better compatibility with MALDI MSI conditions. These can include the use of magnetic nanoparticles, or investigating the binding capabilities of A $\beta$  to metals such as zinc and copper ions.

In comparison to previously used Dynabeads, magnetic nanoparticles would provide a much smaller substrate for A $\beta$  extraction. The reduction in size will help to minimize the unavoidable effects of variations in surface uniformity tissue samples exhibit. This reduction will instead aid in generating a more even layer with fuller coverage of the entire sample section. Retaining the magnetic properties provide an advantage when additional tissue treatments and washes are require without compromising spatial resolution of analyte distribution.

Alternatively, the binding capabilities of A $\beta$  to metals such as zinc and copper ions can be exploited. Although Zn<sup>2+</sup> levels in the extracellular regions of the brain are fairly limited, Zn<sup>2+</sup> concentrations in brain regions most greatly affected by AD such as the hippocampus, amygdala, and cortex are relatively high [1-2]. Zn<sup>2+</sup> bind to histidine residues on A $\beta$  proteins and peptides forming both 1 : 1, and 3 : 1 zinc(II)-A $\beta$  complexes [3]. This interaction induced rapid *in vitro* aggregation of A $\beta$  [2, 4-6]. Like zinc, Cu<sup>2+</sup> was also found to interact with A $\beta$  by binding to the histidine residues. However, it was reported to form 1 : 1 and potentially 2 : 1 Cu(II)-A $\beta$  complexes [7-8]. The binding capabilities of A $\beta$  to metal ions provides a great opportunity to utilize this interaction to enhance detection sensitivity. The use of metal ions Zn<sup>2+</sup> and Cu<sup>2+</sup> provide an added bonus in removing the necessity for an additional substrate appication for SPE, since both copper and zinc have been utilized successfully as either a modification to standard matrices (Cu-CHCA), or as a stand alone matrix (ZnO) [9-10].

## 6.2 References

- [1] Frederickson, C. J.; Giblin, L. J.; Krezel, A., et al.; *Exp Neurol* **2006**, *198* (2), 285-93.
- [2] Frederickson, C. J.; Bush, A. I.; *Biometals* **2001**, *14* (3-4), 353-66.
- [3] Tōugu, V.; Karafin, A.; Palumaa, P.; *J Neurochem* **2007**, *104* (5), 1249-1259.
- [4] Yang, D.-S.; McLaurin, J.; Qin, K., et al.; *European Journal of Biochemistry* **2001**, *267* (22), 6692-6698.
- [5] Huang, X.; Atwood, C. S.; Moir, R. D., et al.; *J Biol Chem* **1997**, *272* (42), 26464-70.
- [6] Bush, A. I.; Pettingell, W. H.; Multhaup, G., et al.; *Science* **1994**, *265* (5177), 1464-7.
- [7] Atwood, C. S.; Scarpa, R. C.; Huang, X., et al.; *J Neurochem* **2000**, *75* (3), 1219-33.
- [8] Ali, F. E.; Separovic, F.; Barrow, C. J., et al.; *Int. J. Pept. Res. Ther.* **2006**, *12* (2), 153-164.
- [9] Wu, Z.; Fernandez-Lima, F. A.; Perez, L. M., et al.; *J Am Soc Mass Spectrom* **2009**, *20* (7), 1263-71.
- [10] Watanabe, T.; Kawasaki, H.; Yonezawa, T., et al.; *Journal of Mass Spectrometry* **2008**, *43* (8), 1063-1071.



# Appendix 1 – Copyright Permission

## SPRINGER NATURE LICENSE TERMS AND CONDITIONS

Oct 17, 2018

This Agreement between Ms. Jasmine Wang ("You") and Springer Nature ("Springer Nature") consists of your license details and the terms and conditions provided by Springer Nature and Copyright Clearance Center.

License Number	4451500345381
License date	Oct 17, 2018
Licensed Content Publisher	Springer Nature
Licensed Content Publication	Journal of The American Society for Mass Spectrometry
Licensed Content Title	Detection of Amyloid Beta (A $\beta$ ) Oligomeric Composition Using Matrix-Assisted Laser Desorption Ionization Mass Spectrometry (MALDI MS)
Licensed Content Author	Jasmine S.-H. Wang, Shawn N. Whitehead, Ken K.-C. Yeung
Licensed Content Date	Jan 1, 2018
Licensed Content Volume	29
Licensed Content Issue	4
Type of Use	Thesis/Dissertation
Requestor type	academic/university or research institute
Format	print and electronic
Portion	full article/chapter
Will you be translating?	no
Circulation/distribution	<501
Author of this Springer Nature content	yes
Title	Matrix-Assisted Laser Desorption/Ionization Mass Spectrometry Imaging of ZP1609 and Amyloid Beta
Institution name	Western University
Expected presentation date	Oct 2018
Requestor Location	Ms. Jasmine Wang Western University Department of Chemistry 1151 Richmond Street London, ON N6A 3K7 Canada Attn: Ms. Jasmine Wang
Billing Type	Invoice
Billing Address	Ms. Jasmine Wang Western University Department of Chemistry 1151 Richmond Street London, ON N6A 3K7 Canada Attn: Ms. Jasmine Wang
Total	0.00 CAD

### Terms and Conditions

#### Springer Nature Terms and Conditions for RightsLink Permissions

**Springer Nature Customer Service Centre GmbH (the Licensor)** hereby grants you a non-exclusive, world-wide licence to reproduce the material and for the purpose and requirements specified in the attached copy of your order form, and for no other use, subject to the conditions below:

1. The Licensor warrants that it has, to the best of its knowledge, the rights to license reuse of this material. However, you should ensure that the material you are requesting is original to the Licensor and does not carry the copyright of another entity (as credited in the published version).

If the credit line on any part of the material you have requested indicates that it was reprinted or adapted with permission from another source, then you should also seek permission from that source to reuse the material.

2. Where **print only** permission has been granted for a fee, separate permission must be obtained for any additional electronic re-use.

3. Permission granted **free of charge** for material in print is also usually granted for any electronic version of that work, provided that the material is incidental to your work as a whole and that the electronic version is essentially equivalent to, or substitutes for, the print version.
4. A licence for 'post on a website' is valid for 12 months from the licence date. This licence does not cover use of full text articles on websites.
5. Where 'reuse in a dissertation/thesis' has been selected the following terms apply: Print rights of the final author's accepted manuscript (for clarity, NOT the published version) for up to 100 copies, electronic rights for use only on a personal website or institutional repository as defined by the Sherpa guideline ([www.sherpa.ac.uk/romeo/](http://www.sherpa.ac.uk/romeo/)).
6. Permission granted for books and journals is granted for the lifetime of the first edition and does not apply to second and subsequent editions (except where the first edition permission was granted free of charge or for signatories to the STM Permissions Guidelines <http://www.stm-assoc.org/copyright-legal-affairs/permissions/permissions-guidelines/>), and does not apply for editions in other languages unless additional translation rights have been granted separately in the licence.
7. Rights for additional components such as custom editions and derivatives require additional permission and may be subject to an additional fee. Please apply to [Journalpermissions@springernature.com](mailto:Journalpermissions@springernature.com)/[bookpermissions@springernature.com](mailto:bookpermissions@springernature.com) for these rights.
8. The Licensor's permission must be acknowledged next to the licensed material in print. In electronic form, this acknowledgement must be visible at the same time as the figures/tables/illustrations or abstract, and must be hyperlinked to the journal/book's homepage. Our required acknowledgement format is in the Appendix below.
9. Use of the material for incidental promotional use, minor editing privileges (this does not include cropping, adapting, omitting material or any other changes that affect the meaning, intention or moral rights of the author) and copies for the disabled are permitted under this licence.
10. Minor adaptations of single figures (changes of format, colour and style) do not require the Licensor's approval. However, the adaptation should be credited as shown in Appendix below.

#### **Appendix — Acknowledgements:**

##### **For Journal Content:**

Reprinted by permission from [the Licensor]: [Journal Publisher (e.g. Nature/Springer/Palgrave)] [JOURNAL NAME] [REFERENCE CITATION (Article name, Author(s) Name), [COPYRIGHT] (year of publication)]

##### **For Advance Online Publication papers:**

Reprinted by permission from [the Licensor]: [Journal Publisher (e.g. Nature/Springer/Palgrave)] [JOURNAL NAME] [REFERENCE CITATION (Article name, Author(s) Name), [COPYRIGHT] (year of publication), advance online publication, day month year (doi: 10.1038/sj.[JOURNAL ACRONYM].)]

##### **For Adaptations/Translations:**

Adapted/Translated by permission from [the Licensor]: [Journal Publisher (e.g. Nature/Springer/Palgrave)] [JOURNAL NAME] [REFERENCE CITATION (Article name, Author(s) Name), [COPYRIGHT] (year of publication)]

##### **Note: For any republication from the British Journal of Cancer, the following credit line style applies:**

Reprinted/adapted/translated by permission from [the Licensor]: on behalf of Cancer Research UK: : [Journal Publisher (e.g. Nature/Springer/Palgrave)] [JOURNAL NAME] [REFERENCE CITATION (Article name, Author(s) Name), [COPYRIGHT] (year of publication)]

##### **For Advance Online Publication papers:**

Reprinted by permission from The [the Licensor]: on behalf of Cancer Research UK: [Journal Publisher (e.g. Nature/Springer/Palgrave)] [JOURNAL NAME] [REFERENCE CITATION (Article name, Author(s) Name), [COPYRIGHT] (year of publication), advance online publication, day month year (doi: 10.1038/sj.[JOURNAL ACRONYM].)]

##### **For Book content:**

Reprinted/adapted by permission from [the Licensor]: [Book Publisher (e.g. Palgrave Macmillan, Springer etc)] [Book Title] by [Book author(s)] [COPYRIGHT] (year of publication)]

**JOHN WILEY AND SONS LICENSE  
TERMS AND CONDITIONS**

Oct 17, 2018

This Agreement between Ms. Jasmine Wang ("You") and John Wiley and Sons ("John Wiley and Sons") consists of your license details and the terms and conditions provided by John Wiley and Sons and Copyright Clearance Center.

License Number	4451501443780
License date	Oct 17, 2018
Licensed Content Publisher	John Wiley and Sons
Licensed Content Publication	Rapid Communications in Mass Spectrometry
Licensed Content Title	Matrix-assisted laser desorption/ionization imaging mass spectrometry of intraperitoneally injected danegaptide (ZP1609) for treatment of stroke-reperfusion injury in mice
Licensed Content Author	Jasmine S.H. Wang, Moises Freitas-Andrade, John F. Bechberger, et al
Licensed Content Date	May 10, 2018
Licensed Content Volume	32
Licensed Content Issue	12
Licensed Content Pages	8
Type of use	Dissertation/Thesis
Requestor type	Author of this Wiley article
Format	Print and electronic
Portion	Full article
Will you be translating?	No
Title of your thesis / dissertation	Matrix-Assisted Laser Desorption/Ionization Mass Spectrometry Imaging of ZP1609 and Amyloid Beta
Expected completion date	Oct 2018
Expected size (number of pages)	140
Requestor Location	Ms. Jasmine Wang Western University Department of Chemistry 1151 Richmond Street London, ON N6A 3K7 Canada Attn: Ms. Jasmine Wang
Publisher Tax ID	EU826007151
Total	0.00 USD
Terms and Conditions	

**TERMS AND CONDITIONS**

This copyrighted material is owned by or exclusively licensed to John Wiley & Sons, Inc. or one of its group companies (each a "Wiley Company") or handled on behalf of a society with which a Wiley Company has exclusive publishing rights in relation to a particular work (collectively "WILEY"). By clicking "accept" in connection with completing this licensing transaction, you agree that the following terms and conditions apply to this transaction (along with the billing and payment terms and conditions established by the Copyright Clearance Center Inc., ("CCC's Billing and Payment terms and conditions"), at the time that you opened your RightsLink account (these are available at any time at <http://myaccount.copyright.com>).

**Terms and Conditions**

- The materials you have requested permission to reproduce or reuse (the "Wiley Materials") are protected by copyright.
- You are hereby granted a personal, non-exclusive, non-sub licensable (on a stand-alone basis), non-transferable, worldwide, limited license to reproduce the Wiley Materials for the purpose specified in the licensing process. This license, **and any CONTENT (PDF or image file) purchased as part of your order**, is for a one-time use only and limited to any maximum distribution number specified in the license. The first instance of republication or reuse granted by this license must be completed within two years of the date of the grant of this license (although copies prepared

before the end date may be distributed thereafter). The Wiley Materials shall not be used in any other manner or for any other purpose, beyond what is granted in the license. Permission is granted subject to an appropriate acknowledgement given to the author, title of the material/book/journal and the publisher. You shall also duplicate the copyright notice that appears in the Wiley publication in your use of the Wiley Material. Permission is also granted on the understanding that nowhere in the text is a previously published source acknowledged for all or part of this Wiley Material. Any third party content is expressly excluded from this permission.

- With respect to the Wiley Materials, all rights are reserved. Except as expressly granted by the terms of the license, no part of the Wiley Materials may be copied, modified, adapted (except for minor reformatting required by the new Publication), translated, reproduced, transferred or distributed, in any form or by any means, and no derivative works may be made based on the Wiley Materials without the prior permission of the respective copyright owner. **For STM Signatory Publishers clearing permission under the terms of the [STM Permissions Guidelines](#) only, the terms of the license are extended to include subsequent editions and for editions in other languages, provided such editions are for the work as a whole in situ and does not involve the separate exploitation of the permitted figures or extracts,** You may not alter, remove or suppress in any manner any copyright, trademark or other notices displayed by the Wiley Materials. You may not license, rent, sell, loan, lease, pledge, offer as security, transfer or assign the Wiley Materials on a stand-alone basis, or any of the rights granted to you hereunder to any other person.
- The Wiley Materials and all of the intellectual property rights therein shall at all times remain the exclusive property of John Wiley & Sons Inc, the Wiley Companies, or their respective licensors, and your interest therein is only that of having possession of and the right to reproduce the Wiley Materials pursuant to Section 2 herein during the continuance of this Agreement. You agree that you own no right, title or interest in or to the Wiley Materials or any of the intellectual property rights therein. You shall have no rights hereunder other than the license as provided for above in Section 2. No right, license or interest to any trademark, trade name, service mark or other branding ("Marks") of WILEY or its licensors is granted hereunder, and you agree that you shall not assert any such right, license or interest with respect thereto
- NEITHER WILEY NOR ITS LICENSORS MAKES ANY WARRANTY OR REPRESENTATION OF ANY KIND TO YOU OR ANY THIRD PARTY, EXPRESS, IMPLIED OR STATUTORY, WITH RESPECT TO THE MATERIALS OR THE ACCURACY OF ANY INFORMATION CONTAINED IN THE MATERIALS, INCLUDING, WITHOUT LIMITATION, ANY IMPLIED WARRANTY OF MERCHANTABILITY, ACCURACY, SATISFACTORY QUALITY, FITNESS FOR A PARTICULAR PURPOSE, USABILITY, INTEGRATION OR NON-INFRINGEMENT AND ALL SUCH WARRANTIES ARE HEREBY EXCLUDED BY WILEY AND ITS LICENSORS AND WAIVED BY YOU.
- WILEY shall have the right to terminate this Agreement immediately upon breach of this Agreement by you.
- You shall indemnify, defend and hold harmless WILEY, its Licensors and their respective directors, officers, agents and employees, from and against any actual or threatened claims, demands, causes of action or proceedings arising from any breach of this Agreement by you.
- IN NO EVENT SHALL WILEY OR ITS LICENSORS BE LIABLE TO YOU OR ANY OTHER PARTY OR ANY OTHER PERSON OR ENTITY FOR ANY SPECIAL, CONSEQUENTIAL, INCIDENTAL, INDIRECT, EXEMPLARY OR PUNITIVE DAMAGES, HOWEVER CAUSED, ARISING OUT OF OR IN CONNECTION WITH THE DOWNLOADING, PROVISIONING, VIEWING OR USE OF THE MATERIALS REGARDLESS OF THE FORM OF ACTION, WHETHER FOR BREACH OF CONTRACT, BREACH OF WARRANTY, TORT, NEGLIGENCE, INFRINGEMENT OR OTHERWISE (INCLUDING, WITHOUT LIMITATION, DAMAGES BASED ON LOSS OF PROFITS, DATA, FILES, USE, BUSINESS OPPORTUNITY OR CLAIMS OF THIRD PARTIES), AND WHETHER OR NOT THE PARTY HAS BEEN ADVISED OF THE POSSIBILITY OF SUCH DAMAGES. THIS LIMITATION SHALL APPLY NOTWITHSTANDING ANY FAILURE OF ESSENTIAL PURPOSE OF ANY LIMITED REMEDY PROVIDED HEREIN.
- Should any provision of this Agreement be held by a court of competent jurisdiction to be illegal, invalid, or unenforceable, that provision shall be deemed amended to achieve as nearly as possible the same economic effect as the original provision, and



the legality, validity and enforceability of the remaining provisions of this Agreement shall not be affected or impaired thereby.

- The failure of either party to enforce any term or condition of this Agreement shall not constitute a waiver of either party's right to enforce each and every term and condition of this Agreement. No breach under this agreement shall be deemed waived or excused by either party unless such waiver or consent is in writing signed by the party granting such waiver or consent. The waiver by or consent of a party to a breach of any provision of this Agreement shall not operate or be construed as a waiver of or consent to any other or subsequent breach by such other party.
- This Agreement may not be assigned (including by operation of law or otherwise) by you without WILEY's prior written consent.
- Any fee required for this permission shall be non-refundable after thirty (30) days from receipt by the CCC.
- These terms and conditions together with CCC's Billing and Payment terms and conditions (which are incorporated herein) form the entire agreement between you and WILEY concerning this licensing transaction and (in the absence of fraud) supersedes all prior agreements and representations of the parties, oral or written. This Agreement may not be amended except in writing signed by both parties. This Agreement shall be binding upon and inure to the benefit of the parties' successors, legal representatives, and authorized assigns.
- In the event of any conflict between your obligations established by these terms and conditions and those established by CCC's Billing and Payment terms and conditions, these terms and conditions shall prevail.
- WILEY expressly reserves all rights not specifically granted in the combination of (i) the license details provided by you and accepted in the course of this licensing transaction, (ii) these terms and conditions and (iii) CCC's Billing and Payment terms and conditions.
- This Agreement will be void if the Type of Use, Format, Circulation, or Requestor Type was misrepresented during the licensing process.
- This Agreement shall be governed by and construed in accordance with the laws of the State of New York, USA, without regards to such state's conflict of law rules. Any legal action, suit or proceeding arising out of or relating to these Terms and Conditions or the breach thereof shall be instituted in a court of competent jurisdiction in New York County in the State of New York in the United States of America and each party hereby consents and submits to the personal jurisdiction of such court, waives any objection to venue in such court and consents to service of process by registered or certified mail, return receipt requested, at the last known address of such party.

#### **WILEY OPEN ACCESS TERMS AND CONDITIONS**

Wiley Publishes Open Access Articles in fully Open Access Journals and in Subscription journals offering Online Open. Although most of the fully Open Access journals publish open access articles under the terms of the Creative Commons Attribution (CC BY) License only, the subscription journals and a few of the Open Access Journals offer a choice of Creative Commons Licenses. The license type is clearly identified on the article.

##### **The Creative Commons Attribution License**

The [Creative Commons Attribution License \(CC-BY\)](#) allows users to copy, distribute and transmit an article, adapt the article and make commercial use of the article. The CC-BY license permits commercial and non-

##### **Creative Commons Attribution Non-Commercial License**

The [Creative Commons Attribution Non-Commercial \(CC-BY-NC\) License](#) permits use, distribution and reproduction in any medium, provided the original work is properly cited and is not used for commercial purposes.(see below)

##### **Creative Commons Attribution-Non-Commercial-NoDerivs License**

The [Creative Commons Attribution Non-Commercial-NoDerivs License \(CC-BY-NC-ND\)](#) permits use, distribution and reproduction in any medium, provided the original work is properly cited, is not used for commercial purposes and no modifications or adaptations are made. (see below)

##### **Use by commercial "for-profit" organizations**

Use of Wiley Open Access articles for commercial, promotional, or marketing purposes requires further explicit permission from Wiley and will be subject to a fee.

Further details can be found on Wiley Online Library

<http://olabout.wiley.com/WileyCDA/Section/id-410895.html>

# Jasmine Wang

## Curriculum Vitae

### EDUCATION

---

- 2012 - Present      **Ph.D.**, Physical & Analytical Chemistry  
Western University, London, ON  
Supervisors: Dr. Ken Yeung and Dr. Shawn Whitehead
- Research Focus:
- Method development for the analysis of proteins and peptides using MALDI imaging.
  - Tissue preparation techniques to improve detection sensitivity and spatial resolution.
  - A $\beta$  detection using MALDI MS
- Conferred June 2012      **Honours B.Sc.**, Double Major in Chemistry and Biochemistry  
University of Toronto, Toronto, ON  
Minor: Psychology

### RESEARCH EXPERIENCE

---

- 2012 – Present      **Graduate Research Assistant**  
*Western University*
- Researched a variety of novel techniques for targeted protein and peptide analysis in MALDI MS imaging;
  - Adapted and developed methods for enhancing signal detection of peptides/proteins within complex samples and tissue sections;
  - Established standard operating procedures; and
  - Maintained, serviced, and constructed laboratory equipment.
- Sept. 2012 - May 2016      **Graduate Teaching Assistant**  
*Western University*
- Ran laboratory sessions for undergraduate chemistry courses;
  - Presented pre-laboratory lessons and implemented safe laboratory practices;
  - Facilitated laboratory experiments and provided guidance in laboratory techniques; and
  - Performed regular assessments to provide constructive feedback for students.

- Sept. 2014 -  
May 2015
- Interim MALDI Mass Spectrometry Facility Manager**  
*London Regional Proteomics Facility*
- Provided technical support and consultation services to peers and colleagues;
  - Planned and executed sample analysis, for MS and MS/MS data acquisition, peptide mass fingerprinting, and MALDI MSI services;
  - Developed standardized operating procedures to improve work flow;
  - Promoted facility services and educated clients on MALDI MS sample preparation methodologies; and
  - Performed daily troubleshooting, maintenance, and diagnostics to solve instrumental errors and complications.
- May 2011 -  
May 2012
- Laboratory Assistant**  
*University of Toronto*
- Facilitated the development of undergraduate instruction manuals for Advanced Organic Synthesis and Bio-Organic Chemistry; and
  - Compiled the necessary information and filmed instructive videos on NMR theory and sample preparation for the undergraduate teaching website.
- Feb. 2011 -  
May 2012
- Research Assistant**  
*University of Toronto*
- Completed undergraduate thesis in the Development of a novel NMR technique for clay-xenobiotic interactions; and
  - Provided laboratory assistance in the study of soil contamination effects on the biological activity of living organisms.

## **VOLUNTEER EXPERIENCE**

- Sept. 2012 –  
May 2016
- Outreach Volunteer**  
*Let's Talk Science*
- Organized and led outreach events for elementary schools to demonstrate core scientific principles, and to encourage students to develop a passion for science.

## PUBLICATIONS

---

**Wang, J.S.H.**, Whitehead, S.N., Yeung, K.K.-C. Detection of amyloid beta (a $\beta$ ) oligomeric composition using matrix-assisted laser desorption ionization mass spectrometry (MALDI MS). *J Am Soc Mass Spectrom* 2018; 29(4):786-795. doi: 10.1007/s13361-018-1896-z.

**Wang, J.S.H.**, Freitas-Andrade, M., Bechberger J.F., Naus, C.C., Yeung, K.K.-C., Whitehead, S.N. Matrix-assisted laser desorption/ionization imaging mass spectrometry of intraperitoneally injected danegaptide (ZP1609) for treatment of stroke-reperfusion injury in mice. *Rapid Communications in Mass Spectrometry* 2018; 32(12):951-958. doi: 10.1002/rcm.8115.

Ibrahim, H.; Jurcic, K.; **Wang, J.S.H.**; Whitehead, S.N.; Yeung, K.K.-C. 1,6-diphenyl-1,3,5-hexatriene (DPH) as a novel matrix for MALDI MS imaging of fatty acids, phospholipids, and sulfatides in brain tissues. *Anal Chem* 2017; 89(23):12828-12836. doi: 10.1021/acs.analchem.7b03284.

## CONFERENCE PROCEEDINGS

---

**Wang, J.S.H.**, Bechberger, J.F., Freitas-Andrade, M., Naus, C.C., Whitehead, S.N., Yeung, K.K.-C. MALDI IMS Detection of Intraperitoneally Injected Dipeptide, ZP1609. 65<sup>th</sup> Annual *American Society for Mass Spectrometry Conference* (Indianapolis, USA, June 2017). Poster.

Bechberger, J. F., Freitas-Andrade, M., **Wang, J. S.-H.**, Yeung, K. K.-C., Whitehead, S. N., Hansen, R. S., Naus, C. C. Danegaptide Enhanced Astrocyte Gap Junctional Coupling and Reduces Ischemic Reperfusion Brain Injury in Mice. *International Symposium on Cerebral Blood Flow, Metabolism, and Function*. (Berlin, Germany, April 2017). Poster.

**Wang, J. S.-H.**, Jurcic, K., Whitehead, S. N., Yeung, K. K.-C. Detection of Amyloid-Beta Oligomer Composition with MALDI MS. 63<sup>rd</sup> Annual *American Society for Mass Spectrometry Conference* (St. Louis, USA, June 2015). Poster.

**Wang, J. S.-H.**, Jurcic, K., Whitehead, S.N., Yeung, K.K.-C., Oligomerization Study of Amyloid Beta using MALDI-TOF Mass Spectrometry. *Annual Society of Neuroscience Conference* (Washington D.C., USA, Nov 2014). Poster.

**Wang, J. S.-H.**, Jurcic, K., Whitehead, S.N., Yeung, K.K.-C., Method of amyloid beta detection using MALDI-TOF mass spectrometry. 34<sup>th</sup> Annual *Southern Ontario Neuroscience Association Conference* (London, ON., May 2014). Poster.